Development of Short-term Photovoltaic Forecasting and Application to Energy Management System

太陽光発電の短期発電量予測法の開発と電力需給制御への適用）

by

IMAM WAHYUDI FARID

D140188

Graduate School of Engineering

Hiroshima University

March 2018

ABSTRACT

Renewable energy resources (RESs) have attracted significant attention due to their reduced environmental impacts. In particular, active installation of photovoltaic (PV) power generation is being strongly promoted in Japan. However, the PV output is generally uncertain due to the spatially and time-varying changing solar radiation. Therefore, it is necessary to achieve a stable power supply by using controllable generator groups, which correspond to existing thermal power and/or diesel generators, based on a well-suited generation planning, operation and control policies. On the other hand, if one can predict the amount of solar radiation accurately, it will then be possible to make efficient operational plans for electric power storages as well as for existing thermal and hydraulic generators. In addition, the proper reserve margins are kept in oder to maintain the security of power systems by analyzing the prediction error and its statistical distribution. Thus, development of an accurate prediction technique and the application to advanced energy management technology are generally regarded as an important task in recent power system.

The main objective of this work is to develop a simple and reliable PV forecasting method that can be applied to energy magement system (EMS). First, a new day-ahead PV forecasting method is proposed by using only weather report data that are provided by the Japan meteorological agency (JMA) and are available to the public. Secondly, a novel approach based on the correlation analysis is developed to realize the high accuracy prediction for the real-time PV forecasting. In above two approaches for PV forecasting, the multiple neural networks (NNs) based on a weather clustering technique are used to obtain the predictions and the confidence intervals (CIs). Finally, these forecasting methods are applied to the EMS controller, where the prediction and CIs are effectively provided to maintain the robust power system security. These demonstrations for supply and demand management are presented to confirm the effectiveness and robustness of the proposed PV forecasting approaches.

ACKNOWLEDGEMENT

First of all, I want to give my high praise to Allah about the opportunity, knowledge, ability and healthy body and mind to finish this thesis book. I really thanks to god about all the goodness.

Also, I really thanks to god for giving me a best supervisor, professor Naoto Yorino. Thank you very much for your comments, patience, suggestion, motivation, and his support during I stay in Hiroshima University, Japan. I learned so much about everything's in this live. Not only about research, also about how to face the future and how to face a human. Without his help, maybe I will not be a person like now. I owe so much thing to you.

I would like to express my greatest gratitude for Prof. Yoshifumi Zoka and Prof. Yutaka Sasaki for help me, thank you so much for everything. Also for all members of EPESL laboratory, thank you very much for your kindness and team work. I would also like to thank to Prof. Takahashi Katsuhiko and Prof. Nishizaki Ichirou for helping me. Thank you very much for your brilliant comments and suggestions.

Last but not the least, I would like to thank my family: my wife Beta Golda Nisa, my parents, my wife's family, my brothers, my sisters, and my friends for supporting my life, thank you so much. Also for my doctoral degree friends and sensei in ITS Surabaya, Thank you very much. ありがとうございます .

Imam Wahyudi Farid

2018

TABLE OF CONTENTS

LIST OF FIGURES

LIST OF TABLES

Chapter 1

Introduction

1.1 Background

Renewable energy generators are expected to grow rapidly in the following years. Also, renewable energy uses non-fossil consumption power generation, and therefore placing renewable energy resources as a best option for long-term power generation. Wind-turbine generations and photovoltaic (PV) generations are the most favorable renewable energy generations among others. Around 20% until 30% of the renewable energy resources is estimated to increase in the next 15 until 20 years. In Japan, PV is strongly promoted to support the power generation in power system grid. [1] mentioned the cumulative PV installed is around 42GW, where 153 MW is allocated for off-grid and 41,879 MW for grid-connected. This capacity value was calculated in the end of 2016. This value reveals that renewable energy is currently being strongly increased and promoted. However, the weakness of the PV is the uncertain value for each day production. This uncertainty is due to the climate and weather changes. The uncertainty on PV output can cause a problem for power system grid. For example, a non-predictable PV output can cause the power system to fluctuate and become unstable. This is a high-risk for the current power system which has been running normally for years. Therefore, a simulator of power sources including thermal power or existing generator and renewable energy sources are necessary to simulate and prepare the power sources calculation. A small power system grid as an example could be built and applied. The power system grid could include generation planning, control and operation.

It is for this reason that a good estimation of PV output is necessary to prepare the PV sources in the power system grid. PVs are clean and safety energy sources. However, they are prone to cause degradation of power quality as well as grid security due to unforeseen weather conditions. Continuous sunlight intermittency, especially during cloudy days, incurs sudden intense changes in their outputs such as unpredictable significant ramp effect. The enhancement of renewable energy requires additional ramping abilities to maintain the grid stability. PV output estimation should propose high accuracy in its results. It should also be

applicable in the power system grid. Development of sophisticated operating technology is a key subject.

Through this research, we analyze the error and the distribution result where error value represents the prediction result and the target date. Based on these calculations, the reserve margin of PV forecast result could be applied on the supply-demand control or the power system simulator. Therefore, to obtain the best prediction result, it is necessary to develop the prediction method. It is also necessary to highlight the development of supply-demand control as it is an important target. We obtain the value of confidence interval (CI) through this stage. We also set the CI value as a reliable range for the PV forecast result.

In this research, we express "robust power system security" to mention the power system security hardiness or generally known as robustness of power system security. References [2-4] mentioned the ideal boundary of power system security. The items set to maintain the power system is secure and will prevent worst-case possibilities such as blackouts, load shading, etc. CI is expected to avoid these damaging conditions. We also proposed a power system simulator or "supply-demand manager" to apply the CI setting and analyze the response. References [5-7] focus on the supply-demand manager (SDM) as a tool for the CI setting application. In the SDM part, we can provide the operational planning, day-ahead planning manager, real-time operation manager and real-time control manager. SDM is also an example of remote island power system grid.

To obtain a good CI setting, we should obtain a good forecast result. Here we summarize the various of PV forecast. Reference [8] is a literature for day-ahead forecasting in small-scale PV generator. This paper provides 24-h-ahead forecasting using a forecasting tool. They use three locations; San Diego, Braedstrup and Catania and use four methods of RBFNNs (Radial Basis Feedforward Neural networks), least square Support Vector Machine (L- SVM), *k*NNs and weighted *k*NNs as engines model. On the other hand, reference [9] uses the spatial-temporal solar to obtain a very-short term solar forecasting. The spatial-temporal solar forecasting framework is based on the vector auto-regression framework. Other than the spatial-temporal framework, solar generation observation that collects using the smart meter and distribution transformer controllers is also used as a comparison. Not only do researchers use one

forecasting method, some researchers also use a hybrid method to obtain the short-term PV forecast. [10,11] both use a hybrid method to obtain the solar power forecasting. In reference [10] the authors use Florida data set and a combination of gradient-descent optimization and feedforward artificial neural network (ANN) to model the data. To determine the ANN parameters, the author uses meta-heuristic optimization model, known as shuffled frog leaping algorithm (SFLA). [11] use self-organizing map (SOM) and learning vector quantization (LVQ) to classify the historical data input for 1-day ahead forecast. For the PV power output forecast, the authors use support vector regression (SVR) for the data input. A probabilistic method is used by [12] as short-term PV power forecasting. The probabilistic method is based on a competitive ensemble of different base predictors. Also, another method known as the determination method is used by [13] to forecast the PV output. The NN is trained by the output data based on the fuzzy logic. The report weather data which is used as input data and fuzzy logic determine the insolation forecast. Another researcher [14] uses aerosol data to improve the PV power forecasting model. Aerosol index (Ai) is used because it could indicate the particular matter in the atmosphere, and the authors of the research also mentioned that they found a strong linear correlation between Ai and solar radiation attenuation. [15] creates a model of the solar irradiance using grid point value (GPV) data analysis. This method is convenient for the efficiency of PV system.

Support vector machine (SVM) was also used by [16,17] to forecast the PV power output. [16] use the combination of satellite images and SVM to model the solar power prediction. The authors analyze 4 years of satellite images from the past and develop the satellite images. Other than that, recurrent neural network (RNN) was used by [18] to develop the correlation between solar radiation and timescale-related variations of weather item such as wind speed, humidity and temperature. RNN was combined with wavelet to obtain the solar radiation prediction in the wavelet domain. [19], constructive neural networks (CoNNs) were used by the authors to obtain the solar radiation prediction. CoNNs train the input data, which include historical data of temperature, humidity, wind speed and weather type, and then the process starts with one hidden unit in the hidden layer. Another hidden unit is added again if the NNs need to improve the mapping capability until it reaches the minimum NN. [20] models the power forecasting based on the nonlinear system

identification. The authors use data in Kuwait and suitable for a high non-linear change in the PV system.

An intelligent method was used by [22] to obtain the day-ahead hourly forecasting. The first step in classifying the historical data, the authors use fuzzy *k*-means, which then is followed by the second step of training the data trained using radial basis function neural network (RBFNN). The third step which aims to optimize the RBFNN parameters, the authors use harmony search algorithm (HSA), while for the forecasting process, the fuzzy inference is used in the research.

In the researches, not only do authors disclose the power output forecast, but the application of PV output is also described along with the forecast result. [24] apply the PV prediction in the distribution of voltage regulation. This paper discusses about the overvoltage limit violation because of PV sources in the power system grid. A very short duration of PV power forecast, about 15 seconds, is utilized to avoid the upper limit of voltage regulation and overvoltage. [5] use the PV output in a larger scale compared to [24]. They mention a feasible operation region for the PV output limitation area. In the power system, the application of PV output is also used by some authors in unit commitment (UC). [26] use the PV output prediction for the efficiency of uncertainty management in the high penetration of renewable energy in the power system grid. [27] places its focus in the time-scale adaptive dispatch. The time-scale is used for renewable energy power supply system on islands. This system is adjusted online based on the CI setting from the PV forecast error. [28] use correlation analysis of insolation in two different locations. The data are measured by the authors using an actinometer. In [29] the authors identify two parameters of prediction which is, first, based on its moving direction and second, based on the speed of insolation. Other researchers process the cloud images to forecast the power fluctuation. The data research is obtained through records conducted on ground. Different with [30], they use data from weather satellites to forecast the PV power output. Based on our identification, the imagery data, the amount of insolation from the recorded device, etc., requires a complicated process as the data is not easily obtained by the researchers. In this research, we use a simple and reliable data from Japan Meteorological Agency (JMA) that could be easily accessed and free at any time required. Other than that, the accuracy of PV output forecast is also considered as an important parameter.

Hence, in this research, we provide the CI setting for power system grid application system.

1.2 Objective and Scope of the Study

The main objective of this research is the development of short-term PV output forecasting. In this PV output forecasting, we propose a simple and reliable data to be modeled and forecasted. Furthermore, the result of short-term PV output forecasting is used as information on EMS controller.

In this case, the short-term of PV output forecasting are divide into two cases of PV output forecast which are day-ahead PV output forecast and real-time PV output. The first section of our focus is the day-ahead PV output. This subject is targeted to be applied on the day-ahead planning manager. The detail of day-ahead PV output forecast discusses about day-hour order of PV output forecast. Our simple and reliable data proposed in this research is modeled and forecasted using NN. JMA provides the simple data that can be accessed easily and at any time. The day-ahead PV output forecast with 30-minute intervals will be applied on the unit commitment planning. According to the day-ahead UC planning, this time interval is necessary to obtain a better start/stop generator schedule.

The second section of our focus in the research of short-term PV output forecasting is the real-time PV output forecast. In this case, JMA data will be used once again to obtain the result. In real-time PV output forecast, the step is similar to the day-ahead PV output forecast. A more detailed step of the forecasting will be described in the following section. In the early stage of the research, JMA data is collected from the website, and data for each point or area is processed using neural network. Then, we calculate the gap time among the area and use each area forecast result to obtain the next neighborhood area. SRCA method is used to obtain the neighboring PV output result. The real-time PV output is conducted at 5-minute intervals. The real-time PV output result will be used as unit commitment calculation in the same day. The results are not only used in unit commitment, but they are also used for DELD calculation in the same day. To avoid weather changes, a standby power source will be prepared.

The last aim of this research is to apply the PV output result on the power system. For the initial step, we provide an EMS controller that represent an electricity grid. In this EMS, renewable resources, battery and generator are provided as power electricity sources. Not only do we provide electricity sources, we also provide a controller and electricity demand. All of these are included in the UC planning manager.

1.3 Outline of the Thesis

This thesis book consists of six chapters which will discuss the following:

Chapter 1

This chapter presents the background of this study, including the characteristics of the PVs.

Chapter 2

This chapter describes the conventional PV forecasting methods and techniques.

Chapter 3

In this chapter, the author provides a more detailed explanation about a new approach to predict the day-ahead PV output. To obtain the day-ahead PV output, the author only uses public data which will then be modeled using multiple NNs. The data will further be tested using the testing data and be evaluated for the result. Then, the prediction and CIs are obtained and applied to day-ahead planning manager of EMS controller.

Chapter 4

This chapter provides a novel method to estimate the real-time PV outputs by the correlation analysis.

Chapter 5

In chapter 5, the thesis performs the application in the EMS controller by using the proposed PV forecasting. The day-ahead and real-time PV forecasting are applied to the unit commitment and the dynamic economic load dispatch, respectively.

Chapter 6

The last chapter of the thesis presents the summary of the major achievements. Furthermore, future research works are provided to continue this research.

Chapter 2

Power Forecasting Methods and Techniques

2.1 Introduction

Previous works and research have reported various methods which can be used in predicting the PV output solely based on publicly available weather data. However, the methods used by the authors to obtain and process the raw data prior to forecasting the PV output tend to be complicated. Such methods do not propose an effective and simple data processing and forecasting, resulting in inefficient application of the method on EMS controllers. These power forecasting methods are substantially inapplicable due to their complicated and inconvenient implementation. Others have also reported that existing forecasting tend to be sophisticated [60-63] based on a variety of methods to forecast PV output power, adding up to the complexity nature of these methods. Several of the power forecasting methods used by researchers include numerical weather prediction [64,25], sky imagery [65,66], and neural network [67,68].

Through the research, we utilize simple data and reliable method that can be applied to the energy management operation to achieve an applicable research result. The data used in this research is the public historical insolation and weather (temperature, wind speed, and precipitation) data which can be easily obtained from the meteorological agency website of Japan. Since PV output forecast has become an important issue in energy management planning, a reliable method particularly 1 until 5 minutes forecast is substantial for real-time PV output forecasting. Recently, real-time PV output forecast requires a sophisticated data processing [69,70]. Neural network (NN), one of the most common modeling forecast method, is commonly used by researchers to model and forecast the PV output. However, NN process need more computation time for modeling and forecasting. This is one of the laxity in NN method [71]. In real-time PV forecast, computation time is one of the important matter in yielding results. Real-time PV forecast is presented for up to 1 hour in advance with 5-minutes intervals. This forecast requires a fast calculation and high accurate prediction to be applied on a real-time operation and planning of generators or batteries.

2.2 Photovoltaic (PV) Power System

PV output forecast is a complicated issue faced by many researchers. One reason behind this is the high number of weather uncertainty which is one of the most difficult process to undertake in the forecasting approach. Some researchers have reported using several forecasting methods to obtain a reliable and precise result. This is achieved through the estimation of error value between the forecast output and the weather data where the smaller the error values are, the more reliable and precise the results are.

One of the biggest challenges in the field of renewable energy sources (RES) is their vulnerability and their volatile nature as it depends on changing matters such as weather conditions. While conventional power plants offer concrete resources, which can be accessed on demand, resources of non-conventional power plants for renewable energy, on the other hand, cannot be accessed on demand such as wind and solar production. The changing nature of these resources play a vital role on the production of renewable energy, and it is on these issues that the power output of PV system heavily relies on. Power production from PV energy sources depends on weather conditions of cloud coverage and incidence angle of the sun's radiation which are always changing. With the power output highly dependent on these weathers changing conditions, it is crucial to develop accurate and precise forecasts in order to run a smoother integration of renewable energy into the electricity grid.

2.3 Forecasting Methods

Various work on PV output prediction have co-existed with the development of renewable energy sources (RES). Research on this specific field, and renewable resources output in general, is vital to the development of RES as they heavily rely on naturally replenished resources. Being a natural entity replenished on a human timescale, these resources are not equipped with certainty and predictability in terms of the number of output as they are inextricably linked to the continuous change of uncontrollable weather and other natural conditions.

Inevitably, this creates an immense impact on renewable energy and its development, including renewable energy from PV.

An attempt to map and predict the output from PV have been conducted in various research over the past several years, resulting in several forecasting models. There exists various PV prediction methods in the literature such as the day-ahead forecasting for small-scale PV [8], the spatial-temporal solar very short-term forecasting [9], the hybrid algorithms for short-term PV prediction [10,11], the probabilistic ensemble methods [2], the determination methods [3], research using aerosol data [14], grid point value (GPV) [15], support vector machine (SVM) [16,17], recurrent neural network (RNN) [8], constructive neural networks (NNs) [19], nonlinear system identification models [20], the Markov switching models [21], the intelligent methods for day-ahead hourly forecasting [22], and the statistical methods [23]. Applications of the PV predictions are presented for the distribution voltage regulation [24], for the large-scale grid [25], for the unit commitment (UC) [26], and for the time-scale adaptive dispatch [7]. The reference [8] proposes a PV prediction method for local distribution control system based on the correlation analysis of the observed data. Recent methods use cloud images that are observed from the ground [29] or that are obtained from weather satellites [30].

However, these complicated methods require access and availability of special data such as meteorological image data, solar data from the radiation meters at power grid substations, etc., which are not easily obtainable in practice. Furthermore, these methods focus their attention on the accuracy of obtained predictions and there are practically no examinations on the CI metric, among others. There are a number of methods available in present day used to forecast PV output which will further be discussed in the following section to serve as reference and review for this research.

2.3.1. Statistical Models (AR, ARIMA, NN, etc.)

One common method in making predictions based on a variety of data input is the statistical model. With a mathematical approach, statistical modelling will generate an approximate reality to the data input and process the approximation into a prediction. It is often known as the data-generating process as it predicts

information based on collected or sampling data and population understanding. Statistical modelling has been applied in various forms of programs which among others include autoregressive (AR), autoregressive-moving average model (ARIMA), and neural network (NN). [29] use AR and ARIMA to model and forecast the solar radiation in Bogota. The author uses basic AR formula here,

$$X_t = \alpha_0 + \sum_{l=1}^{p} \alpha_l X_{t-l} + \varepsilon_t \quad (1)$$

Where α_0 set in constant value and ε_t is a zero-mean white noise with constant variance σ_t^2 . Then, the authors also use ARIMA model to forecast the solar radiation. Here the ARIMA model formula,

$$W_{t+h} = -\sum_{j=1}^{h-1} \Psi_j \alpha_{t+h-j} - \sum_{j=h}^{\infty} \Psi_j \alpha_{t+h-j} \quad (2)$$

Another author also uses statistical time series model of solar radiation and outdoor temperature as data input and Kalman filter as forecast method. [30] use the temperature room because their calculation method requires a time series model of external climate. [30] another researcher uses ARX method to obtain the online short-term solar power forecasting.

2.3.2. Cloudy Imagery and Satellite based Models

Cloudy imagery and satellite-based models focus in cloudy imagery data. Some researchers use several devices to observe the sky movement from one point to another. The data is based on the observation result. Generally, the researchers use the clearness indices to convert the cloud situation into number value. The clearness indices (some researchers reported using clearness index or CI) is on the ration scale of 0 to 1. This value is obtained from the cloudy imagery pixel. There are several categories of the cloudy imagery pixel result. A clear sky, a high density cloudy sky and a low density cloudy sky are the classes that are generally used by the researchers in this area.

Several recent studies for cloudy imagery and satellite-based model are mentioned below. [36] use 80 PV systems that are installed in the rooftop in Tuscon, AZ region. The PV systems are used as ground-based irradiance sensors, the PV distributed on 50 km x 50 km area. Figure 1 is the example of the imagery satellite.

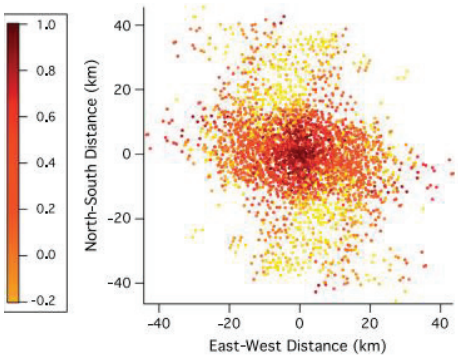

Figure 1. Top: Spatial correlation between station pairs for one day as a function of separation in the east–west as well as north–south directions

The authors record the data at 15-minute interval and not only focus on the sky imager. [37] use statistical smoothing techniques to find the clear sky model. [38] use cloudiness indices as input data and radial basis function (RBF) neural network to predict the solar radiation.

2.3.3. Numerical Weather Prediction (NWP) Models

Numerical weather prediction (NWP) or often known as numerical forecasting offers a mathematical model as an attempt to understand the pattern in weather prediction. Numerical forecasting is conducted through complex supercomputers which generate predictions based on data of the atmosphere and ocean according to the current weather condition. Though the model has been tested and designed in the 1920s, realistic and promising results were produced only until the advent of computer simulation in the 1950s. Many weather variables such as temperature, wind and possibility of precipitation are forecasted through this model. These predictions are generated through high-speed computers which integrates fundamental equations of hydrodynamics and a modeled atmosphere in a mathematical approach.

While numerical forecasting offers many promising results, inaccuracy in its equations often leads to some errors in the predictions. Another flaw of this method is the number of gaps between the initial data, ultimately resulting in imprecise output. The number of people with access to the computer data is also very limited. [64] use three individual validation of global horizontal irradiance multi-day forecast models. They use this model for three areas; US, Canada and

Europe. All of the forecast models are based on directly or indirectly to NWP. [40] use NN to localize the precipitation forecast that is obtained from the NWP prediction. They use the middle Atlantic region of US data for their research.

2.3.4. Hybrid Models

Another forecasting method presented in earlier works is the hybrid model. Hybrid forecasting proposes a program by combining regression, data smoothing, and other stages of techniques to attain forecasting results which compensate flaws of individual forecasting methods. The methods used in hybrid forecasting include Vanguard Dampened Trend, Log Theta, Theta, NN, NWP and clear sky model. [11] use hybrid method for one-day ahead forecasting. Their research focuses on hourly PV power output. They integrate the self-organizing map (SOM) to classify the data input. Also, learning vector quantization (LVQ) is used to classify the historical data PV while Support vector regression (SVR) is used to comprehend the historical data. [39] use hybrid *k*-means and nonlinear autoregressive neural network (NAR) model to obtain a better PV output forecast. The *k*-means method is used to extract the data. Not only to extract, the method was also used to model the data and find the data patterns. Once the data has been modeled, NAR is used as a forecasting method.

2.4 Summary

As reflected above through the various types of power forecasting methods for renewable energy, it is apparent that the need of a forecasting model for RES is crucial. Many have proposed various kinds of prediction models, applying a different approach for every type while adjusting to the needs, different type of available data, the efficiency and effectiveness of the techniques used, and other significant features. However, undoubtedly many challenges are faced when dealing with weather uncertainty which can impact on the data used in present models. Flaws and weaknesses are present on the forecasting methods, demanding a constant development and research in the field of weather forecasting for renewable energy, which in this case focuses on PV output. One of the challenges

faced by the models is the limited amount of available data and its complexity. Many required data and made available publicly are inconvenient and offer a certain degree of uncertainty. With this particular challenge as a highlight, this research aims to provide a method of forecasting PV output by using only simple and reliable data to improve its accuracy and effectivity. It will also give a bigger possibility of usage and application as the necessary data are made publicly available and easily obtained.

Chapter 3

Day-ahead 24-hours Power Forecasting

3.1. Introduction

This chapter focuses on the discussion of day-ahead 24 hours PV output forecasting. In the previous chapter, it is explained how other researchers use different kinds of methods to obtain day-ahead PV output forecast, and many of them were challenged with complicated circumstances concerning the data. They require a complicated data processing before being able to be used as input for their method. Not only did it require complicated data processing, but many of the data used in the previous researches were inaccessible data, making it an even more difficult situation to improve the PV output forecast. In this chapter, a more detailed explanation about the day-ahead PV output forecast which uses a simple and reliable data is described. [39] use a simple and efficient algorithm to forecast the solar radiation. A decomposition process from geostationary satellite data is necessary to obtain the data input, meaning the input data require a non-simple process.

In this research, the primary focus of day-ahead PV output forecasting is placed on the following 24 hours of the day. Calculation of the day-ahead forecast will be conducted based on several steps as shown in Figure 2. This detailed process will be taken step by step to ensure that the calculated forecast is performed in a methodized manner from the beginning until the CI results are obtained. Results from the day-ahead power forecasting will be utilized. The solar power prediction shall function as a tool to balance the total power production and is placed in the electricity grid. The research result shall be conducted on a start-stop UC plan implemented among existing generators along with the batteries.

To obtain day-ahead forecasting results, PV output predictions are set the same with the day-ahead UC planning time interval. The forecasting unit would be handling at 30-minutes interval time on collecting PV output data to further process on day-ahead forecasting. The results from these forecasting will then be included in the UC planning. In the next section, the research proposes a new method which

uses a group of neural networks assigned for every weather cluster for the target time.

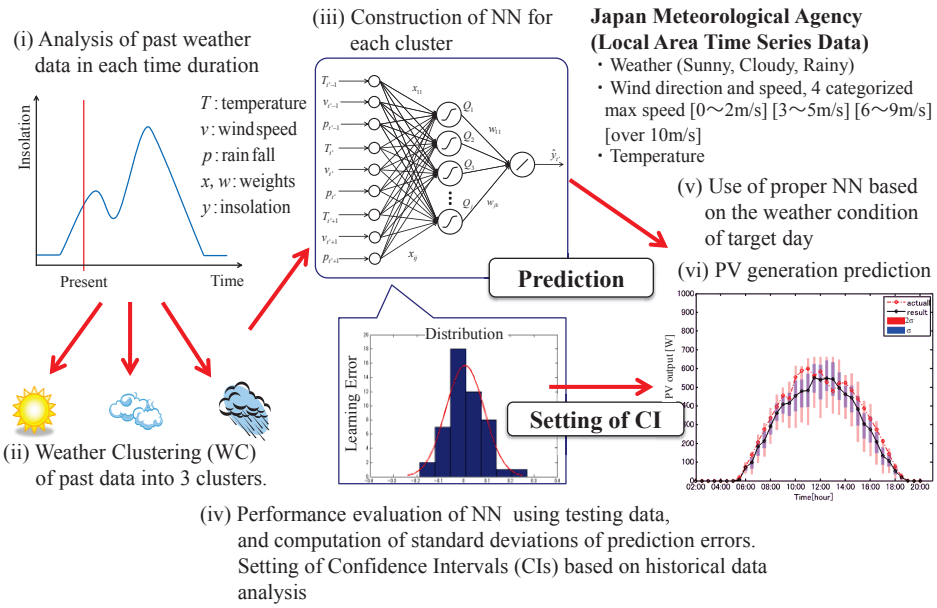

Figure 2. The proposed scheme of PV output prediction.

The proposed scheme for the PV output forecast is detailed through six calculation steps.

1. The first step of the PV output forecast involves a thorough analysis on previous weather data in each time duration. The data being analyzed includes an intensive feature such as the temperature, windspeed, rainfall, and insolation which altogether have an impact on the weather condition. The data are downloaded through the JMA website. Currently, we use temperature, windspeed, insolation and rainfall data only since these kinds of weather conditions have a direct impact to the insolation value. The data downloaded for the research is from 2009 until 2012. More explanation about data processing will be described below.
2. Once the past data have been analyzed, they are put into clusters according to the weather clustering (WC). Analyzed data are categorized based on the weather conditions. There are three types of weather clusters; sunny, cloudy, and rainy condition. These clusters are based on the Japan Meteorological

Agency which presents the weather clusters according to the local area time series data.

3. Upon completion of weather clustering, the forecasting process shall proceed with the third step of the PV output forecasting which involves the construction of Neural Network (NN) for each of the weather cluster formed in the figure 2.
4. After the Neural Network has been set for every weather condition cluster, an evaluation on its performance can be conducted using testing data. This evaluation shall be performed in the following phase of the forecasting model. The NN on each cluster will be evaluated by testing data and computation of standard deviations for prediction errors.
5. Then, the next step is CI setting. The standard deviation that is calculated before, will be used as appropriate setting for confidence intervals (CI) based on historical data analysis.
6. The last step is applying the CI evaluation to the EMS controller. The forecasting process is applied using the proper NN based on the weather condition on the target day. This will result in the PV output prediction.

3.2. Data Clustering by Weather Condition

This section of the research presents a detailed explanation on the data clustering process. Figure 3 shows the JMA data which are made available through their website.

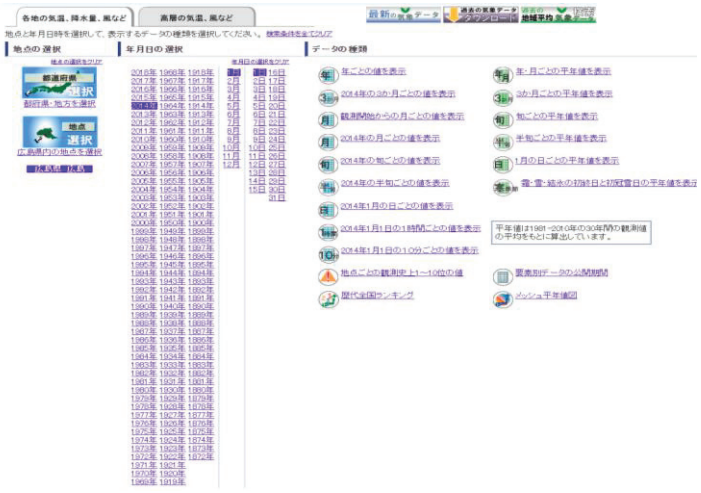

Figure 3. Weather data from JMA website

In the JMA website, there are many historical data that could be easily accessed for free. The weather data starts from 1872 until the current day. According to the website, the data is not fully complete in terms of 10 seconds interval time. Data with this interval time only applies to data from 2000 until current day data.

After accessing the JMA website, user should choose the necessary date and time interval. In this step, the user should check properly to download the necessary data through the website. Figure 4 shows the time interval before year 2000.


前年 前月 前日 翌日 翌月 翌年　日ごとの値 1時間ごとの値 10分ごとの値

広島 1951年1月1日 (1時間ごとの値)

時	気圧(hPa)		降水量	気温	露点温度	蒸気圧	湿度	風向・風速(m/s)		日照時間	全天日射量	雪(cm)		天気	雲量	視程
	現地	海面	(mm)	(℃)	(℃)	(hPa)	(%)	風速	風向	(h)	(MJ/m²)	降雪	積雪			(km)
1			--													
2			--													
3			--													
4			0.0													
5			0.0													
6			0.1													
7			0.1													
8			0.1													
9			0.0													
10			--													
11			0.0													
12			0.0													
13			--													
14			--													
15			--													
16			--													
17			--													
18			--													
19			--													
20			--													
21			--													
22			--													
23			--													
24			--													

Figure 4. The JMA data website in year 1961

Based on Figure 4, there are 13 kinds of weather data that are recorded by JMA. The data is available for 24 hours. Figure 4 also shows that there is no data available in 1st January 1951. It means not all the data is available in the JMA website for every time. In year 1951, the data time interval is also available for every hour. However, data is not yet available for 10-second interval.

日ごとの値

一覧表 | グラフ | 見出しの固定 | メニューに戻る

主な要素 | 詳細（気圧・降水量） | 詳細（気温・蒸気圧・湿度） | 詳細（風） | 詳細（日照・雪・その他）

前年 | 前月 | 前日 | 翌日 | 翌月 | 翌年 | 月ごとの値 | 旬ごとの値 | 半旬ごとの値 | 日ごとの値

広島 1951年1月（日ごとの値） 主な要素

日	気圧(hPa) 現地 平均	気圧(hPa) 海面 平均	降水量(mm) 合計	降水量(mm) 最大 1時間	降水量(mm) 最大 10分間	気温(℃) 平均	気温(℃) 最高	気温(℃) 最低	湿度(%) 平均	湿度(%) 最小	風向・風速(m/s) 平均風速	風向・風速(m/s) 最大風速 風速	風向・風速(m/s) 最大風速 風向	風向・風速(m/s) 最大瞬間風速 風速	風向・風速(m/s) 最大瞬間風速 風向	日照時間(h)	雪(cm) 降雪 合計	雪(cm) 最深積雪 値	天気概況 昼 (06:00-18:00)	天気概況 夜 (18:00-翌日06:00)
1			0.3	0.1	0.1	5.2	10.9	0.8												
2			—	—	—	4.0	9.8	0.5												
3			—	—	—	3.3	11.4	−1.1												
4			—	—	—	2.3	7.1	−1.8												
5			—	—	—	3.8	10.0	−0.4												
6			0.1	0.1	0.0	4.0	7.9	−0.6												
7			10.7	1.6	0.5	4.0	6.9	1.6												
8			—	—	—	4.2	12.1	0.0												
9			5.2	1.5	0.6	5.7	9.3	0.7												
10			9.5	3.1	0.8	7.9	9.4	6.3												
11			—	—	—	8.1	11.7	5.1												
12			0.1	×	0.0	2.0	5.6	−1.1												
13			0.0	0.0	0.0	−0.8	2.5	−2.9												
14			0.0	0.0	0.0	0.4	6.9	−3.6												
15			—	—	—	2.7	9.2	−1.0												
16			—	—	—	3.0	9.3	−2.1												
17			—	—	—	5.4	12.6	0.3												
18			0.0	0.0	0.0	5.5	11.2	−0.7												
19			12.5	1.8	0.4	6.6	8.1	4.8												
20			—	—	—	7.0	11.3	2.4												
21			1.0	0.5	0.3	−0.7	2.6	−3.0												
22			0.0	0.0	0.0	0.0	5.1	−3.9												
23			0.0	0.0	0.0	2.1	4.3	−1.8												
24			—	—	—	5.1	6.8	3.0												
25			—	—	—	7.1	9.1	5.7												
26			0.2	0.2	0.1	5.1	9.7	2.7												
27			—	—	—	4.3	9.6	0.1												
28			—	—	—	4.2	11.8	−1.0												
29			—	—	—	4.8	13.3	−1.7												
30			—	—	—	5.0	11.8	1.1												
31			—	—	—	4.9	12.2	−0.4												

Figure 5. JMA data for January 1951

.

Based on Figure 5, in January 1951, only daily data for each month is available. Also, not every weather data appears in the website. Only precipitation data and temperature data are available. Figure 5 describes the lowest, maximum and average daily temperature data. The temperature data uses ºC as its units. In another column, the precipitation data is available, but it is not the same as temperature data. The precipitation data is only available for the 1st, 6th, 7th, 9th, 10th, 12th ~ 14th, 18th, 19th, 21st ~ 23rd, and 26th of January 1951.

一覧表 | グラフ | 見出しの固定 | メニューに戻る

前年 | 前月 | 前日 | 翌日 | 翌月 | 翌年 | 日ごとの値 | 1時間ごとの値 | 10分ごとの値

広島 2009年1月1日 （1時間ごとの値）

時	気圧(hPa) 現地	気圧(hPa) 海面	降水量 (mm)	気温 (℃)	露点温度 (℃)	蒸気圧 (hPa)	湿度 (%)	風向・風速(m/s) 風速	風向・風速(m/s) 風向	日照時間 (h)	全天日射量 (MJ/m²)	雪(cm) 降雪	雪(cm) 積雪	天気	雲量	視程 (km)
1	1009.8	1016.6	--	0.7	-1.8	5.3	83	3.9	北							
2	1009.4	1016.2	--	0.6	-2.1	5.2	82	1.9	北北東							
3	1009.7	1016.5	--	0.1	-2.3	5.2	84	2.7	北北東					◑	2	20.0
4	1009.6	1016.4	--	0.5	-2.0	5.3	83	2.1	北北東							
5	1009.4	1016.2	0.0	0.6	-2.1	5.2	82	4.0	北							
6	1009.5	1016.3	0.0	0.6	-1.5	5.5	86	2.4	北					○	1	20.0
7	1009.9	1016.7	--	0.3	-2.1	5.2	84	2.7	北北東		0.00					
8	1009.8	1016.6	--	0.5	-1.7	5.4	85	1.4	北北東	0.4	0.10					
9	1010.4	1017.2	--	1.9	-1.3	5.5	79	1.1	東北東	1.0	0.62	0	--	◑	2	30.0
10	1010.1	1016.8	--	4.1	-4.1	4.5	55	1.3	北東	1.0	1.19					
11	1009.8	1016.5	--	5.0	-5.4	4.1	47	2.3	北北東	0.5	1.26					
12	1008.8	1015.5	--	6.2	-4.5	4.4	46	0.8	北東	0.3	1.19			◑	8	35.0
13	1008.3	1014.9	--	6.4	-5.6	4.0	42	3.0	北北東	0.6	1.56					
14	1008.4	1015.0	--	6.6	-5.1	4.2	43	3.0	北北西	0.5	1.26					
15	1009.4	1016.1	0.0	5.3	-2.1	5.3	59	6.1	北	0.1	0.59	--	--	●	10-	8.00
16	1009.9	1016.6	0.0	4.1	-0.9	5.7	70	3.7	北	0.4	0.56					
17	1010.4	1017.1	0.0	3.2	-0.4	5.9	77	1.5	北北東	0.1	0.19					
18	1011.3	1018.1	0.0	2.9	0.3	6.2	83	3.7	西	0.0	0.00			☁	10	10.0
19	1011.5	1018.3	0.5	2.7	0.0	6.1	82	1.6	西南西							
20	1012.2	1019.0	0.0	2.8	0.1	6.1	82	1.7	南西							
21	1012.6	1019.4	0.0	2.7	0.3	6.2	84	2.2	北北東			0	--	●	10	15.0
22	1013.0	1019.8	0.0	2.5	0.1	6.1	84	2.1	西							
23	1012.6	1019.4	0.0	2.9	0.0	6.1	81	1.7	北							
24	1012.9	1019.7	0.0	2.8	0.4	6.3	84	1.2	東南東							

Figure 6. JMA data for January 2009

Compared to Figure 6, weather data for January 2009 appears to be more complete than January 1951. In contrast to the data of January 1951, in 2009 the website provides 13 kinds of weather data. The user could use all of this data easily. Also, the data time interval is available in more detail. There are 10 seconds time interval for each data that could be accessed in the JMA website. Figure 7 below shows the 10 second time interval data.

一覧表　グラフ　　見出しの固定　メニューに戻る

前年　前月　前日　翌日　翌月　翌年　　日ごとの値　1時間ごとの値　10分ごとの値

広島 2009年1月1日(10分ごとの値)

時分	気圧(hPa)		降水量	気温	相対湿度	風向・風速(m/s)				日照時間
	現地	海面	(mm)	(℃)	(%)	平均	風向	最大瞬間	風向	(分)
00:10	1010.0	1016.8	---	0.9	83	2.7	北	4.6	北	
00:20	1009.9	1016.7	---	0.7	83	3.4	北	5.4	北	
00:30	1009.7	1016.5	---	0.8	83	1.4	東北東	2.1	北東	
00:40	1009.8	1016.6	---	0.8	83	1.6	北	3.9	北	
00:50	1009.7	1016.5	---	0.7	82	3.7	北北東	4.5	北北東	
01:00	1009.8	1016.6	---	0.7	83	3.9	北	5.1	北北東	
01:10	1009.6	1016.4	---	0.7	82	3.7	北北東	5.1	北	
01:20	1009.6	1016.4	---	0.6	82	3.5	北	4.7	北	
01:30	1009.5	1016.3	---	0.6	83	3.5	北	4.7	北	
01:40	1009.5	1016.3	---	0.7	82	2.2	北北東	3.7	北	
01:50	1009.4	1016.2	---	0.6	82	0.9	北東	1.9	北	
02:00	1009.4	1016.2	---	0.6	82	1.9	北北東	3.9	北北西	
02:10	1009.6	1016.4	---	0.6	82	2.7	北北東	4.3	北	
02:20	1009.6	1016.4	---	0.3	84	2.8	北	3.8	北北東	
02:30	1009.7	1016.5	---	0.4	84	2.2	北	3.3	北	
02:40	1009.6	1016.4	---	0.3	84	2.4	北	3.5	北北西	
02:50	1009.6	1016.4	---	0.2	84	2.2	北	3.8	北	
03:00	1009.7	1016.5	---	0.1	84	2.7	北北東	3.8	北北東	
03:10	1009.6	1016.4	---	0.1	85	2.9	北北東	4.8	北	
03:20	1009.6	1016.4	---	0.3	84	1.8	北東	2.7	北北東	
03:30	1009.7	1016.5	---	0.3	84	1.8	北	2.6	北	
03:40	1009.7	1016.5	---	0.5	84	1.3	北	1.9	北	
03:50	1009.6	1016.4	---	0.4	83	2.4	北北東	3.6	北北東	
04:00	1009.6	1016.4	---	0.5	83	2.1	北北東	2.9	北北東	
04:10	1009.6	1016.4	---	0.5	83	2.2	北	3.2	北北西	
04:20	1009.5	1016.3	0.0	0.5	83	3.3	北北東	4.3	北北東	
04:30	1009.6	1016.4	0.0	0.6	82	3.3	北北東	4.1	北北東	
04:40	1009.5	1016.3	---	0.6	83	2.0	北北東	4.2	北北西	
04:50	1009.4	1016.2	0.0	0.7	81	4.3	北	6.2	北	
05:00	1009.4	1016.2	0.0	0.6	82	4.0	北	5.0	北	
05:10	1009.5	1016.3	0.0	0.4	83	3.9	北	5.0	北	
05:20	1009.5	1016.3	---	0.4	85	3.2	北北東	4.6	北北東	
05:30	1009.6	1016.4	---	0.4	85	1.1	北東	3.3	北北東	
05:40	1009.4	1016.2	---	0.5	86	0.7	北	1.4	北	
05:50	1009.4	1016.2	---	0.5	86	2.1	北	3.2	北	

Figure 7. JMA data for January 2009 in 10 seconds time interval

In this figure, the data time starts from 00.10 until 24.00. There are 144 data and nine kinds of weather items data in a day. From this data, we could select the temperature, wind speed average, and the precipitation of rain. The data is combined with the PV system at Hiroshima University. Our detailed preprocessing data is described in the following two steps:

1. **Step 1**

In the first step, we use data that could be accessed easily from the JMA website. [33] the data is made available and accessible for the public. The website offers 3-hour weather data. The data used for this research is described as follows:

(1) Temperature, in this book symbolized as (T) in ^{o}C,

(2) Maximum wind speed (v) in m/s,

(3) Probability of the precipitation (p), (with the precipitation value of 1, if observed, and 0, if not observed).

(4) Weather class (sunny, cloudy, rainy, and snowy).

To maximize the data research, wind speed is divided into 4 levels of speed. First is wind speed of 0-2 m/s, and the second class of speed starts from 3 until 5 m/s, while the third class is for wind speed of 6 m/s until 9 m/s, and the last class is over than 10 m/s of wind speed.

2. **Step 2**

Weather condition plays the biggest influence in determining the amount of solar radiation. Based on the JMA website, there are no classifications for weather conditions. Therefore, in this research, we classify the historical weather data into three categories of weather condition. The first category is sunny, and the second category is cloudy while the last category is rainy. The weather classification is based on the radiation thresholds. Once the weather conditions have been clustered, then NNs are constructed for every weather class.

A thorough description of the proposed data classification is stated in the following two points:

1. The JMA data that could be accessed from the website, is combined with our local data which is obtained from the PV that is installed in the Hiroshima University rooftop. The PV capacities are 40 kW. Both data are a historical weather data and is used for the local prediction.
2. For the second point, data from the Ministry of Economy, Trade and Industry [31] is used for the global PV generation forecasting.

The following is an example of data usage. We consider the past, present and the following months as target data. Three months before, the present month and three months after the present month are used to model and forecast the amount of insolation. For example, if we are going to forecast a day in a month in 2012 such as August 2012, we shall use data from 2009 until 2011 as the training phase of neural network. As previously explained, we shall also use data from July, August, and September 2009 until 2011. For the timing base data, we shall also use data from 3 hours before the target data, during the target data and 3 hours after the target data. To calculate and verify the network, data in July 2012 is used as the testing data. We also have 100 different NNs with random value for the weight. We

construct these NNs for each weather classification. Back propagation (BP) is chosen to model the historical data. After we construct NNs, and train and test them, the mean absolute error (MAE) is calculated to be used as comparison to the prediction result. One important thing to do before using weather data is to convert all the input value into the same value. This process is described as the normalization process.

3.3 Construction of Neural Networks

In this section, the construction of NNs is described in detail. This section also includes the third step of day-ahead PV forecasting. As mentioned above, we use 3-hour basic data. We construct the NNs using the classification input data. The construction of NNs is equal to the training phase of NNs. For example, for cases of rainy condition, we shall use the rainy weather data. Figure 8 describes the NNs. The network consists of three layers, in which the output $\hat{y}_{t'}$ describes the amount of solar radiation at the specific time of *t'*.

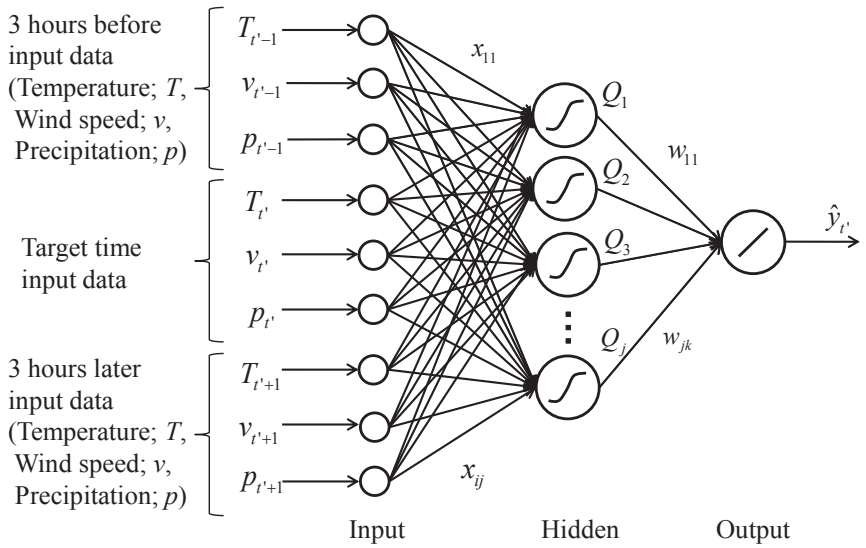

Figure 8. 3-layer neural network

The 3 layers of NN are constructed to model the weather data. The 3 layers of NN consist of input layer, hidden layer and output layer. For each layer, the neuron represents the calculation process inside. In this case, there are nine numbers of neuron in input layer, with *j* as number of neuron in the hidden layer and one neuron for the output layer. All neurons in the input layer represent the value of the

weather data. Input data is symbolized as (T, v, p). As mentioned before, the data used for 3 hours before the target time is represented as $t' - 1$, while for the target time the data is represented as t' and for 3 hours after the present data we describe it as $t' + 1$ in figure 8.

Between the input layer and the hidden layer, each neuron in these two layers are fully connected to each other. For every connection of neurons from input layer and hidden layer, x_{ij} represents the input weight value and w_{ij} represents the output weight. In this stage, the number of weight value is determined randomly. The neuron in the hidden layer serve as a multiplication calculation between the input value and weight input. The result of this multiplication is transformed by the activation function. In this research, "logsig" activation function is selected to calculate the multiplication result between the input value and input weight. Also, Q describes the output result for the calculation process in the hidden neurons. For the training phase, the result is determined by using the backpropagation (BP) training method.

In the NN construction, there are two main phases to construct NN. First is the training phase and the second is the testing phase. Training phase is an important key to obtain the best value of input and output weight. This phase should be constructed well, so that the error from the testing phase is small. Input data for training and testing phase are represented as follows:

(1) Weather classification data,
(2) Temperature represented as T,
(3) 4 classes of Wind speed which is represented as v,
(4) The amount of solar radiation described as Precipitation p,

In the training phase of the backpropagation method, all data input will be multiplied by the input weight one by one. Formula 1 shows the multiplication process between data input and input weight.

$$\widehat{y_t} = \sum_k^i w_{ik} Q_j (\sum_j^i x_{ij}\, input) \qquad (2)$$

After $\widehat{y_t}$ is obtained from the first forward phase, the difference in value between $\widehat{y_t}$ value and the target value will be evaluated. After the delta value is

obtained, the next step is the backward process. Backward process is necessary to update the output and input weight. Forward and backward process is known as the iteration process. This process will be iterated more than 100 times. In this research, we will use 20.000 times of iteration. The iteration will stop until the delta between the training output and the target output is small or the differences are adequate.

3.4 Performance Evaluation and CI Setting

The following is the fourth step in the day-ahead PV output forecasting. In the performance evaluation step, we use the test data to verify and evaluate the NNs. This will result in the value of the PV output and the calculation of the error value.

In this step, we also set the CI setting and value. CI value is analyzed by considering the prediction errors. CI setting divides the CI results into two range which are the permissibility of maximum and minimum limit of the PV output reliable case. The result is considered as a reliable data for the PV output prediction result. To obtain the prediction error, standard deviation (σ) is used as the testing result. The CI value is the range of $\pm\sigma$, $\pm 2\sigma$. Figures 9 describes the CI setting in detail. This CI value will be an effective feasible operation limit for PV output forecasting in power system grid. The CI setting is used for the operation planning and the real-time case as robust security for the power system grid.

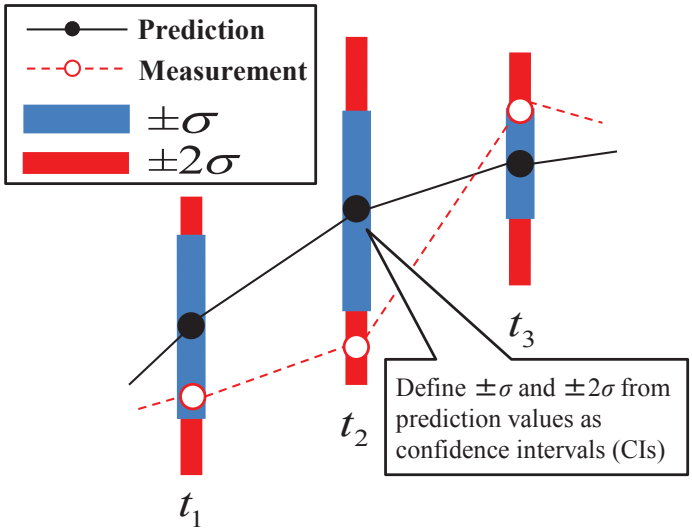

Figure 9. Setting method of CIs

Figure 9 shows that the blue area is the first standard deviation area of day-ahead PV output. The blue area represents the first range of CI or $\pm\sigma$ while the red area describes the second range of CI setting or $\pm 2\sigma$.

After the CIs range is obtained, the result of CIs for each month in a year is provided in figure 10. The CI calculation for each month have been completed and reported. Weather classification and non-classification are provided as a comparison result.

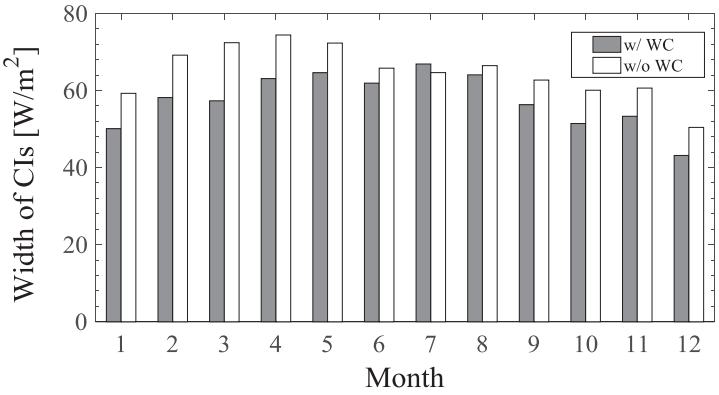

Figure 10. CIs in 2012

From figure 10, the result shows that weather with classification has a small interval variance in a year. The CIs value also changes between each month. This is due to the weather season and weather condition. Compared to others, the CIs result between April until September is higher due to the sunny season or summer season. Figure 10 also shows that December 2012 has the lowest width of CIs. This value appears in the result because Japan is in snowy or winter season. We also noted a difference between results with cluster and without cluster. CIs result of data without cluster is higher than CI result with cluster data. Based on the probability calculation, the result shows that the difference value between recorded data and the prediction result could still be more than 80% of the probability. Also, for the two types of classification result, it could be confirmed that the result with weather classification is better than non-weather classification.

In the two graphs below, Figure 11 and 12 confirm that the result of two CIs, namely $\pm\sigma$ or $\pm 2\sigma$ become better by the weather classification. Based on Figure 11

and 12, it is also proven that the CI reliability is increased and improved because of the weather classification.

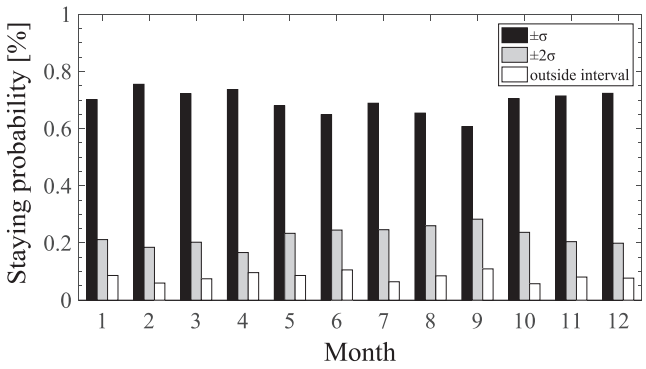

Figure 11. Staying probabilities with weather clustering

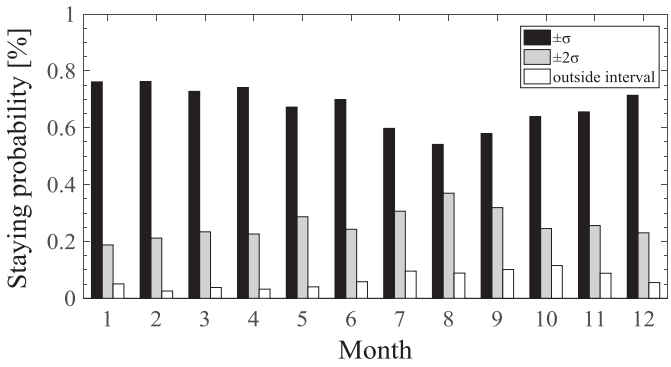

Figure 12. Staying probabilities without weather clustering

Based on figure 11 and figure 12, the staying probability of CIs in figure 13 is smaller than in figure 12. The black bar in figure 12 is smaller than the black bar in figure 13, meaning the CIs width using the first range reliable shall be applied on the EMS controller. In figure 13, the 2nd until 6th months of year 2012, the outside interval probability is higher than figure 12, but the second interval or the gray bar of CIs is higher than the first interval. This result confirms that weather classification as our proposed method is a good way to improve the PV output forecast.

3.5 Estimation of PV Outputs

The PV output forecast result is achieved by applying the measurement data and the JMA data from the website. As previously mentioned, the 30-minute interval according to the UC planning shall use the linear interpolation process.

$\hat{y}_{t'}$ is the output of NNs or amount of solar radiation forecasting. This value should be converted to the PV output generation or $\hat{P}_{t'}$. [76] is the reference formula for converting the solar radiation forecasting result to the PV output generation. The following is the formula,

$$\hat{P}_{t'} = \left(K / G_S\right) \cdot P_{AS} \cdot \hat{y}_{t'} \tag{3}$$

K is the constant value that represents the monthly comprehensive design factor, while G_s, represents the amount of solar radiation intensity in the standard test condition with the units in kW/m^2, and the last one is the standard solar cell array output or P_{AS}.

To obtain the value of K, in this research we use formula (4). The following is the monthly comprehensive design factor formula,

$$K = K_{HD} \cdot K_{PD} \cdot K_{PA} \cdot K_{PM} \cdot \eta_{IND} \cdot K_{PT} \tag{4}$$

The solar radiation yearly variation of correction coefficient is represented as K_{HD}, while the aging correction coefficient is represented as K_{PD}. The value of array circuit correction coefficient is represented as K_{PA}. We also use K_{PM} for the array load matching correction coefficient. η_{IND} represents the power conditioner effective efficiency, and the last coefficient for temperature correction factor is symbolized as K_{PT}. To convert the solar radiation value to the PV output, all these coefficients should be used and prepared in the calculation formula. Also, all of these coefficients will be determined based on the PV system condition in which we use the PV system in the Hiroshima University rooftop.

3.6 Case Studies

In this part, the case studies of day-ahead PV output forecasting are described. From the beginning, we pre-process the input data for day-ahead PV forecast as mention in Figure 2 as the first step. In this section, if some data are missing, we calculate the missing data using the interpolation linear. However, the missing data should be in the acceptable range. Otherwise, the data in that day will not be used. In another case, if the data in that day is not available in the JMA

website, we consider using the same condition as three hours before. We also assume that the next three hours have the same value or condition. For example, if the JMA website mentions that at 12:00 o'clock it is a sunny day, we assume the data from 10:31 until 13:30 is sunny as well. This case applies on the entire simulation data.

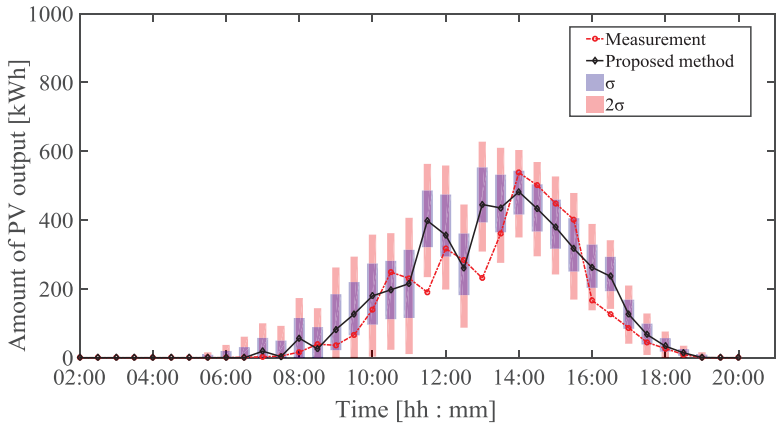

Figure 13. PV forecasting with weather clustering

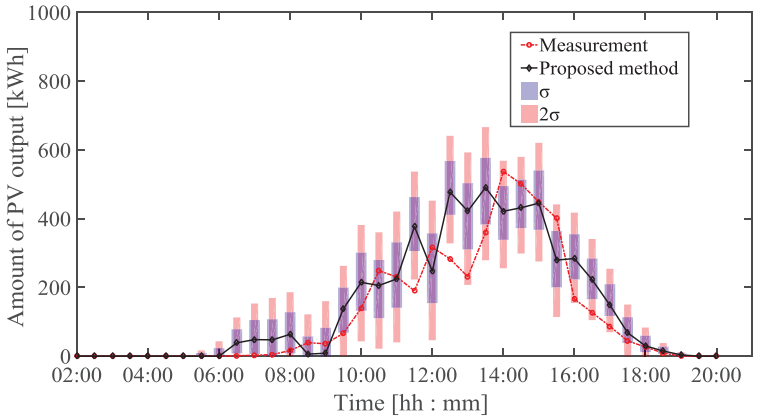

Figure 14. PV forecasting without weather clustering.

Figures 13 and 14 show the amount of PV output forecast result. As shown in the figures, the amount of PV output fluctuates by the time. As we mentioned before, we use 30-minute time interval and apply it in the vertical axis, starting from 02:00 until 20:00. We establish the figure every two hours because of the figure space. The purple area that extends vertically in the black line is the first value of ±σ, meaning that this color is the first CI range. Then, the red area is the value of ± 2σ which is the second CI range. For the weather marks, which are shown in the bottom of the figure, it represents the time weather, starting from 2, 3, 6, 8, 10, 14,

16, and 20. If the weather is changing slowly, we have also prepared for this condition. The result also shows that our method can predict accurately. For the CI setting, we set the CI value the same as the generation output forecast. For example, there is a case in which the PV could produce power in small number. This situation generally happens in the early morning or late evening. Because of that, the CI variance is also small and applies in both range. Also, for the sunny day or non-cloudy or rainy day, the amount of PV output is big, so that the CI setting also has a big range.

As shown in figure 13 and 14, we could find a big CI range at 14:00. This area is bigger than early morning time or late evening because the PV power output is also big. In this condition, we can set the maximum of the CI range same as the PV output forecast result. If we compare the weather with classification and without classification, it can be concluded that the CI variance is smaller in the weather classification method.

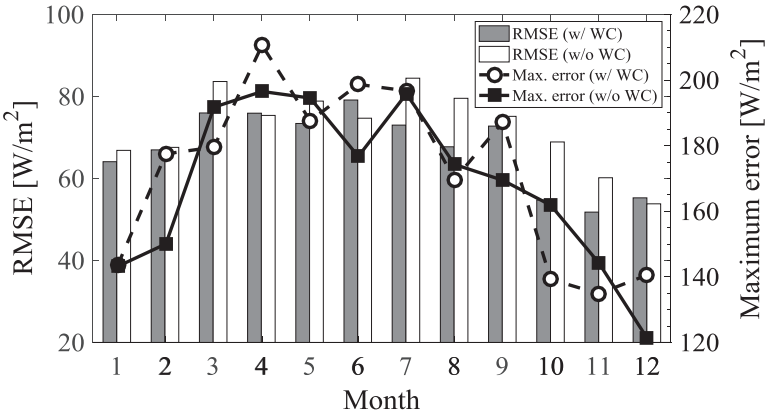

Figure 15. RMSE and maximum errors in 2012

Figure 15 shows the monthly result in a year. The root mean square error (RMSE) is used to obtain the error prediction. Equation (5) is the RMSE formula. N represents the data number, while $\hat{P}_s$ (t) represents the PV power generation predicted value in *t* certain time. P_s (t) is the measurement value in certain *t* time, with units in [W/m^2].

We also provide the average prediction error and the maximum prediction error monthly in a year. In this case, we chose the year 2012 as an example.

$$RMSE = \sqrt{\frac{1}{N}\sum_{t=1}^{N}\left(P_s(t) - \hat{P}_s(t)\right)^2} \tag{5}$$

When we use the weather classification for the PV forecast, we realize that the average errors are smaller than those in the data without weather classification. The maximum errors in several specific months in a year also increased. However, our classification weather has a weakness as well. The weakness is the data weather assumption will be considered the same as the previous or the following three hours. The method also could not keep up with the weather changes during 3 hours.

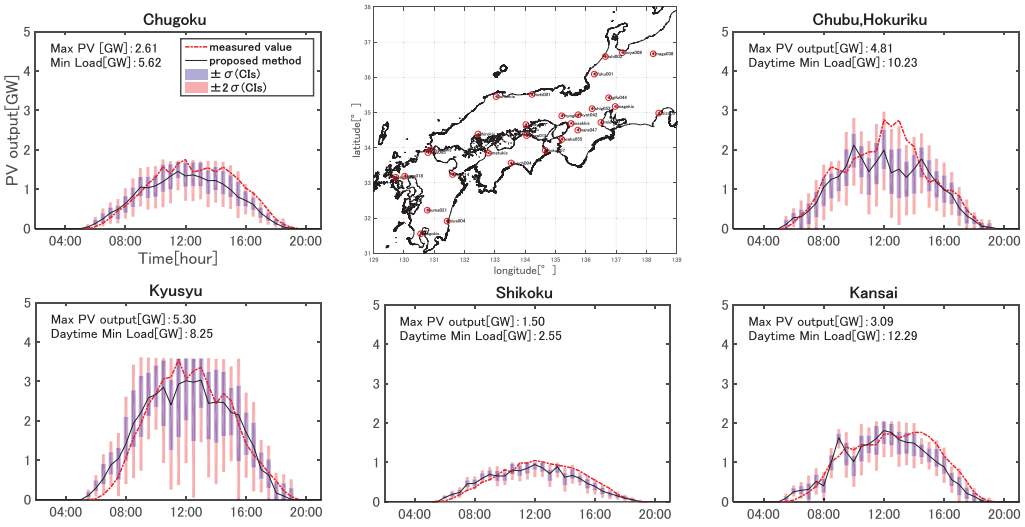

Figure 16. Day-ahead PV forecast on August 3, 2012

3.7 Summary

This chapter can be summarized as follows:

1. This chapter focuses on the explanation of day-ahead 24-hours PV output forecasting. The researchers face several complex circumstances about the data input.
2. We proposed a simple data that can be easily obtained from the website. In our research we use the JMA website.
3. There are six steps to use our simple data in obtaining the PV output forecast. The first step of the PV output forecast involves a thorough analysis on previous weather data in each time duration. Once the past data have been analyzed, the data are put into clusters according to the weather clustering (WC). There are

three types of weather clusters; sunny, cloudy, and rainy condition. Upon completion of weather clustering, the forecasting process shall proceed with the third step of the PV output forecasting which involves the construction of Neural Network (NN) for each of the weather cluster. After the Neural Network has been set for every weather condition cluster, an evaluation on its performance can be conducted using testing data. Then, the next step is CI setting. The standard deviation that was previously calculated, will help to set the appropriate confidence intervals (CI) based on historical data analysis.

4. After obtaining the CI setting, the result is applied to the EMS controller.

Chapter 4

Real-time 5-minutes Power Forecasting

4.1. Introduction

In this section, the authors focus on real-time forecasting of PV. The real-time PV forecasting provides a PV output forecast at less than 10 minutes intervals using ELM and SRCA. In general, real-time PV output forecast requires high accuracy and high-speed forecasting process to operate a target system.

We also develop the SRCA method to obtain the real-time PV output. The time interval of real-time demand and real-time PV output forecast is up to 1 hour and 5-minute intervals in advanced. This time interval is used in the forecasting target day. However, the process runs in 5-minutes interval and will be used as UC simulation in the same day. We also provide the DELD of the generators and batteries as calculation parameters. In order to deal with the weather changes and unpredictable PV output, we prepare a stand-by operating reserve and a spinning reserve at the same time as the real-time PV output simulation. The following is the real-time forecast procedure.

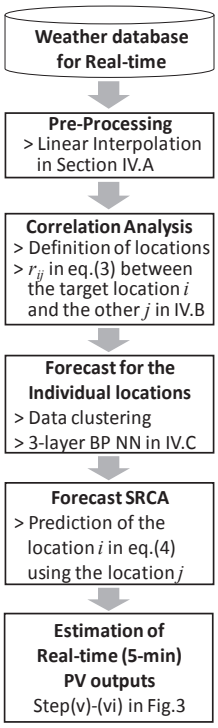

Figure 17. Real-time PV forecast

Figure 17 shows the real-time PV output forecast process. Weather database analysis is the starting point in obtaining the real-time PV output forecast. The same data is used for the day-ahead forecast, and it is also used as real-time PV forecast database. The following is the data type repetition. We use 3-hour weather data, T, v, p. In real-time case, we use weather cluster as well, so in the preprocessing data, we pre-process the data that is going to be used in our research. We cluster it into three categories (sunny, cloudy, rainy, and snowy).

The same method for constructing NNs is used as described in Section III for the day-ahead PV forecasts. This method is also applied into real-time PV forecast for individual areas. The difference is only in the time interval data that is used for the real-time case. All the data that is provided for every 3 hours by JMA is transformed into 5-minute basis data in the pre-processing section of figure 17 by using the interpolation scheme in the pre-processing part. The data for individual locations are used to construct the NNs, which are then used for real-time predictions of the target areas and other locations. The same procedures as given in steps (ii) to (vi) of figure 17 are performed using 5-minute basis data. Consequently, the estimation of real-time PV outputs is obtained.

4.2. Correlation Analysis between the Target and the Other Areas

In this section, we shall explain in detail about the SRCA method. We use the SRCA method as real-time forecast in 5 minutes interval. Fundamentally, SRCA is considered the gap correlation between several areas. The amount of insolation is calculated between two or more neighboring areas.

Furthermore, due to the delay of fluctuation of solar radiation actual value characteristics, we may obtain stable prediction accuracy of all times. However, if the solar radiation suddenly changes, it is possible to obtain high prediction error at some extent. To solve these problems, we applied the real-time PV output prediction method according to the SRCA model that has considered the amount of solar radiation in other region.

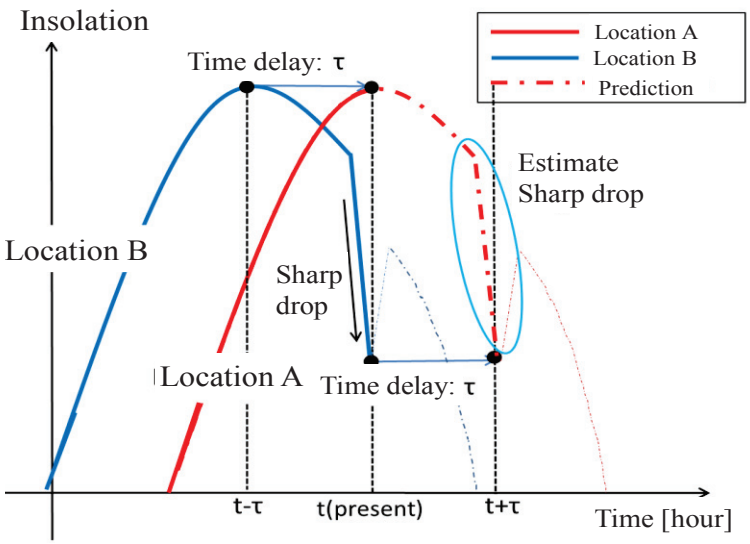

Figure 18. Proposed SRCA method

SRCA stands for Solar Radiation Correlation Analysis, which is a method that is expected to be applied in remote islands. As figure 18 shows, there are more than one area for the SRCA method. These areas are going to evaluate the correlation between the target location and the other location. This method analyzes the distance between two or more areas. In figure 8, there are two different areas that are separated by t- τ . In figure 18, the blue line represents location B while the red line represents location A. The concept of this research is based on the idea of the cloud movement which will also be used for the solar radiation pattern. In this concept, we split the areas into upstream and downstream areas or points. Our prediction object and target compile the real-time forecast. Based on the upstream and downstream areas, the gap time is obtained. The solar radiation data which has similar value will then be used for real-time forecasting. It is calculated using the SRCA method, and the location is chosen based on the result.

4.3. Forecasting for the Individual Areas

Based on the description of figure 18, an individual area is initially forecasted before forecasting other points or areas. In this section, the individual area is forecasted using NN and ELM. This part is necessary to obtain the PV output forecast for individual areas. The results and timing process are then compared between the NN and ELM method.

4.3.1. Neural Network Models using Data Clustering

Same as the day-ahead PV output forecast, we construct NN for each season to obtain the real-time PV output forecast. The data clustering used to model and forecast the data is the same one used for day-ahead PV output forecast. There are three classes of weather clusters; sunny, cloudy, and rainy condition. The same data is also used for input data. The NN architecture is also the same as figure 8.

Its performance and effectiveness are also calculated in the process. A conventional method namely the auto regressive (AR) method is chosen as a comparison method. The error results are then compared based on the average and maximum error.

4.3.2. Extreme Learning Machine Model

In this research, apart from NN, the ELM method is also used to model and forecast the individual areas. The ELM method is used since its algorithm could perform the training phase time faster than NN. The training phase time is necessary to construct a robust network. Therefore, the results of real-time PV output forecast could be informed to the power system operator immediately. Additionally, ELM also does not require an iterative process.

Empirical calculation proves that ELM can process generalization better and faster than neural network [73]. The basic idea of ELM lies in the single hidden layer feed forward network. The architecture of ELM is shown in figure19.

The mode and forecasting process is conducted through 7 steps as shown in figure

1. Set the input and output data, labeled as $\boldsymbol{X}$, $\boldsymbol{Y}$, respectively.
2. Set the number of nodes in the hidden layer. This step is symbolized as $\boldsymbol{L}$.
3. Set the activation function for the nodes in the hidden layer. Generally, the "logsig" activation function is used for the training phase. Formula 6 shows this calculation.
4. Set the weight input and bias input randomly. The input weight can be mentioned as $\boldsymbol{W}$ and the bias input as $\boldsymbol{b}$.
5. Calculate the hidden layer and maintain it as one matrix. This step is similar to the part Q in chapter 3, while in figure 18, it is labeled as $\boldsymbol{M}$. Through this step,

not only do we obtain the multiplication result but also the results of the activation function calculation.

$$\boldsymbol{M} = logsig\ (\sum_j^i x_{ij}\ input) \quad (6)$$

6. Calculate and analyze the output weight of single layer neural network. This step is labeled as β.

$$g(\boldsymbol{M}) \cdot \beta = \boldsymbol{Y} \quad (7)$$

$$\beta = \boldsymbol{H}^{+} \cdot \boldsymbol{Y} \quad (8)$$

In step 6, β is directly connected with $\boldsymbol{Y}$, which is the output of ELM. To obtain the value of β, ELM uses the method of Moore-Penrose generalized inverse. In this case, β is the calculation result of $g(\boldsymbol{M})$.

$\boldsymbol{H}^{+}$ is the Moore-Penrose generalized inverse of $\boldsymbol{H}$ [72]. The calculation of $\boldsymbol{H}^{+}$ is mentioned in (4).

$$\boldsymbol{H}^{+} = (\boldsymbol{H}^{T}\boldsymbol{H})^{-1}\boldsymbol{H}^{T} \quad (9)$$

In this part, the β value must be calculated correctly to obtain a small error between the forecast result and the data output.

7. Calculate the error between the forecast result and the data output. $\hat{\boldsymbol{Y}}$ represents the output result. To calculate the error, the RMSE formulation is used.

Ultimately, ELM provides a faster learning speed than general neural network algorithm. For the implementation of ELM, it provides a simpler process based on the matrix Moore-Penrose generalized inverse.

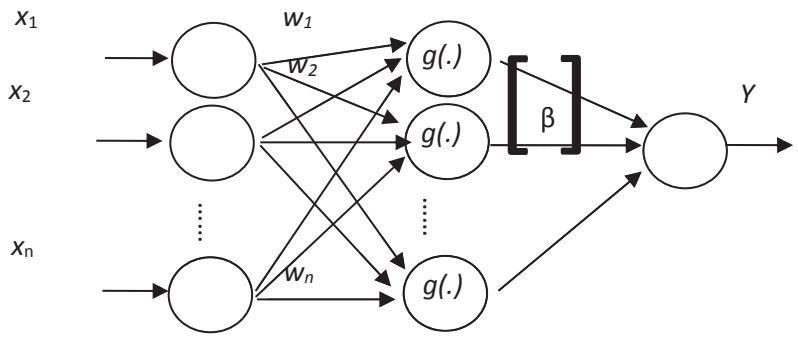

Figure 19. ELM Architecture.

x_i: input data, i=1…n, w_i: weight between input and middle layer, i=1…n.

4.4. Forecasting the Target Area using Correlation Factors

In this section, the correlation factor is used to determine the PV output of the neighborhood area. We derive solar radiation correlation coefficient or represented as (*rij*) of the prediction target point (*i)* and other points (*j)* for every 5 mins. Then, we extract the solar radiation amount through the past data in a certain period of point (*i)*. After that, the solar radiation amount is extracted through the past data in the same time window period of point *j*, and τ minutes before point *i* period as stated in the following:

$$r_{ij}(\tau) = \frac{\sum_t \left(x_i(t) - \bar{x}_i\right)\left(x_j(t-\tau) - \bar{x}_j\right)}{\sqrt{\sum_t \left(x_i(t) - \bar{x}_i\right)^2}\sqrt{\sum_t \left(x_j(t-\tau) - \bar{x}_j\right)^2}} \tag{10}$$

t : time (min), τ : time interval (min), x_j : other point solar radiation amount (kW/m^2), x_i : predicted point solar radiation amount (kW/m^2), $\bar{x}$: x period average (kW/m^2).

In the next step, the gap time τ is changed by 5 minutes, and the correlation coefficient is calculated. This is performed by selecting the gap time τ_{max} with the highest correlation and using the τ_{max} before solar radiation amount of point *j* to point *i* solar radiation prediction.

To obtain prediction with high accuracy, we performed real-time correlation analysis with multiple spots. Areas with high correlation are selected, and each correlation coefficient are set as main object. The prediction results of each spot are then integrated. As a specific method, correlation analysis is performed towards multiple spots. The correlation coefficient of every area r*ij* is emphasized, and then calculated for its weighted average value of the solar radiation prediction as shown in the following formula (11).

$$\hat{Y}_i(t) = \frac{\sum_\tau \sum_j \left(r_{ij}(\tau) \cdot \hat{y}_{ij}(t-\tau)\right)}{\sum_\tau \sum_j r_{ij}(\tau)} \tag{11}$$

$\hat{y}_{ij}(t)$ denotes the predicted solar radiation value at location *i* by using location *j* at time *t* [kW/m^2], and $\hat{Y}_i(t)$ denotes the predicted solar radiation value at

location i by all screened locations at time t [kW/m^2].

Figure 17 shows the prediction concept in real-time. Conventional authors have considered the prediction method [19,74,75]. As a simple real-time prediction method, we propose AR (autoregressive) model according to the least squares method of the predicted area's past data. This is a useful technique to avoid excessive error and can ensure accuracy to certain level. Although it enables high accuracy prediction for the latest time, error tends to increase as the predicted time elapses.

4.5. Estimation of PV Outputs

This section shall provide the estimation of PV output. Similar to chapter 3, an individual area is modeled and forecasted which is proceeded with the forecasting of PV output using the SRCA calculation. A more detailed explanation on the process shall be provided in the following chapter.

4.6. Case Studies

This section of chapter 4 shall provide case studies of real-time PV output forecast. As previously mentioned, multiple areas are calculated in obtaining the real-time PV output forecasting and also the analysis for each PV output forecast area. For the individual area forecasting, the NN and ELM methods are used as forecasting method.

ELM is applied as a regression analysis which can obtain the PV output forecast. Real-time PV forecast with 10-second intervals is presented in this section. Table 1 shows that the increasing number of hidden nodes can affect the CPU time.

No. of Hidden Nodes	Forecast Error (ELM)	Forecast Error (NN)	CPU Time [s] (ELM)	CPU Time [s] (NN)
50	2.00	12.4	0.16	4.17
100	1.50	10.7	0.26	4.23
150	3.76	10.9	0.43	4.31
200	1.79	14.0	0.63	5.18

Table 1. Comparison of Forecast Error and CPU Time between ELM and NN

Table 1 indicates that the forecast accuracy is strongly influenced by the meteorological data. It is proof that the type of meteorological data has a strong correlation with the amount of insolation. Several number of hidden nodes are selected. This treatment is necessary to compare the error and CPU time between the NN and ELM methods. Based on table 1, the error value has a declining tendency after the number of hidden nodes is changed from 50 to 100 number of nodes. On the other hand, the error has an increasing trend when 150 number of nodes is used. This situation occurs due to the different variable setting of ELM and NN. After that, 200 number of hidden nodes is used to model the data input using the ELM and NN method. After the PV output in the individual areas are forecasted, the SRCA method is used to calculate the real-time PV output forecast.

The following is an explanation on the error calculation for real-time PV forecast. The prediction error rate (ε) and maximum prediction error rate (η) are used to obtain the error value. The formula is as stated in the equations (12) and (13) below. These two methods can be used as a comparison for the prediction accuracy. Many researchers use this formula to obtain the prediction accuracy. While in this research, this method is used because the value of solar radiation is a value that shows the maximum number of solar radiation in a day.

$$\varepsilon = \frac{100 \times \sqrt{\frac{1}{m}\sum_{l=1}^{m}\left(\hat{X}_l - X_l\right)^2}}{\frac{1}{m}\sum_{l=1}^{m} Q} [\%] \qquad (12)$$

$$\eta = 100 \times \left| X_{\max} - \hat{X}_{\max} \right| / Q_{\max} \quad [\%] \tag{13}$$

The predicted solar radiation value is symbolized as $\hat{X}$, while $\hat{X}_{\max}$ is the value of the predicted solar radiation that causes the maximum prediction error, and the actual value of solar radiation is symbolized as X. The amount of the actual value solar radiation used to calculate the maximum prediction error is represented as X_{max}, while the extraterrestrial solar radiation is described as Q, and the last Q_{max} represents the maximum value of the extraterrestrial solar radiation.

Table 2 provides the accuracy result of this method. The table shows the real-time PV output forecast in June 2012. Real-time PV forecast for 60-minutes and 10-minutes ahead are also provided in figure 20 and 21. The results of the AR model are also provided and compared in the graphs. Based on figure 20, the η value which uses the AR model increases from 5 minutes to 10 minutes. This shows that the SRCA method has similar results with the AR model.

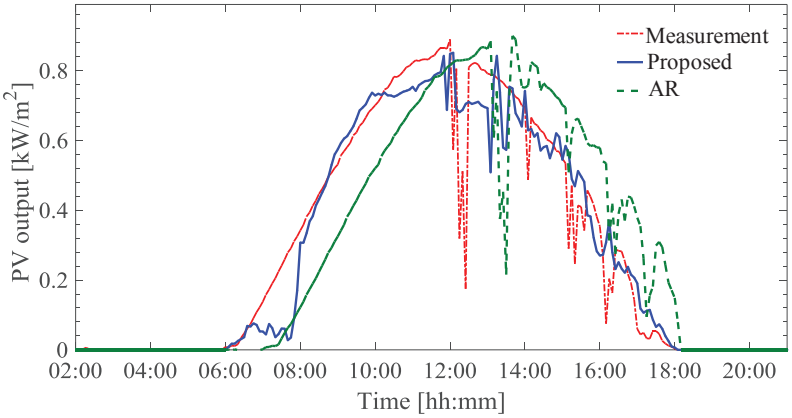

Figure 20. 60-min ahead predictions

Figure 20 shows that the proposed method could follow the measurement data pattern. At 06.00 until 08.00, the blue line does not match with the measurement and AR result. The same pattern also appears for the SRCA result from 08.00 until 10.00 where the blue line does not match with the measurement line. The same situation is also proven through table 2. In the 60-minute ahead forecast result, the value of average and maximum error is the biggest among others. After 08.00, the forecast result is in the same flow as the measurement and AR method.

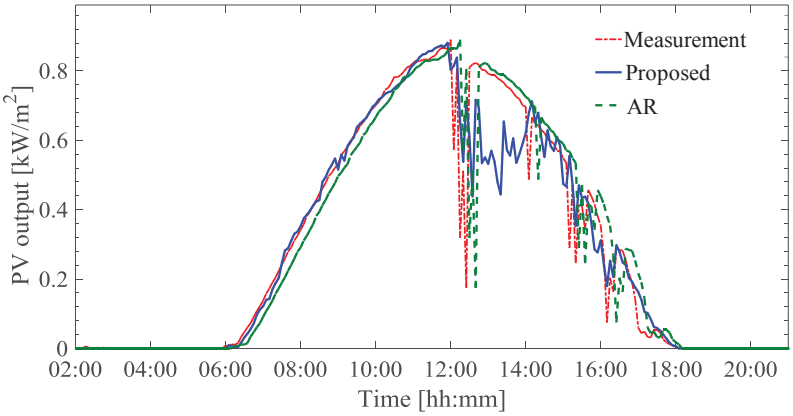

Figure 21. 10-min ahead predictions

Figure 21 shows that the 10-minute ahead forecast is better than the 60-minute ahead forecast. In this case, 10-minute ahead forecast line flow is closer to the measurement and AR result. The biggest error occurs in 12.00 until 14.00. This error can be seen through the blue line which, representing the SRCA method, has a different pattern with the measurement data.

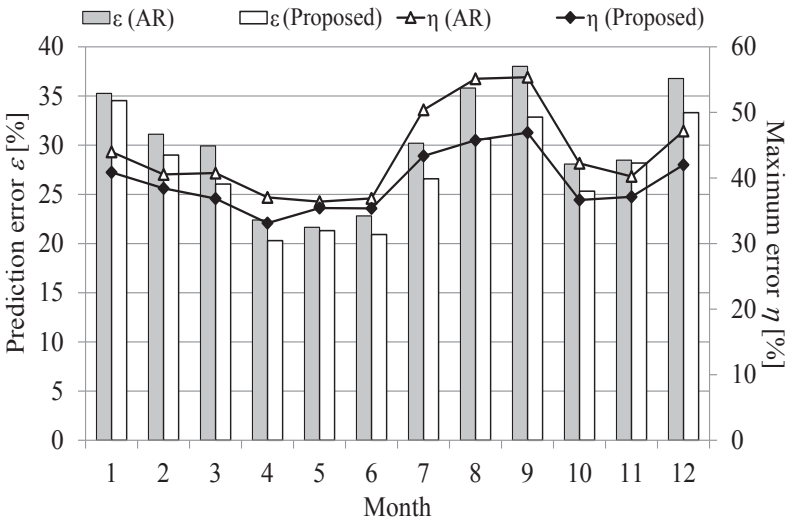

Figure 22. Prediction errors

Figure 22 shows the monthly forecast error rate of the 30-minute ahead forecast. This figure describes the proposed error which increases during the 7th until 9th month. The lowest error value occurs in the 4th until 5th month. We also compared the result of the proposed method with the AR method to compare our result with the conventional method. The result shows that the proposed method has the same pattern in increasing or decreasing trend in a year.

Table 2. Prediction errors in June 2012

		5min ahead	10min ahead	20min ahead	40min ahead	60min ahead
SRCA	Av. Error ε [%]	16.09	19.00	20.75	23.76	25.07
	Max Error η [%]	16.50	18.47	19.84	21.20	22.26
AR	Av. Error ε [%]	32.87	36.74	36.56	39.10	40.65
	Max Error η [%]	31.43	32.48	33.91	34.89	35.12

The following is the forecasting results for all seasons in different weather and season conditions. The data used is from October until December 2011, also January until September 2012. The available data is preprocessed using the proposed preprocessing method. By using this method, writers of this research are interested in forecast using an advanced calculation such as lamp fluctuation. Based on the result, the proposed method has similar results with the conventional method. This is proven by the average error result and maximum error result. Additionally, this research also provides the MAE result for each season and the comparison with the AR method as well. In conclusion, non-sophisticated data could obtain a reliable result for PV power system simulator. The proposed method also shows that it is applicable and useful enough to be used in real cases. The forecast accuracy also shows that public data could be useful.

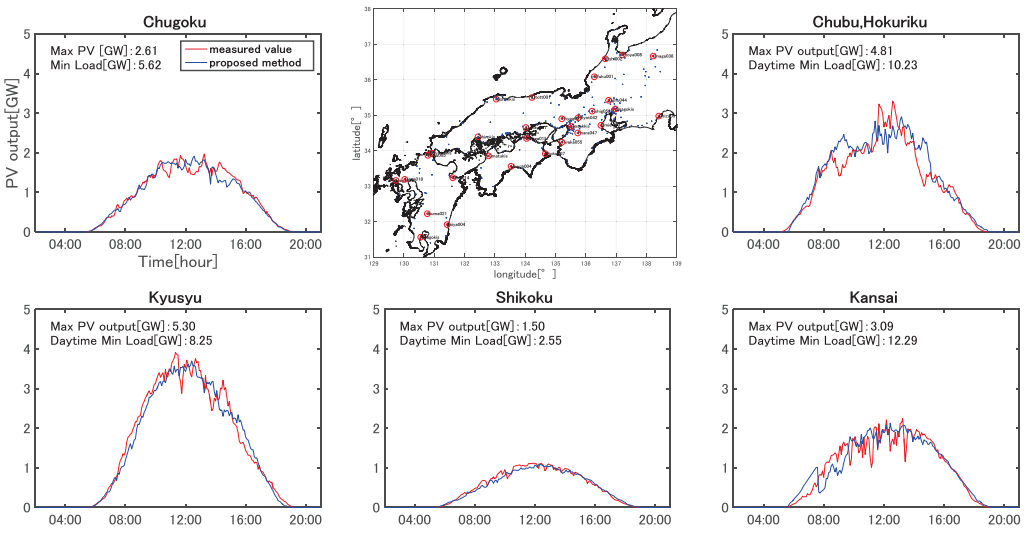

Figure 23. Real-time PV forecast on 3rd Aug. 2012

4.7. Summary

This chapter could be summarized as follows:

1. This chapter discusses in detail about the real-time PV output forecast.
2. The data used in this section is the same as day-ahead PV output forecast. The difference with day-ahead PV output forecast is the interval data time in which a 5-minute interval time is used in this section.
3. We could perform an individual area forecast before using the SRCA method.
4. For the individual area forecast, the NN and ELM method are used as the forecasting method. These two methods are compared to obtain a faster CPU time and a better error calculation.
5. The prediction error rate ε and the maximum prediction error rate η, are used as indices for comparing the prediction accuracy.
6. Results of the proposed method are compared with the results from the AR method to see how it compares with the conventional method.

Chapter 5

Application to the Energy Management System (EMS)

5.1. Introduction

This chapter focuses on the application of the PV output forecast. As mentioned in the previous chapter, the EMS controller is provided to represent a small-scale power system grid. The EMS controller architecture is shown in figure 24. This controller is an attempt in facing the uncertainties of renewable energy resources. This chapter establishes a novel methodology for stochastic dynamic economic load dispatch (SDED). This methodology becomes necessary to guarantee secure operation in real-time scenarios [41]. This concern is common to various widely adopted power systems, where smart gird projects make use of all available controls including demand response [42]. In order to fully utilize controllable generators, the development of a stable and reliable load dispatching method is extremely important in dealing with uncertainties [43] [3].

Various approaches have been proposed concerning SDED problem, which are classified into two approaches. The first approach continuously performs static economic load dispatch (ELD) at each interval by considering the ramp rate constraints [44], [45]. The second approach establishes the generation schedule (GS) by solving a single optimization problem. The approach includes various analytical technique in programming [49], improved simulated annealing [46], [47], hybrid approach of Hopfield neural network and quadratic programming (QP) [48], variable scaling hybrid differential algorithm [50], re-dispatch algorithms by using QP, linear programming (LP) and the Danzig Wolfe's decomposition technique [51], a multi-stage algorithm [52], and the interior point method [53] However, these conventional approaches cannot fully handle the large amount of uncertainties which arise from the power system operations. Hafiz et al. [5] and Yorino et al. [6] have proposed time-sequence dynamic feasible region (TDF) approach to fully utilize ramp rate capabilities of controllable generators against uncertainties. The concept of Robust Power System Security [54] has been proposed by Okumoto et al. where safe-side treatment of uncertainty is suggested for important constraints related to system collapse.

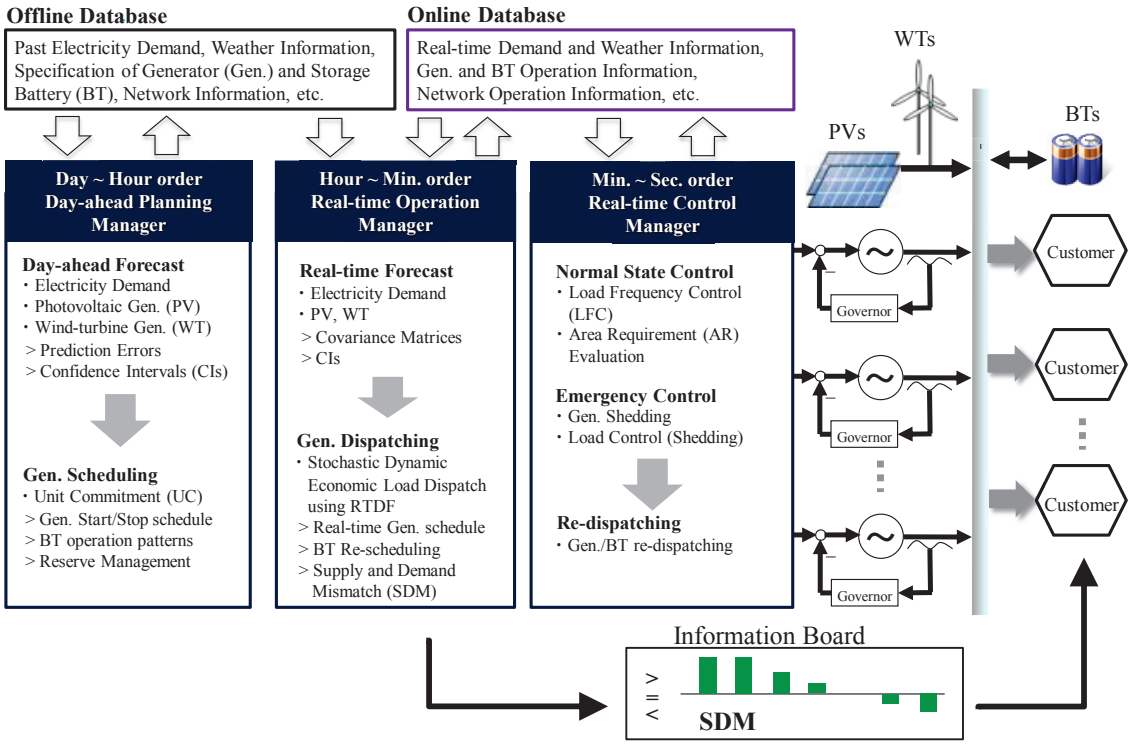

Figure 24. The proposed micro-EMS controller

A detailed explanation about the EMS controller will be described in the following section.

5.2. Outline of the proposed EMS Controller

The research target is to develop a robust micro-EMS controller against uncertainties [55]. Figure 1 shows the configuration of the proposed management system: there are mainly three functions responsible for day-ahead operation planning, minute-order real-time operation, and second-order real-time control. Based on the prediction of RES outputs, the system manages the existing generators, storage battery (BT) and controllable demands in optimal manner.

This section shall provide a more detailed view about new energy management method based on the Robust Power System Security. The proposed method is applied to micro energy management system (micro-EMS) controller (Fig. 1), where load and RES predictions are available online. Confidence intervals (CIs) of the RES prediction errors are based on the required reliability of system operation against system collapse. This outline consists of four parts of EMS

controller which will be described in the following, starting from the beginning until the end.

The first step is day-ahead and real-time forecasting parts which describes on how to obtain the forecast result. The forecast result has been described in detail in the preceding chapter. Then, the next step is UC calculation with battery. In this section, UC calculation and formulation are described in detail. The third component is dynamic economic load dispatch (DELD) part and the last is frequency control part. We first carry out PV output forecast and its error analysis. A weather clustering method has been proposed for this purpose in [55]. A covariance matrix of PV output errors is calculated, while CIs of the PV forecast errors are based on the required reliability against system collapse. The covariance matrices will be used in real-time GS in (44) for line flow control, while CIs are used in day-ahead unit commitment (UC) in (28) and real-time RTDF computation in (31) which is further used in real-time SDED in (45) to guarantee the supply and demand balance and reserve management.

In general, the proposed EMS controller consists of three parts; the first part is the planning manager, the second part is the operation manager, and the last part is optimization. As mentioned in figure 24, operation manager includes the description on day-hour order PV output forecast. The day-hour PV output forecast is the first step in the day-ahead planning. In this research, the day-hour PV output forecast is included in the section of day-ahead and real-time forecasting. Day-hour PV output planning is involved on the day-ahead planning manager calculation with a more detailed explanation below. The second part of EMS controller is hour-minutes PV output order. This part is necessary in obtaining the real-time operation manager. It requires a historical database to obtain the real-time PV output forecast. The last part is minute-second order for real-time control manager.

5.2.1. Day-ahead and Real-time Forecasting Parts

Figure 24 shows the day-ahead and real-time forecasting parts. The forecasting section is part of planning manager and operation manager. Day-ahead forecasting consist of day-hour PV output order. In day-hour PV output order, offline and online database is necessary for the forecasting process. Weather

information or weather database is necessary for the forecasting part. In this research, wind speed, temperature, and probability of the precipitation data are necessary as weather offline database. After the day-ahead PV output forecast is obtained, the next step is the calculation of a simulated day-ahead planning manager. For day-ahead planning manager calculation, past electricity demand, specification of existing generator, storage battery capacity and grid information are all necessary. If the wind-turbine data is possible to have, this data also can be included for the day-ahead planning manager. The EMS controller is prepared to calculate the day-ahead planning manager.

These data are required for day-ahead planning manager. This calculation generates a generator scheduling for day-ahead planning manager. The generator scheduling will be re arranged if the calculation result obtain a better combination than before. In GS, the renewable resources begin to be considered if these resources plan are to be merged in the existing power system grid. Then, the next step is UC part with storage battery.

5.2.2. Unit Commitment (UC) Part with Storage Battery

UC part with storage battery is involved in the planning manager section. This manager provides an updated schedule of the output pattern for the limited resources. The output is represented as a 24-hour GS which also comprises the BT operation schedule, where the unit time is 30 minutes. Existing techniques for the UC can be fully utilized in the optimization process. The optimization process is described in detail below. Uncertainties related to the prediction and fluctuation of PV are handled particularly [55]. The storage battery data is included in UC calculation.

5.2.3. Dynamic Economic Load Dispatch (DELD) Part

In power system, there are a lot of number of unit commitment problems. This research proposes a new algorithm for UC and stochastic dynamic economic load dispatch. This method should be efficient for the real-time and the day-ahead generator scheduling (GS). Not only efficient, the proposed method also offers a simple weather data usage that could be accessed easily. Then, this simple weather

data could obtain a reliable PV output forecast that can be applied for GS. Besides that, the method also offers a security treatment for power system. This treatment could guarantee that the PV resources will not interrupt the existing power system. The proposed method can effectively treat the PV forecasting error by setting the CI range.

In this research, we propose a new energy management method based on robust power system security. The proposed method updates the day-ahead GS a few times a day and provides 1-hour GS every 5 minutes in real-time operation. There are two treatments for this main research:

1. CIs and covariance matrix of prediction errors are used respectively in deterministic feasibility detection and probabilistic line flow management. The former realizes effective safe-side reserve management, while the latter handles soft constraints of line overloading. The approach is considered a new approach in handling uncertainties.
2. This research also proposes a new algorithm to realize the proposed uncertainty treatment, which include (1) an improved TDF, Robust TDF (RTDF) that effectively treats CIs, (2) an improved SDED method which combines RTDF, QP and liner stochastic load flow (SLF), and (3) an improved UC algorithm for day ahead 24-hour GS.

The advantages of this proposed method are that the supply and demand balance is kept to the maximum (high feasibility of dispatch) under uncertainties in real-time power system operations. In case of a critical situation when the forecasted load cannot match with the existing generator's capability, the method will detect the minimum amount of supply and demand mismatch in advance (1-hour before) and handle it reliably for the considered time horizon.

5.2.4. Frequency Control Part

This section of the chapter shall discuss in detail regarding the frequency control. In our EMS controller, the frequency control is also maintained in the permitted ranges of frequency. Therefore, this research provides three main controller parts, namely day-ahead operation planning, minute-order real-time operation and second-order real-time control. Based on the PV output forecast, the

system could manage the existing generators to maintain their frequency in the stable range. It is a challenge to maintain the power system frequency in the stable range due to the RES that have a high of uncertainties value.

5.3. Problem Formulation

5.3.1. Optimization stage I for UC using Day-ahead PV Forecasting

1.. Formulation for Stage I Optimization

The optimization problem is formulated with N_G controllable generators in a time horizon of T intervals ahead from the current moment as follows.

Minimize:

$$C^{DH}(\boldsymbol{P_G}, \boldsymbol{u}) = \sum_{t=1}^{T}\sum_{k=1}^{N_G} u_{kt} \cdot f_{kt} + \sum_{m=1}^{N_P}\sum_{k=1}^{N_G}\left(u_{kT_{Pm}} - u_{kT_N}\right) \cdot suc_k \tag{14}$$

$$f_{kt} = a_k P_{Gkt}^2 + b_k P_{Gkt} + c_k \tag{15}$$

suc_k : start-up cost [$] of k-th generator

Subject to:

i. Supply and demand balance constraints.

$$\sum_{k=1}^{N_G} P_{Gkt} + B_{dt} - B_{ct} = E[P_{Dt}] - E[P_{PVt}] - E[P_{WTt}] \tag{16}$$

ii. Upper and lower output of generator constraints.

$$P_{Gk}^{\min} \cdot u_{kt} \le P_{Gkt} \le P_{Gk}^{\max} \cdot u_{kt} \tag{17}$$

iii. Ramp-rate constraints.

$$-\delta_k \cdot \Delta t \le P_{Gk(t-1)} - P_{Gkt} \le \delta_k \cdot \Delta t \tag{18}$$

iv. Start/stop variables constraints.

$$0 \le u_{kt} \le 1 \tag{19}$$

v. Minimum continuity down time constraints.

$$\begin{aligned} &if \quad (1-u_{kt})\cdot u_{k(t-1)} = 1 \\ &then \quad \sum_{t}^{t+mdt} (1-u_{kt}) = mdt_k \end{aligned} \tag{20}$$

vi. Minimum continuity up time constraints.

$$\begin{aligned} &if \quad u_{kt}\cdot(1-u_{k(t-1)}) = 1 \\ &then \quad \sum_{t}^{t+mut} (1-u_{kt}) = mut_k \end{aligned} \tag{21}$$

vii. BT charge/discharge output limits constraints.

$$0 \le B_{dt} \le B_d^{\max} \tag{22}$$

$$0 \le B_{ct} \le B_c^{\max} \tag{23}$$

With switching constraint:

$$B_{ct}\cdot B_{dt} = 0 \tag{24}$$

viii. BT upper and lower bounds of the state of charge.

$$B_s^{\min} \le B_{st} \le B_s^{\max} \tag{25}$$

ix. Dynamic transition of BT state of charge.

$$B_{st} = B_{s(t-1)} + \{B_{ct} - B_{dt}/\eta\}\cdot\frac{\Delta t}{60} \tag{26}$$

x. Line flow limits between node *i* and *j*.

$$-F_{ij}^{\max} \le F_{ijt} \le F_{ij}^{\max} \tag{27}$$

xi. DC power flow equation (36) in the next section

xii. Operating reserve power constraints.

$$\sum_{k=1}^{N_G} P_{Gk}^{\max}\cdot u_{kt} + B_{dt} - B_{ct} \ge \ddot{P}_{nt} + R_t \tag{28}$$

$$\sum_{k=1}^{N_G} P_{Gk}^{\min} \cdot u_{kt} + B_{dt} - B_{ct} \le \underset{\cdots}{P}_{nt} \tag{29}$$

where, $P_{nt} = P_{Dt} - P_{PVt} - P_{WTt}$,

$$\ddot{\ddot{P}}_{nt} = P_{Dt} - \underset{\cdots}{P}_{PVt} - \underset{\cdots}{P}_{WTt} ,$$

$$\underset{\cdots}{P}_{nt} = P_{Dt} - \ddot{\ddot{P}}_{PVt} - \ddot{\ddot{P}}_{WTt} .$$

With the following description: C^{DH}: generation cost [$] for day-ahead GS, u_{kt}: start/stop variables of k-th generator at time t, P_{Gkt}: power output [MW] of k-th generator at time t, $\boldsymbol{P_G} \in \mathrm{R}^{N_G \times T}$: vector of P_{Gkt} (k=1,..,N_G, t=1,..,T), $\boldsymbol{u} \in \mathrm{R}^{N_G \times T}$: vector of u_{kt}, a_k, b_k, c_k: quadratic cost coefficients of k-th generator, T_{Pm}: time [min] at local maximum electricity demand (m=1,…,N_P), N_P: number of peak time, T_N: time [min] at minimum electricity demand, B_{ct}, B_{dt}: charge and discharge output power [MW] of BT at time t, respectively, P_{Dt}: electricity demand [MW] at time t, P_{PVt}: PV outputs [MW] at time t, P_{WTt}: WT outputs [MW] at time t, $E[\cdot]$: expected value [MW] at time t, $P_{Gk}^{\max}$, $P_{Gk}^{\min}$: maximum and minimum outputs [MW] of k-th generator, respectively, δ_k: ramp-rate limit [MW/min] of k-th generator, Dt: computational interval [min], mut_k, mdt_k: Minimum operating time [min] and minimum waiting time [min] of k-th generator, respectively, B_c^{max}, B_d^{max}: charge and discharge maximum power [MW] of BT, respectively, B_{st}: state of charge (SOC) [MWh] of BT at time t, B_s^{max}, B_s^{min}: maximum and minimum SOC bounds [MWh] of BT, respectively, h: charge/discharge efficiency of BT, F_{ijt}: line flow [MW] from node i to j governed by DC power flow equation, F_{ij}^{max}: maximum allowable line flow [MW] between node i and j, R_t: operating reserve power [MW] at time t, P_{nt}: net electricity demand at time t, $\ddot{\ddot{P}}_{nt}$, $\underset{\cdots}{P}_{nt}$: upper and lower bounds [MW] of P_{nt} including CIs of RES prediction at time t, respectively.

Solution procedure will be given in the following section. After obtaining the solution, this research proposes to fix the start/stop time schedules and the BT charge/discharge operation, and then perform the next steps as below.

A. RTDF and Supply-Demand Mismatch using CIs

TDF is defined as the region of generator output P_{Gkt} reachable from a specified operating point and satisfying all constraints (16)-(18) with load forecasts $\hat{P}_{Dt}$ for t=1,..,T. TDF evaluation algorithm was proposed in [5] and [6], where the present operating point t=0 is used as a starting point to achieve reachable points successively in forward direction to t=T. TDF result from this calculation is represented as $TDF(t, \hat{P}_{Dt})$, which implies the region defined by the upper and lower limits of each generator output at each time t=1…T.

In this research, Robust TDF (RTDF) is defined by considering CIs around the latest load predictions $\hat{P}_{Dt}$:

$$RTDF(t, \hat{P}_{Dt}) = \left\{ TDF(t, \hat{P}_{Dt} + M_{Ut}) \bigcap TDF(t, \hat{P}_{Dt} - M_{Lt}) \right\} \tag{30}$$

"$\bigcap$" implies the intersection. M_{Ut} and M_{Lt} are the assumed upper and lower limits of prediction errors, respectively. RTDF is obtained as the upper and lower bounds pair $\overline{\alpha}_{kt}$ and $\underline{\alpha}_{kt}$ (k=1,..,N_G, t=1,..,T) as follows.

$$\underline{\alpha}_{kt} \le P_{Gkt} \le \overline{\alpha}_{kt} \tag{31}$$

Calculation of RTDF is performed in each control cycle before stage II optimization in section III-*D*.

Once the upper and lower limits are obtained, any output values P_{Gkt} inside the limits (31) will be guaranteed as reachable if the latest load forecast errors appear inside CIs, $[\hat{P}_{Dt} - M_{Lt}, \hat{P}_{Dt} + M_{Ut}]$. In this algorithm, when $\overline{\alpha}_{kt} < \underline{\alpha}_{kt}$ is detected, RTDF is nonexistence and the supply-demand mismatch (SDM) is computed by (32).

$$SDM = \begin{cases} \underline{\alpha}_{kt} - \overline{\alpha}_{kt} & (when\ \overline{\alpha}_{kt} < \underline{\alpha}_{kt}) \\ 0 & (when\ \overline{\alpha}_{kt} \ge \underline{\alpha}_{kt}) \end{cases} \tag{32}$$

When SDM is detected, it must be compensated by additional power provision or load reduction. After the management of SDM, the RTDF is recalculated to confirm that the SDM disappears. Then, the optimization process is

continued.

B. Stochastic Load Flow [20]-[22]

The prediction errors of loads and RESs result are in the line flow of uncertainty. Line flow constraints are treated in a probabilistic manner. Assuming the normal distribution for the prediction error characteristic, linear DC power flow calculation method is used to provide the most efficient computation. The SLF method is applied in such a way that the probability of constraint violation is less than a specified value for each line. The stochastic network constraint is represented as in the following form.

$$LBF_l \le F_l = \sum_{j=1}^{N_n} S_{lj} P_j \le UBF_l \tag{33}$$

UBF_l and LBF_l are the upper and lower bounds [MW] with respect to the transmission line l, F_l: amount of line flow [MW], N_n: number of nodes, S_{lj}: conversion matrix, P_j: injection power [MW] into node j.

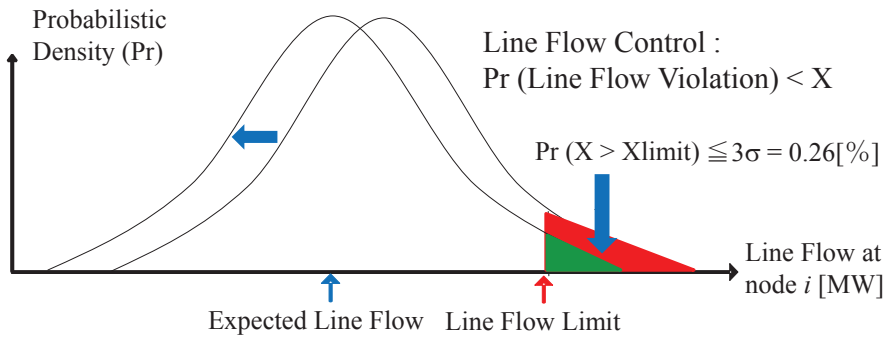

Figure 25. Stochastic control of line flow

The formulation of (33) is provided in the following equation. Based on the DC power flow method, the following relationships hold.

$$\boldsymbol{S}_N \boldsymbol{\theta} = \boldsymbol{P} \tag{34}$$

$$\boldsymbol{F} = \boldsymbol{S}_C \boldsymbol{\theta} \tag{35}$$

Where, $\boldsymbol{\theta} \in \mathrm{R}^{Nn\times 1}$: voltage angle matrices [rad], $\boldsymbol{P} \in \mathrm{R}^{Nn\times 1}$: real power injection matrices [p.u.], $\boldsymbol{F} \in \mathrm{R}^{Nl\times 1}$: real power line flow [p.u.], $\boldsymbol{S}_N \in \mathrm{R}^{Nn\times Nn}$:

node susceptance matrices [p.u./rad], $\boldsymbol{S_C} \in \mathrm{R}^{Nl \times Nn}$: line susceptance matrices. From (34) and (35), the following is obtained:

$$\boldsymbol{F} = \boldsymbol{S_C}\boldsymbol{S_N}^{-1}\boldsymbol{P} = \boldsymbol{S} \cdot \boldsymbol{P} \tag{36}$$

Node injection $\boldsymbol{P}$ is represented as

$$\boldsymbol{P} = \boldsymbol{P_G} - \boldsymbol{P_D} \tag{37}$$

Where $\boldsymbol{P_D}$ is a probabilistic variable consisting of loads and RES outputs (negative demands), while $\boldsymbol{P_G}$ corresponds to a variable of conventional generator outputs to be determined in the optimization process. Therefore, the expected value $E[\boldsymbol{P}]$ of node injection power $\boldsymbol{P}$ is represented by the following expression:

$$E\left[\boldsymbol{P}\right] = \boldsymbol{P_G} - E\left[\boldsymbol{P_D}\right] \tag{38}$$

Then, the mean value vector and covariance matrix of line flow are represented as follows:

$$E\left[\boldsymbol{F}\right] = \boldsymbol{S}\left[\boldsymbol{P_G} - E\left[\boldsymbol{P_D}\right]\right] = \boldsymbol{S} \cdot \boldsymbol{P_G} - \boldsymbol{S} \cdot E\left[\boldsymbol{P_D}\right] = [\mu_i] \tag{39}$$

$$\begin{aligned} Cov\left[\boldsymbol{F}\right] &= E[(\boldsymbol{F} - E[\boldsymbol{F}])(\boldsymbol{F} - E[\boldsymbol{F}])^T] \\ &= \boldsymbol{S} \cdot E[(\boldsymbol{P} - E[\boldsymbol{P}])(\boldsymbol{P} - E[\boldsymbol{P}])^T] \cdot \boldsymbol{S}^T \\ &= \boldsymbol{S} \cdot Cov[\boldsymbol{P}] \cdot \boldsymbol{S}^T = [\sigma_{ij}] \end{aligned} \tag{40}$$

Where, $Cov[\boldsymbol{P}] = \begin{pmatrix} b_{11} & b_{12} & \cdots & b_{1n} \\ b_{21} & b_{22} & \cdots & \vdots \\ \vdots & \vdots & \ddots & b_{(n-1)n} \\ b_{n1} & \cdots & b_{n(n-1)} & b_{nn} \end{pmatrix}$.

The diagonal element b_{nn} is variance of $\boldsymbol{P_D}$, the non-diagonal element is the covariance (*Cov*) of PV generation outputs.

The probability density function for line flow *l* may be described using the elements from (39) and (40):

$$\xi_{F_l}(F_l) = \frac{1}{\sqrt{2\pi}\sigma_{ll}} \exp\left\{-\frac{1}{2}\frac{(F_l - \mu_l)^2}{\sigma_{ll}^2}\right\} \tag{41}$$

To constrain the violation probability to a value less than *X*, threshold *b* is defined

by the following equations.

$$X \geq 1 - \int_{-\overline{F_l}}^{\overline{F_l}} \xi_{F_l}(x)dx \tag{42}$$

$$\overline{F_l} - \beta \cdot \sigma_{ll} \geq \left| E\left[F_l\right] \right| \tag{43}$$

Further substitution of (43) into (41) yields stochastic load flow constraint below, where (44) is identical with (33).

$$-\overline{F_l} + \beta \cdot \sigma_{ll} + D_l \leq \sum_{j=1}^{N_n} S_{lj} P_j \leq \overline{F_l} - \beta \cdot \sigma_{ll} + D_l \tag{44}$$

Where , $D_l = \sum_{j=1}^{N_n} S_{lj} E\left[P_D^l\right]$.

5.3.2. Optimization stage II for DELD using Real-time PV Forecasting

The optimization problem (Stage II) is formulated with N_G controllable generators in a time horizon of T intervals ahead from the current moment as follows.

Minimize:

$$C^{RT}(\boldsymbol{P_G}, \boldsymbol{u}) = \sum_{t=1}^{T} \sum_{k=1}^{N_G} (a_k P_{Gkt}^2 + b_k P_{Gkt} + c_k) \tag{45}$$

Subject to:

(16), (18), (31), (44).

Constraints (31) and (44), which are explained in sections III-*B* and *C,* are the novel treatment of uncertainties by the proposed method. That is, the important constraint of the supply and demand balance is treated in deterministic manner by RTDF with CIs to avoid system collapse. On the other hand, soft constraints of line overloading are dealt with by DC probabilistic power flow. Covariance matrix and CIs will be updated frequently in real-time operation, as is presented in the next section.

➢ *Computational Procedures*

This section describes the computation procedure of the proposed method presented in the previous sections. The following procedures are performed in every control cycle.

< Day-ahead 24-hour GS: Stage I > (A few times a day)

Instead of standard approach using Mixed-Integer Linear Programming (MILP), we have developed a special technique by improving the method in [56] to solve the UC problem by using standard QP software. The effectiveness of the proposed technique has been studied in [57].

The day-ahead GS is obtained by using the following algorithm to determine the generator's output $\boldsymbol{P_G}$, its start/stop variable $\boldsymbol{u}$ and BT charge/discharge operation for 24 hours, where unit time is 30 minutes.

Step I-1 Read day-ahead forecast data for loads and RES.

Step I-2 Set iteration number $d = 0$.

Step I-3 Solve (16) by QP to determine $\boldsymbol{P_G}$ and $\boldsymbol{u}$, treated as continuous variables.

Step I-4 Compute unit fuel cost in (46) using present $\boldsymbol{P_G}$.

$$\mu_{kt}^{d} = a_k P_{Gkt} + b_k + c_k / P_{Gkt} \tag{46}$$

Step I-5 Solve the following problem with penalty function (48) using QP algorithm.

Minimize:

$$g(\boldsymbol{P_G}, \boldsymbol{u}, d, \boldsymbol{\mu}^d) = C^{DH}(\boldsymbol{P_G}, \boldsymbol{u}) + h(d, \boldsymbol{\mu}^d) \tag{47}$$

$$h(d, \boldsymbol{\mu}^d) = \sum_{k=1}^{N_G} \sum_{t=1}^{T} \left\{ 10^{-d+2} (d+2) (\mu_{kt})^d \right\} \tag{48}$$

Subject to: (16)-(28), and (36).

Step I-6 $d = d + 1$.

Step I-7 Repeat Steps I-4 to I-6 until the convergence is obtained.

Step I-8 Determine start/stop variables $\boldsymbol{u}$: if u_{kt}>0.5 (threshold) then set u_{kt}=1 else u_{kt}=0.

Step I-9 By fixing $\boldsymbol{u}$, solve the first formula to obtain $\boldsymbol{P_G}$ using QP algorithm.

The obtained start/stop time for generators and BT operation for 24-hour GS will be used in stage II as predetermined schedule. The generator's outputs P_{Gkt} are used as only reference for operators.

< Real-time 1-hour GS: Stage II > (Every 5 minutes)

The real-time GS is carried out to minimize the generator's output and BT charge/discharge operation (if necessary) every 5 minutes.

Step II-1 Read data of day-ahead generator's start/stop variables and BT charge/discharge operations.

Step II-2 Update forecasts (load and RES), covariance matrices, and CIs using most recent data. Perform state estimation to obtain the present operating condition.

Step II-3 Calculate RTDF and Supply-Demand Mismatch (SDM). If SDM is non-zero, arrange relevant reserve by modifying BT operation schedule, or using other resources corresponding to detected value of SDM, and perform RTDF update to confirm zero SDM.

Step II-4 Compute UBF_l and LBF_l.

Step II-5 Solve problem (45) by QP software to obtain GS: P_{Gkt} (k=1,..,N_G, t=5,10,.., 60[min]).

The obtained GS is monitored by system operator, where GS in 5 minutes ahead are sent to the individual generators as real-time control signal.

5.4. Case Studies

1. Simulation Conditions

The proposed method is demonstrated using an example system in figure 26. The generation mix data is from a Japanese smart grid project where the installed PV an WT generation are about 15% of peak load. It is composed of three diesel generators, two load areas with RESs and a BT station. Detail data are given in tables 3. PV prediction data is shown, which has been given by our forecasting method based on the weather clustering type neural network. Typical load patterns are used in the proposed optimization process.

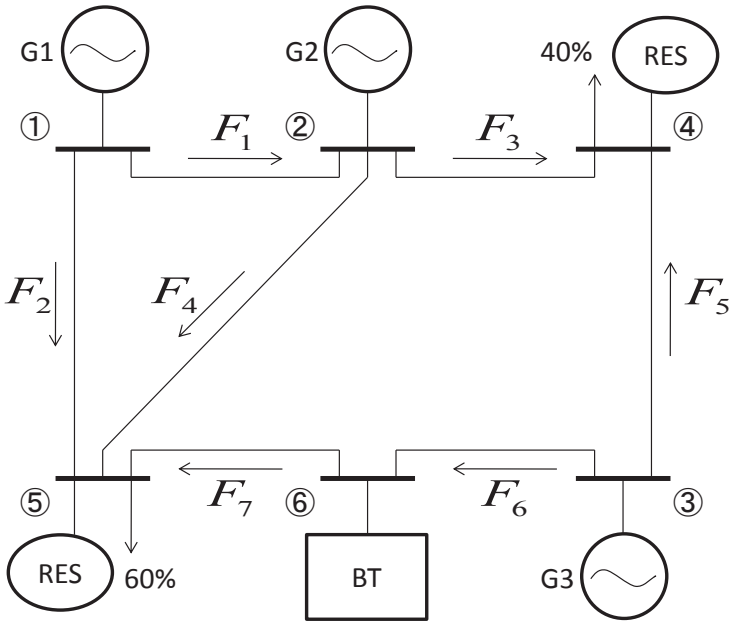

Figure 26. Test Power System

Table 3. specification of generators

k	Output Limit [kW]	Ramp Rate [kW/min]	Start-up Cost (suc_k) [$]	Cost Coefficients[100$]		
				a_k	b_k	c_k
G1	1,000~2,000	66.7	40.00	0.0011	16.416	4,320.00
G2	625~1,250	41.7	25.00	0.0021	17.410	3,667.50
G3	1,125~2,250	75.0	45.00	0.0002	20.178	3,993.70

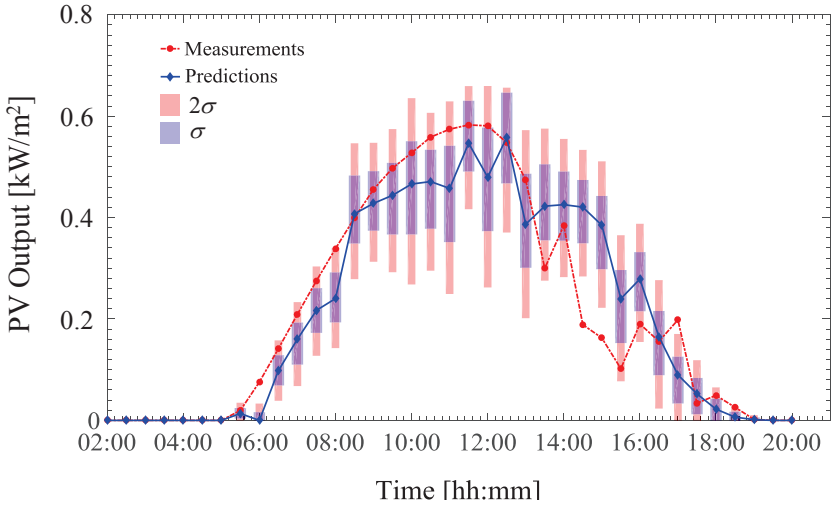

(a) Results of Day-ahead Forecast

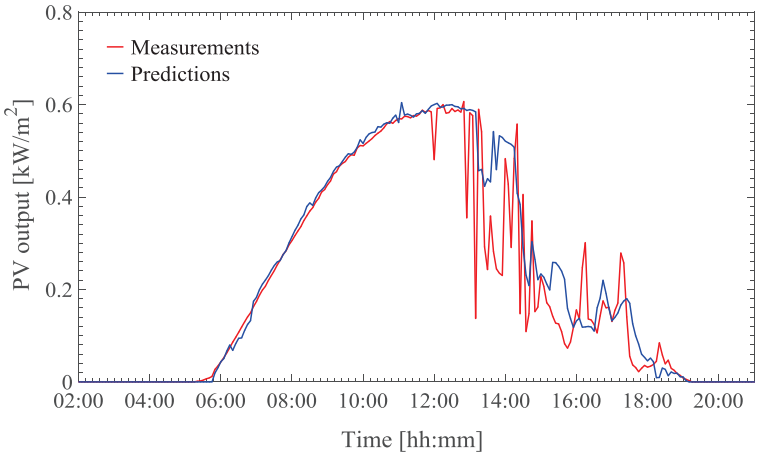

(b) Results of Real-time Forecast.

Figure 27. Forecast results on 4th August, 2012

- *Stage I optimization*

Figure 28 shows the result of stage I optimization, describing 24-hours GS for generators (P_{G1}, P_{G2}, P_{G3}), BT operation (P_{BT}=B_d-B_c), electricity demand (P_D), net electricity demand (P_n), PV output (P_{PV}) predictions, WT outputs (P_{WT}), and SOC of BT (B_s). Note that G2 starts up at 11:00 and shuts down at 18:15 shown in Table II, which will be fixed in the stage II optimization.

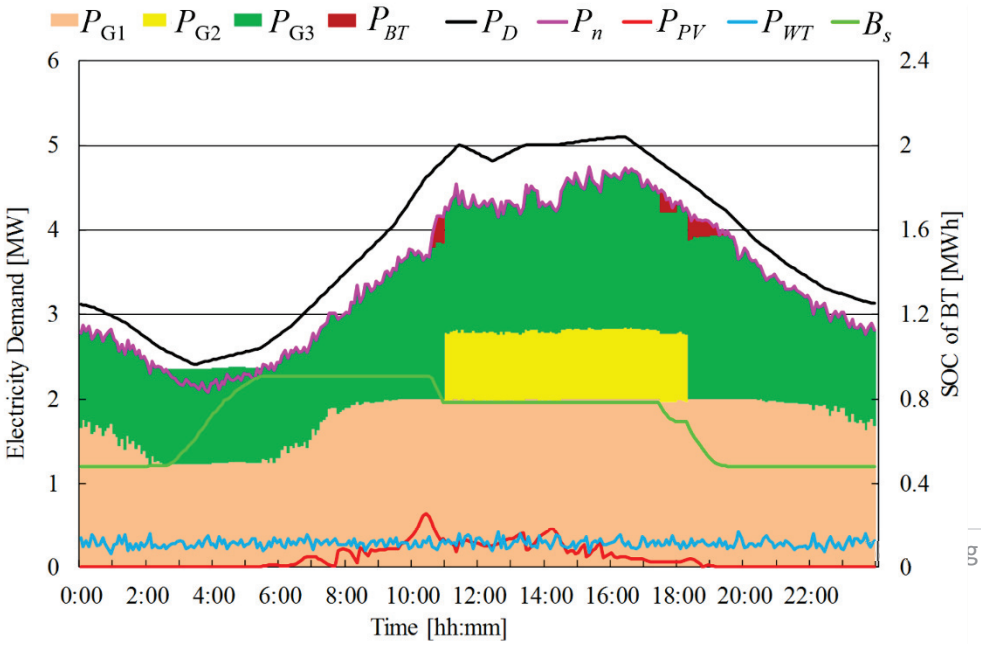

Figure 28. Day-ahead 24-hour GS

Tabel. 4 Start-up and shut-down times data from day-ahead UC

Demand	Unit k	Start-up time	Shut-down time
Weekday	G1	-	-
	G2	11:00	18:15
	G3	-	-

- *Stage II optimization*

1-hour GS is computed and updated every 5 minutes based on real-time PV prediction data. The upper and lower tolerances of prediction errors in net demands (load – RES) are set as a linear function of time as follows:

$$M_{Ut} = M_{Lt} = \hat{P}_{Dt} \times \frac{t}{T} \times \gamma \tag{49}$$

Where, $\hat{P}_{Dt}$ $(t=0,1,\ldots,T)$ are the most recent forecasted net power demands. T=60 [min], t: prediction time (t=0 for present operating point), g is a parameter representing 1 hour ahead maximum prediction error, and g = [0%, 10%, 20%] will be examined. Allowable constraint violation for line flow is set to X=3s =0.26[%] in this examination.

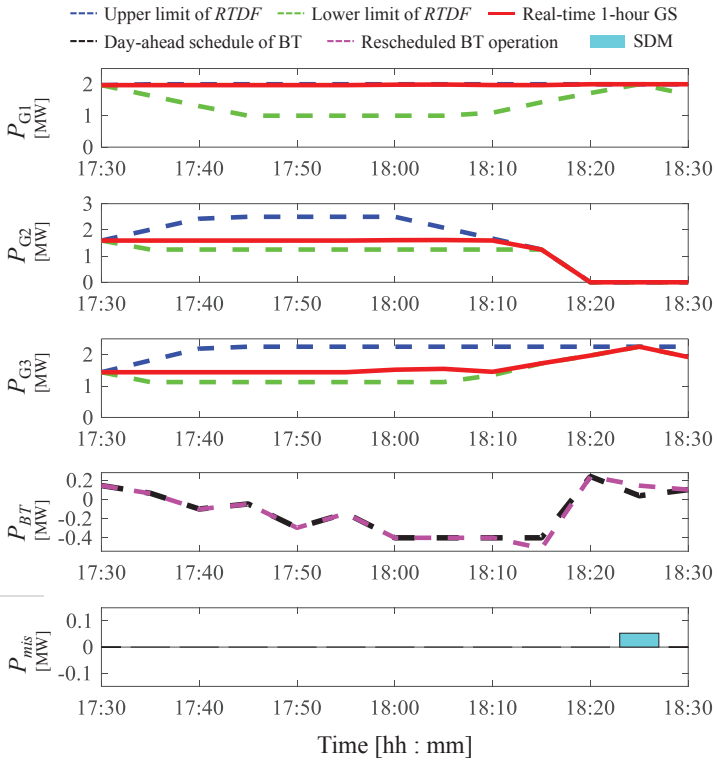

Figure 29. Real-time 1-hour GS with RTDF and SDM

Figure 29 shows the result of stage II optimization obtained at 17:30 (weekday, γ=10%). The upper and lower limits of RTDF and 1-hour GS for each generator are provided. The GS at 5 minutes ahead (17:35) is sent to each generating unit as a control signal. RTDF implies reachable area from the operating point at 17:30. The larger RTDF, the larger system capability that copes with uncertainty is expected. RTDF computation also successfully provides SDM 1-hour before the operation, which is given as P_{mis} that appears at 18:25. This advantageous characteristic come from the RTDF computation which identifies the feasible region with high accuracy. Note that the detected SDM is managed by the rescheduling of the BT operation 1-hour before by the proposed method. If BT cannot cope with the situation, we can prepare additional action such as demand response or load shedding at 18:25.

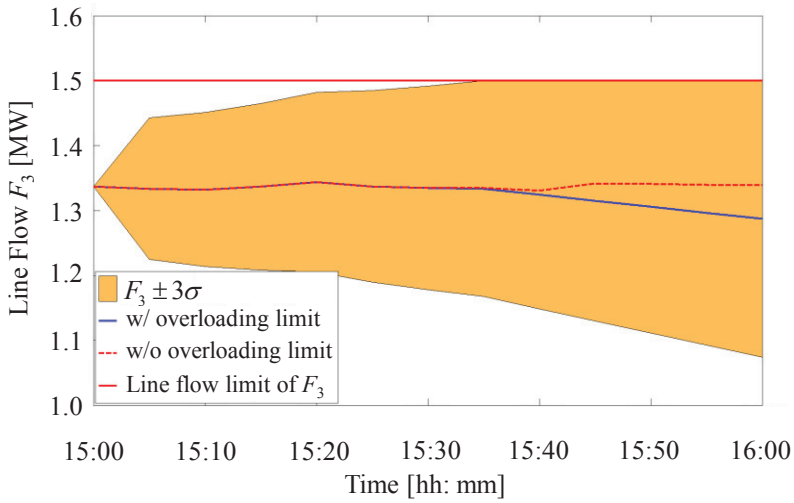

Figure 30. Line Flow with 3σ allowable intervals at line F_3.

Figure 30 shows the scheduled F_3 line flow, which may vary inside 3σ allowable intervals. The result shows that SLF works successfully to avoid overloads in stage II optimization. Figure 8 describes the simulated results after 24-

hour operations by the proposed real-time optimized control method. Descriptions of wave forms are given below the figure caption. We see that the PV prediction 1-hour ahead in the 2nd graph is erroneous. Nevertheless, the proposed method successfully treats the uncertainties to control generators as seen in 4-6th graphs, Rescheduled BT operation in the 7th graph has completely absorbed the SDM detected in figure 31. As a result, the frequency deviations are suppressed less than 0.2 Hz as observed in 8th graph. The frequency fluctuation has been analyzed by the simulator in the proposed micro-EMS controller. The frequency deviations increase mainly due to PV output fluctuations as well as the prediction errors in the day time. Thus, the proposed method reliably manages the uncertainties in the real-time power system operation.

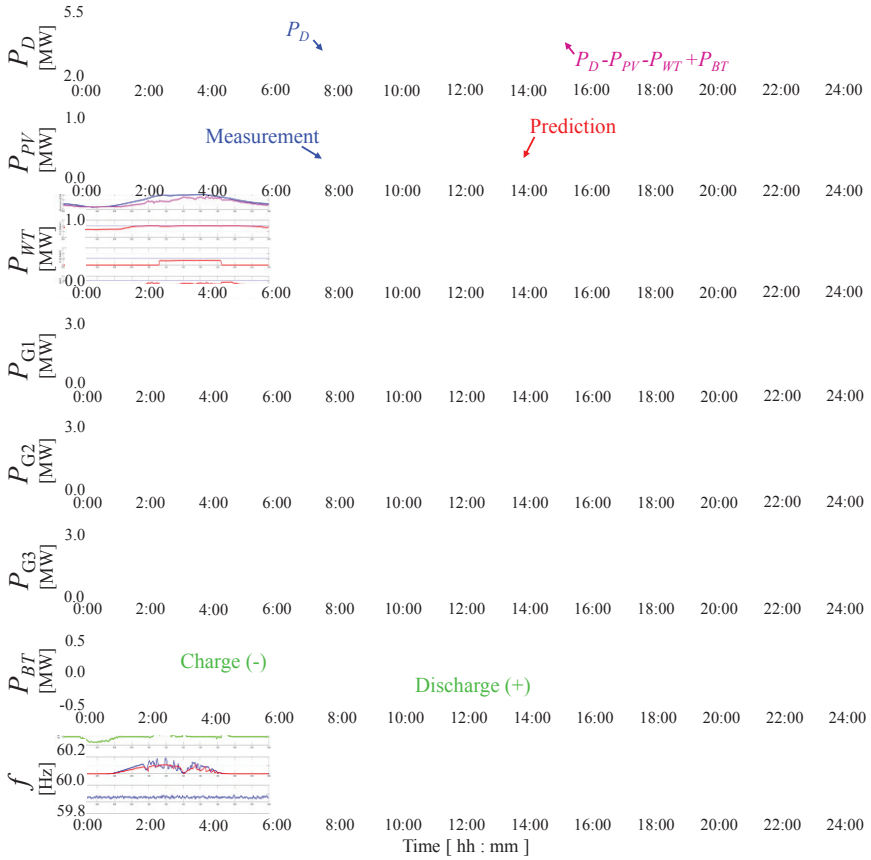

Figure 31. The results of the 24-hour operations.

(From top: 1: P_D and net demand (=P_D-P_{PV}-P_{WT}+P_{BT}) [2~5.5MW], 2: P_{PV} (prediction 1-hour ahead and measurement) [0~1MW], 3: P_{WT} [0~1MW], 4: P_{G1}, 5: P_{G2}, 6: P_{G3} [0~3MW], 7: P_{BT} [-0.5 ~0.5MW], and 8: f system frequency [59.8~60.2Hz], where [*~**] describes full scale of each graph)

Table 5. CPU Time

Number of Generators	Stage I for day-ahead 24-hour GS [sec]	Stage II for real-time 1-hour GS[sec]
3	3.0	0.37 (0.011)
5	4.4	0.44 (0.012)
10	9.4	1.87 (0.054)

Table 4 shows the computational burden (CPU Time), which is evaluated for test power systems with 3, 5, and 10 generators using Intel Core i7, 2.20GHz, 8GB memory. The CPU time on Stage I implies a total computation time from Steps I-2 to I-9 in Section III-*E* for obtaining a day-ahead 24-hour GS. Stage II computation time is for the calculation of Steps II-3 to II-5 in Section III-*E* for obtaining a real-time 1-hour GS that is to be repeated every 5 minutes. Note that the numbers in the blanket imply the computation time for RTDF and SDM.

Integrating large amounts of intermittent RESs into electric power systems causes various difficulties such as the supply and demand balance and frequency problems. In such situations, treatment of uncertainty by means of limited controllable resources is a critical issue for secure power system operations. Frequent evaluation of generation schedule is effective for minimizing prediction errors to establish a reliable operation against sudden changes in RES generations. We propose a new real-time optimization method guaranteeing feasibility of operations. Uncertainties affecting the important constraint of the supply and demand balance are treated in deterministic manner using CIs to avoid system collapse, while those relating to soft constraints of line overloading are dealt with by DC probabilistic power flow. Although the computation time is a critical issue, the proposed method provides a solution for introducing a large amount of RES into a smart grid operation.

The present version of the proposed method utilizes the DC power calculation method which may degenerate the accuracy when applied to low voltage distribution systems with large values of R/X. The use of extended equations based on a distribution power flow [58], [59] seems an interesting trial in the future.

5.5 Summary

This section could be summarized as follows:

1. The research provides an EMS controller represented as a small power system grid. This controller consists of day-ahead operation manager, real-time operation manager and real-time control manager.
2. Integrating large amounts of intermittent RESs into electric power systems causes various difficulties such as the supply and demand balance and frequency problems.
3. The treatment of uncertainty by limited controllable resources is a critical issue for secure power system operations.
4. Frequent evaluation of generation schedule is effective for minimizing prediction errors to establish a reliable operation against sudden changes in RES generations.
5. A new real-time optimization method guaranteeing feasibility of operations is described in this chapter.
6. Although the computation time is a critical issue, the proposed method provides a solution for introducing a large amount of RES into a smart grid operation.

Chapter 6

Conclusions and Future Research

6.1. Conclusions

This research has proposed a day-ahead and a real-time PV generation forecasting method for the supply-demand manager. The performance, capabilities, and effectiveness of our methodology have been verified through extensive simulation results. We have also validated the degree of influence of the prediction error and the CI on the system performance. For the real-time PV forecasting, the SRCA method could be approved as neighborhood-area forecast. This method can be used to predict in an isolated area.

Frequent evaluation of generation schedule is effective for minimizing prediction errors in order to establish a reliable operation against sudden changes in RES generations.

6.2. Future Work

There are still a number of future works that have to be developed for the day-ahead forecast. The aim of this work to improve the prediction accuracy and implement the method on a simulator. This is necessary in studying how significant the impacts on the prediction errors and/or the CI settings.

For a real-time forecast, it is necessary to consider the relationship between the additional weather conditions beside the solar radiation characteristics. Additionally, effective settings for the CIs based on the prediction error analysis, and construction of a detection system for performing short-time lamp fluctuations in advance also remain as topics for our future work.

For the EMS application, the present version of the proposed method utilizes the DC power calculation method which may degenerate the accuracy when applied to low voltage distribution systems with large values of R/X. The use of extended equations based on a distribution power flow [25], [26] seems an interesting trial in the future.

References

[1] H. Yamada and O. Ikki, "National Survey Report of PV Power Applications in JAPAN," *International Energy Agency Photovoltaic Power Systems Programme*, issue date: 22 Aug. 2016.

[2] N. Yorino, Y. Sasaki, E.P. Hristov, Y. Zoka, and Y. Okumoto, "Dynamic load dispatch for power system robust security against uncertainties," *Proc. of 2013 IREP Symp.*, Crete, Greece, Aug. 2013, pp. 1-17.

[3] N. Yorino, M. Abdillah, T. Isoya, Y. Sasaki, and Y. Zoka, "A new method of evaluating robust power system security against uncertainties," *IEEJ Trans. on Elect.and Electron.Eng.*, vol. 10, no. 6, pp. 636-643, Nov. 2015.

[4] N. Yorino, M. Abdillah, Y. Sasaki, and Y. Zoka, "Robust Power System Security Assessment Under Uncertainties Using Bi-Level Optimization," *IEEE Trans. on Power Syst.*, Vol. PP, No. 99, pp.1-11, 2017 (to appear).

[5] H.M. Hafiz, N. Yorino, Y. Sasaki, and Y. Zoka, "Feasible Operation Region for Dynamic Economic Dispatch and Reserve Monitoring," *European Trans. on Electrical Power*, Vol. 22, No. 7, pp.924-936, Oct. 2012.

[6] N. Yorino, H.M. Hafiz, Y. Sasaki, and Y. Zoka, "High-speed Real-time Dynamic Economic Load Dispatch," *IEEE Trans. on Power Syst.*, Vol. 27, No. 2, pp.621-630, May 2012.

[7] Y. Sasaki, N. Yorino, Y. Zoka, and I.F. Wahyudi, "Robust Stochastic Dynamic Load Dispatch against Uncertainties," *IEEE Trans. on Smart Grid*, Vol. PP, No. 99, pp.1-9, 2017 (to appear).

[8] Y. Zhang, M. Beaudin, R. Taheri, and H. Zareipour, "Day-Ahead Power Output Forecasting for Small-Scale Solar Photovoltaic Electricity Generators," *IEEE Trans. Smart Grid*, Vol. 6, No. 5, pp.2253-2262, Sep. 2015.

[9] R.J. Bessa, A. Trindade, and V. Miranda, "Spatial-Temporal Solar Power Forecasting for Smart Grids," *IEEE Trans. Industrial Informatics*, Vol. 11, Vo. 1, pp.232-241, Feb. 2015.

[10] Asrari, T.X. Wu, and B. Ramos, "A Hybrid Algorithm for Short-Term Solar Power Prediction – Sunshine State Case Study," *IEEE Trans. Sustainable Energy*, Vol. 8, No. 2, pp.582-591, Apr. 2017.

[11] H.T. Yang, C.M. Huang, Y.C. Huand, and Y.S. Pai, “A Weather-based Hybrid Method for 1-Day Ahead Hourly Forecasting of PV Power Output,” *IEEE Trans. Sustainable Energy*, Vol. 5, No. 3, pp.917-926, Jul. 2014.

[12] Bracale, G. Carpinelli, and P.D. Falco, “A Probabilistic Competitive Ensemble Method for Short-Term Photovoltaic Power Forecasting,” *IEEE Trans. Sustainable Energy*, Vol. 8, No. 2, pp.551-560, Apr. 2017.

[13] Yona, T. Senjyu, T. Funabashi, and C.H. Kim, “Determination Method of Insolation Prediction With Fuzzy and Applying Neural Network for Long-Term Ahead PV Power Output Correction,” *IEEE Trans. Sustainable Energy*, Bol. 4, No. 2, pp.527-533, Apr. 2013.

[14] J. Liu, W. Fang, X. Zhang, and C. Yang, “An Improved Photovoltaic Power Forecasting Model With the Assistance of Aerosol Index Data,” *IEEE trans. Sustainable Energy*, Vol. 6, No. 2, pp.434-442, Apr. 2015.

[15] A.S. Nin Mohd Shah, H. Yokoyama, and N. Kakimoto, “High-Precision Forecasting Model of Solar Irradiance Based on Grid Point Value Data Analysis for an Efficient Photovoltaic System,” *IEEE trans. Sustainable Energy*, Vol. 6, No. 2, pp.474-481, Apr. 2015.

[16] H.S. Jang, K.Y. Bae, H.S. Park, and D.K. Sung, “Solar Power Prediction Based on Satellite Images and Support Vector Machine,” *IEEE Trans. Sustainable Energy*, Vol. 7, No. 3, pp.1255-1263, Jul. 2016.

[17] J. Shi, W.J. Lee, Y. Liu, Y. Yang, and P. Wang, “Forecasting Power Output of Photovoltaic Systems Based on Weather Classification and Support Vector Machines,” *IEEE Trans. Industry Applications*, Vol. 48, No. 3, pp.1064-1069, May/Jun. 2012.

[18] G. Capizzi, C. Napoli, and F. Bonanno, “Innovative Second-Generation Wavelets Construction With Recurrent Neural Networks for Solar Radiation Forecasting,” *IEEE Trans. Neural Networks and Learning Systems*, Vol. 23, No. 11, pp.1805-1815, Nov. 2012.

[19] L. Ma, N. Yorino, and K. Khorasani, “Solar Radiation (Insolation) Forecasting Using Constructive Neural Networks,” *Proc. of IEEE World Congress on Computational Intelligence (WCCI)*, No.16433, 24-29 July (2016)

[20] Alqahtani, S. Marafi, B. Musallam, and N.E.D. Abd El Khalek, "Photovoltaic Power Forecasting Model Based on Nonlinear System Identification," *Canadian Journal of Electrical and Computer Engineering*, Vol. 39, No. 3, pp.243-250, Summer 2016.

[21] Shakya, S. Michael, C. Saunders, D. Armstrong, P. Pandey, S. Chalise, and R. Tonkoski, "Solar Irradiance Forecasting in Remote Microgrids using Markov Switching Model." *IEEE Trans. Sustainable Energy*, Vol.PP, No. 99, to be appeared.

[22] C.M. Huang, S.J. Chen, S.P. Yang, and C.J. Kuo, "One-day-ahead hourly forecasting for photovoltaic power generation using an intelligent method with weather-based forecasting models," *IET Gener., Transm. Distrib.*, Vol. 9, Vo. 14, pp.1874-1882, 2015.

[23] M.G. De Giorgi, P.M. Congedo, and M. Malvoni, "Photovoltaic power forecasting using statistical methods: impact of weather data," *IET Sci. Meas. Technol.*, Vol. 8, No. 3, pp.90-97, 2014.

[24] S. Ghosh, S. Rahman, and M. Pipattanasomporn, "Distribution Voltage Regulation Through Active Power Curtailment With PV Inverters and Solar Generation Forecasts," *IEEE Trans. Sustainable Energy*, Vol. 8, No. 1, pp.13-22, Jan. 2017.

[25] E. Lorenz, J. Hurka, D. Heinemann, and H.G. Beyer, "Irradiance Forecasting for the Power Prediction of grid-Connected Photovoltaic Systems," *IEEE Journal of Selected Topics in Applied Earth Observations and Remote Sensing*, Vol. 2, No. 1, pp. 2-10, Mar. 2009.

[26] M. Asensio and J. Contreras, "Stochastic Unit Commitment in Isolated Systems With Renewable Penetration Under CVaR Assessment," *IEEE Trans. Smart Grid*, Vol. 7, No. 3, pp.1356-1367, May 2016.

[27] Li, X. Liu, Y. Cao, P. Zhang, H. Shi, L. Ren, and Y. Kuang, "A Time-Scale Adaptive Dispatch Method for Renewable Energy Power Supply Systems on Islands," *IEEE Trans. Smart Grid*, Vol. 7, No. 2, pp.1069-1078, Mar. 2016.

[28] K. Matsuda, K. Arimatsu, K. Yamase, M. Watanabe, J. Yamazaki, and J. Murakoshi, "Short-term Prediction of Photovoltaic Power Generation for Distribution Management System based on Spatial Correlation Analysis," *IEEJ Trans. on Power and Energy*, Vol.134, No.9, pp.759-766, Sep., 2014.

[29] S. Yamamoto, T. Katagi, J. Park, and T. Hashimoto, and T. Hashimoto "A Basic Study to Forecast the Power Fluctuation of the Photovoltaic Power Generation by Image Processing of Clouds," *IEEJ Trans. on Power and Energy*, Vol.119-B, No.8/9, pp.909-915, Aug./Sep., 1999.

[30] K Simose, H. Ohtake, J.G da Silva Fonseca Jr., T. Takashima, T. Oozeki, Y. Yamada, "Analysis of Error Causes of the Irradiation Forecast by the Japan Meteorological Agency Meso-Scale Model," *IEEJ Trans. on Power and Energy*, Vol.134, No.6, pp.518-526, Jun., 2014.

[31] Ministry of Economy, Trade and Industry (METI), http://www.meti.go.jp/english/

[32] Y. Sasaki, N. Yorino, and Y. Zoka, "Probabilistic Economic Load Dispatch Applied to a micro-EMS Controller," *19th Power Systems Computation Conference*, No. ID574, Jul. 2016.

[33] Japan Meteorological Agency: http://www.jma.go.jp/jma/indexe.html Japan Industrial Standard (JIS) C8907, "Estimation method of generating electric energy by PV power system," 2005.

[34] R. Perdomo, E. Banguero, G. Gordilo "Statistical Time Series Models of Solar Radiation for Global Solar Radiation Forecasting In Bogotá," 35th Photovoltaic specialist Conference (PVSC), pp. 2374 – 2379, IEEE, Jun., 2010.

[35] S. Hokoi, M. Matsumoto, "Statistical Time Series Models of Solar Radiation and Outdoor Temperature - Identification of Seasonal Models by Kalman Filter," *Elsevier energy and building*, vol. 15-16, pp. 373-383, 1990.

[36] L. P. A. Vincent, B. E. Adria, D. C. Alexander, L. Michael, K. Kevin, "Intra-Hour Forecasts Of Solar Power Production Using Measurements From A Network Of Irradiance Sensors," *elsevier Solar and Energy*, Vol.97, No.6, pp.58-66, Aug., 2014.

[37] B. Peder, M. Henrik, H. A. Nielsen, "Online short-term solar power forecasting," *elsevier Solar and Energy*, Vol. 83, pp.1772-1783, Jul., 2009.

[38] M. C. Eduardo, M. F. Pedro, E. R. Antonio, "Solar radiation prediction using RBF Neural Networks and cloudiness indices," *International Joint Conference on Neural Networks*, pp.2611-2618, Jul., 2006.

[39] K. Benmouiza, A. Cheknane "Forecasting hourly global solar radiation using hybrid *k*-means and nonlinear autoregressive neural network models," *Elsevier energy Conversion and Management*, Vol. 75, pp.561-569, Jul., 2013.

[40] J. K. Robert, P. Barros "Localized Precipitation Forecasts from a Numerical Weather Prediction Model Using Artificial Neural Networks," *American Meteorological Society*, Vol. 13, pp.1194-1204, Jul., 1998.

[41] J. Zhu, "Optimization of Power System Operation," Wiley-IEEE Press, Second Edition, Jan. 2015.

[42] A. Ipakchi, and F. Albuyeh, "Grid of the future," *IEEE Power and Energy Magazine*, Vol. 7, No. 2, pp.52-62, Feb. 2009.

[43] N. Yorino, Y. Sasaki, S. Fujita, Y. Zoka, and Y. Okumoto, "Issues for Power System Operation for Future Renewable Energy Penetration: Robust Power System Security," *Electrical Engineering in Japan*, Vol. 182, No. 1, pp. 30-38, Jan. 2013.

[44] D.W. Ross, and S. Kim, "Dynamic Economic Dispatch of Generation," *IEEE Trans. on Power App. and Syst.*, Vol. PAS-99, No. 6, pp.2060-2068, Nov. 1980.

[45] T. Li, and M. Shahidehpour, "Dynamic Ramping in Unit Commitment," *IEEE Trans. on Power Syst.*, Vol. 22, No. 3, pp.1379-1381, Aug. 2007

[46] D.N. Simopoulos, S.D. Kavatza, and C.D. Vournas, "Unit Commitment by an Enhanced Simulated Annealing Algorithm," *IEEE Trans. on Power Syst.*, Vol. 21, No. 1, pp.68-76, Feb. 2006.

[47] C.L. Chen, "Simulated Annealing-based Optimal Wind-thermal Coordination Scheduling," *IET Gener. Transm. and Distrib.*, Vol. 1, No. 3, pp.447-455, May 2007.

[48] A.Y. Abdelaziz, M.Z. Kamh, S.F. Mekhamer, and M.A.L. Badr, "A Hybrid HNN-QP Approach for Dynamic Economic Dispatch Problem," *Electric Power Systems Research*, Vol. 78, No. 10, pp.1784-1788, Oct. 2008.

[49] W.G. Wood, "Spinning Reserve Constrained Static and Dynamic Economic Dispatch," *IEEE Trans. on Power App. and Syst.*, Vol. PAS-101, No. 2, pp.381-388, Feb. 1982.

[50] J.P. Chiou, "A Variable Scaling Hybrid Differential Evolution for Solving Large-scale Power Dispatch Problem," *IET Gener. Transm. And Distrib.*, Vol. 3, No. 2, pp.154-163, Feb. 2009.

[51] C.B. Somuah, and N. Khunaizi, "Application of Linear Programming Redispatch Technique to Dynamic Generation Allocation," *IEEE Trans. on Power Syst.*, Vol. 5, No. 1, pp.20-26, Feb. 1990.

[52] F.N. Lee, L. Lemonidis, and K.C. Liu, "Price-based Ramp-rate Model for Dynamic Dispatch and Unit Commitment," *IEEE Trans. on Power Syst.*, Vol. 9, No. 3, pp.1233-1242, Aug. 1994.

[53] G. Irisarri, L.M. Kimball, K.A. Clements, A. Bagchi, and P.W. Davis, "Economic Dispatch with Network and Ramping Constrained via Interior Point Methods," *IEEE Trans. on Power Syst.*, Vol. 13, No. 1, pp.236-242, Feb. 1998.

[54] Y. Okumoto, N. Yorino, Y. Zoka, Y. Sasaki, T. Yamanaka, and T. Akiyoshi, "An Application of Robust Power System Security to Power System Operation for High-penetration of PV," *IEEE Innovative Smart Grid Technologies Europe (ISGT Europe 2012)*, pp.1-7, Berlin, Germany, 14-17 Oct. 2012.

[55] Y. Sasaki, D. Seikoba, J. Okihara, K. Kanaya, Y. Zoka, and N. Yorino, "A Robust Supply and Demand Controller against Uncertainties of Renewable Energy Sources," *18th Power Systems Computation Conference (PSCC2014)*, No. ID352, pp.1-6, Wroclaw, Poland, 18-22 Aug. 2014.

[56] T. Sawa and K. Furukawa, "Unit Commitment using Quadratic Programming and Unit Decommitment," *IEEE PES General Meeting 2012*, pp.1-6, San Diego, CA, 22-26 Jul. 2012.

[57] Y. Sasaki, S. Nobunaga, J. Okihara, Y. Zoka, and N. Yorino, "Development of the DS-Manager for Utilizing the Existing Generators," *The International Conference on Electrical Engineering*, No. 272, pp.1-6, Hong Kong, China, 5-9 Jul. 2015.

[58] K. Mahmoud, N. Yorino, and A. Ahmed, "Optimal Distributed Generation Allocation in Distribution Systems for Loss Minimization," *IEEE Trans. on Power Syst.*, Vol. 31, No. 2, pp.960-969, Mar. 2016.

[59] K. Mahmoud, N. Yorino, and A. Ahmed, "Power Loss Minimization in Distribution Systems Using Multiple Distributed Generations," *IEEJ Trans. on Elec. Electron. Eng*., Vol. 10, No. 5, pp. 521–526, May 2015.

[60] R. K. Swartman, "Correlation of Solar Radiation with Common Parameters in Toronto, Canada," *Solar Energy*, Vol. 13, No. 3, pp. 345-347 (1971).

[61] R. K. Swartman, "Solar Radiation Estimates from Common Parameters," *Solar Energy*, Vol. 11, No.3-4, pp.170-172 (1967).

[62] D. Yang, Z. Dong, T. Reindl, P. Jirutitijaroen, and W. M. Walsh, "Solar Irradiance Forecasting Using Spatio-temporal Empirical Kriging and Vector Autoregressive Models With Parameter Shrinkage," *Solar Energy*, Vol. 103, pp.550-562, (2014).

[63] G. Notton, C. Paoli, S. Vasileva, M. L. Nivet, J. L. Canaletti, and C. Cristofari, "Estimation of Hourly Global Solar Irradiation on Tilted Planes From Horizontal One Using Artificial Neural Networks," *Energy*, Vol. 39, No.1 , pp.166-179 (2012).

[64] R. Perez, E. Lorenz, S. Pelland, M. Beauharnois, G. V. knowe, K. H. Jr., D. Heinemann, J. Remund, S. C. Muller, and W. Traunmuller, "Comparison of Numerical Weather Prediction Solar Irradiance Forecasts in the US, Canada and Europe," *Solar Energy*, Vol. 94, pp.305-326 (2013).

[65] R. Perez, P. Ineichen, K. Moore, M. Kmiecik, C. Chain, R. George, and F. Vignola, "A New Operational Model For Satellite-derived Irradiances: Description and Validation," *Solar Energy*, Vol. 73, No. 5, pp.307-317 (2002).

[66] M. S. Ghonima, et all, "A method for cloud detection and opacity classification based on ground based sky imagery," *Atmospheric Measurement Techniques*, Vol. 5, No. 11, pp. 2881-2892 (2012).

[67] C. Cornaro, "Solar radiation forecast using neural networks for the prediction of grid Connected pv plants energy production (dsp project)," *Proc. on WIRE: Weather Intelligence for Renewable Energies*, 22 October 2014.

[68] G. Capizzi, C. Napoli, and F. Bonanno, "Innovative Second-Generation Wavelets Construction With Recurrent Neural Networks for Solar Radiation Forecasting," *IEEE Trans. on Neural Networks and Learning Systems*, Vol. 23, No.11, pp.1805-1815 (2012).

[69] W. F. Holmgren, A. Lorenzo, M. Leuthold, C. K. K. A. D. Cronin, and E. A. Betterton, "An Operational, Real-Time Forecasting System for 250 MW of PV Power Using NWP, Satellite, and DG Production data," *Photovoltaic Specialist Conference (PVSC)*, No. 14683377, 8-13 June 2014.

[70] A.T. Lorenzo, et.al, "Short-Term PV Power Forecasts Based on a Real-Time Irradiance Monitoring Network," *Photovoltaic Specialist Conference (PVSC)*, No. 14683253, 8-13 June 2014.

[71] M. Benghanem, A. Mellit, S.N. Alamri, "ANN-based modelling and estimation of daily global solar radiation data: A case study. Science Direct," *Energy Conversion and Management*, Vol.50, No.7 , pp.1644-1655 (2009).

[72] Serre, D. Matrices, "Theory and Application," Springer, New York(2002).

[73] G.B. Huang, Q.Y. Zhu, and C.K. Siew, "Extreme learning machine: Theory and applications," *Neurocomputing*, Vol. 70, pp.489-501 (2006).

[74] Y. Sasaki, K. Kanaya, D. Seikoba, J. Okihara, Y. Zoka, and N. Yorino," Probabilistic Constrained Dynamic Economic Load Dispatch for Renewable Energy Sources," *Grand Renewable Energy 2014 International Conference and Exhibition (2014)*.

[75] L. Ma and K. Khorasani, "Constructive feedforward neural networks using Hermite polynomial activation functions," *IEEE Trans. on Neural Networks*, Vol. 16, No. 4, pp.821-833 (2005).

[76] Japan Industrial Standard (JIS) C8907, “Estimation method of generating electric energy by PV power system,” 2005.

Appendix

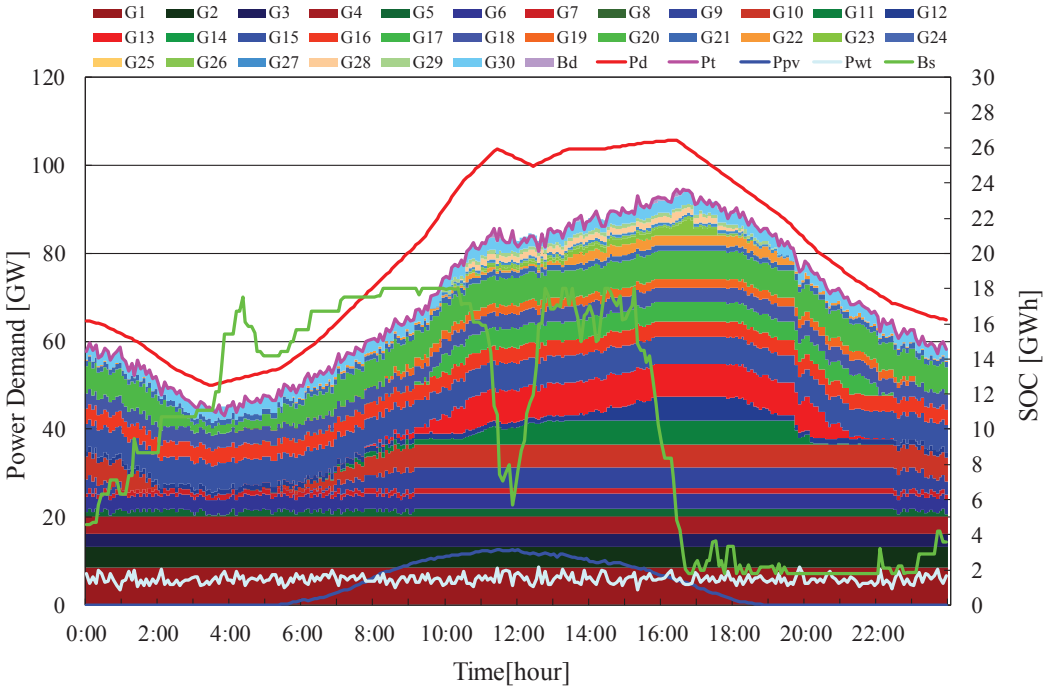

(a) Day-ahead 24-hour GS in Case 1.

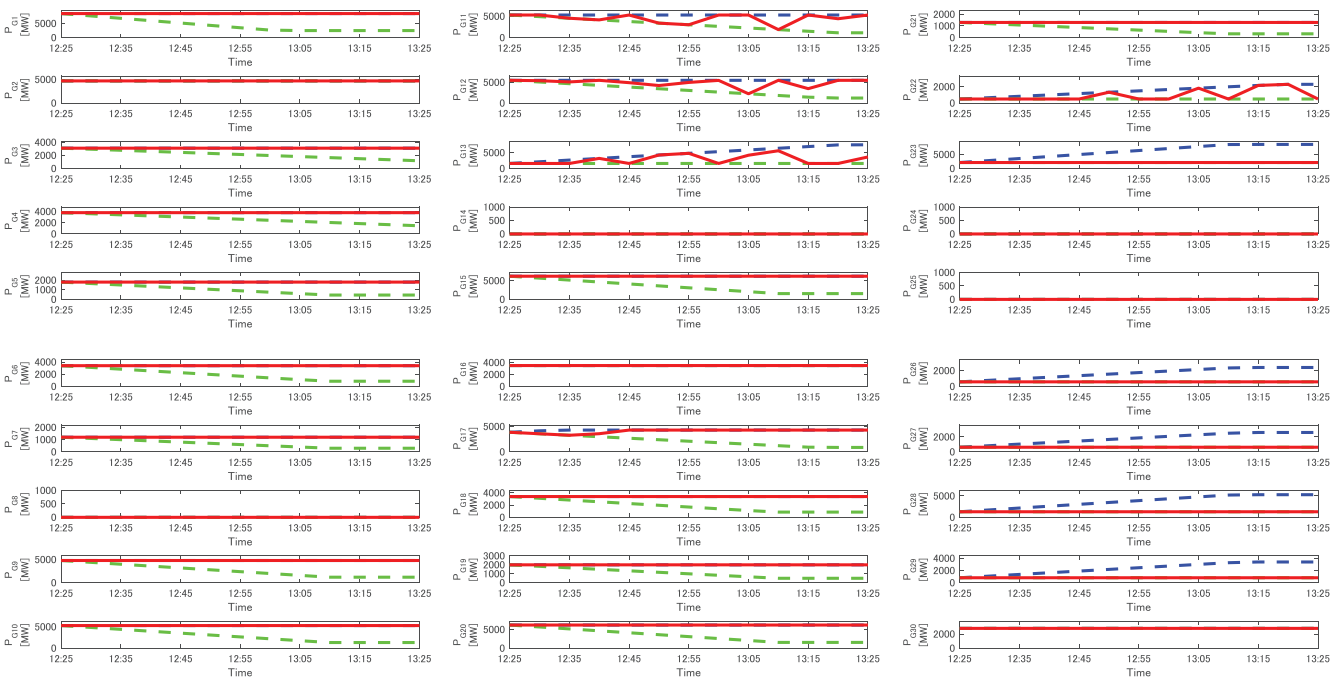

(b) Real-time 1-hour GS with RTDF in Case 1

Day-ahead 24-hour GS and Real-time 1-hour GS with RTDF for West Japan Power System Model in Case 1.

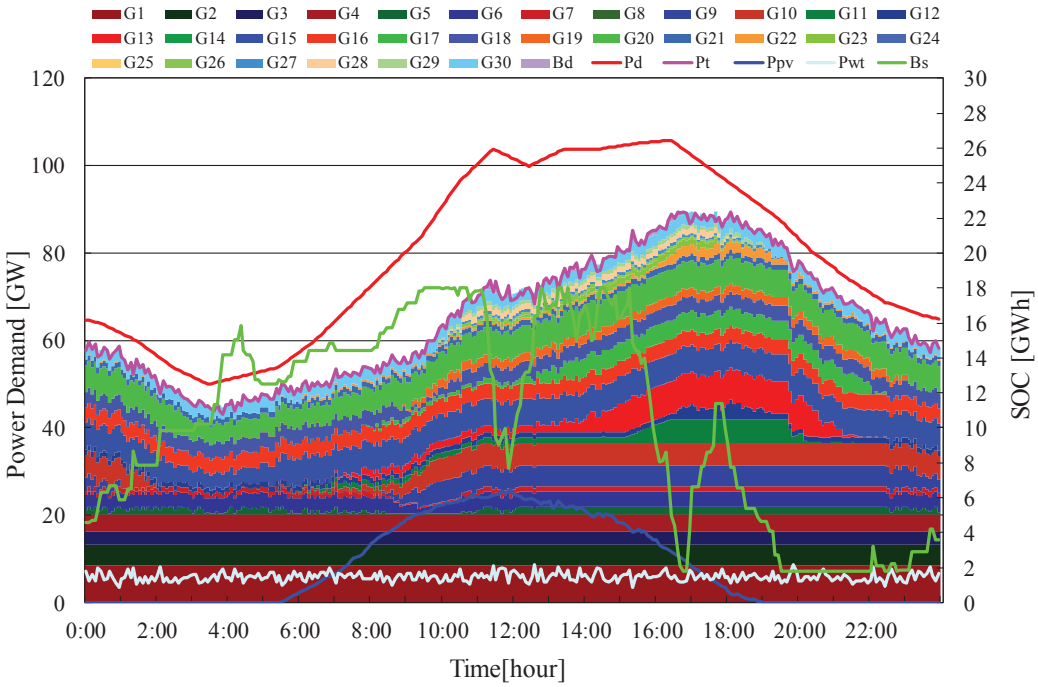

(a) Day-ahead 24-hour GS in Case 2.

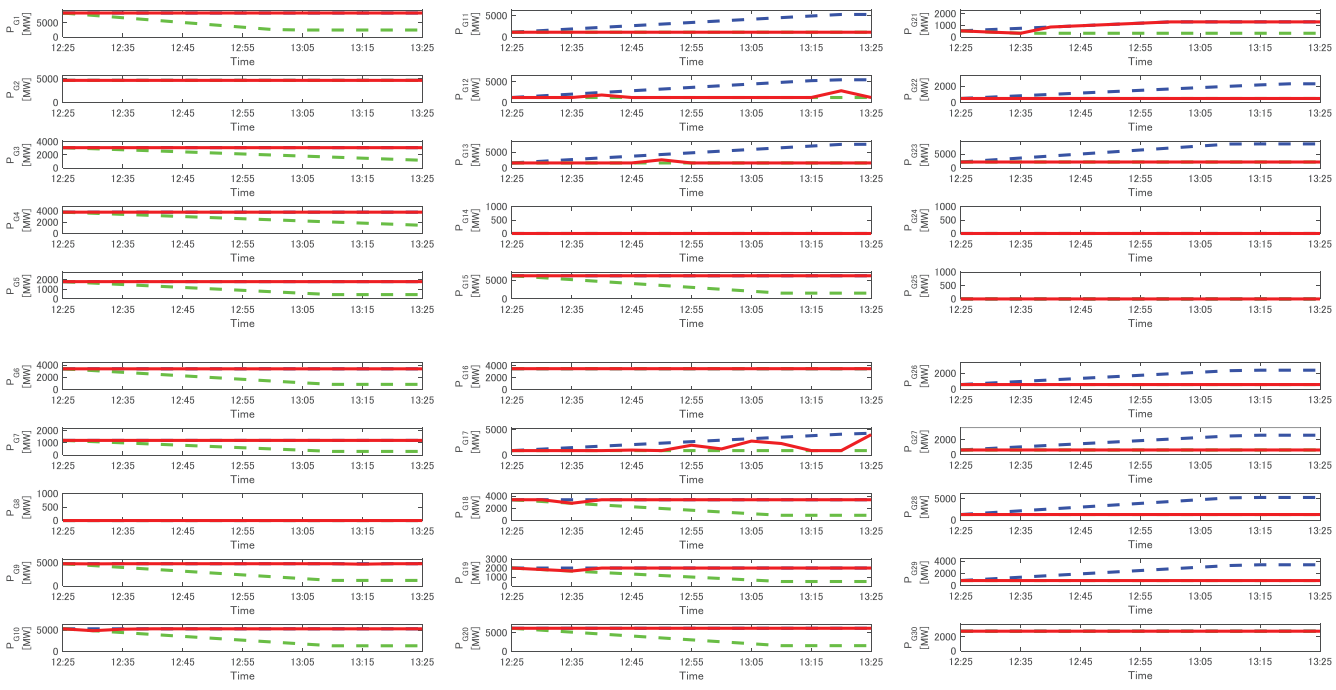

(b) Real-time 1-hour GS with RTDF in Case 2

(c)

Day-ahead 24-hour GS and Real-time 1-hour GS with RTDF for West Japan Power System Model in Case 2.

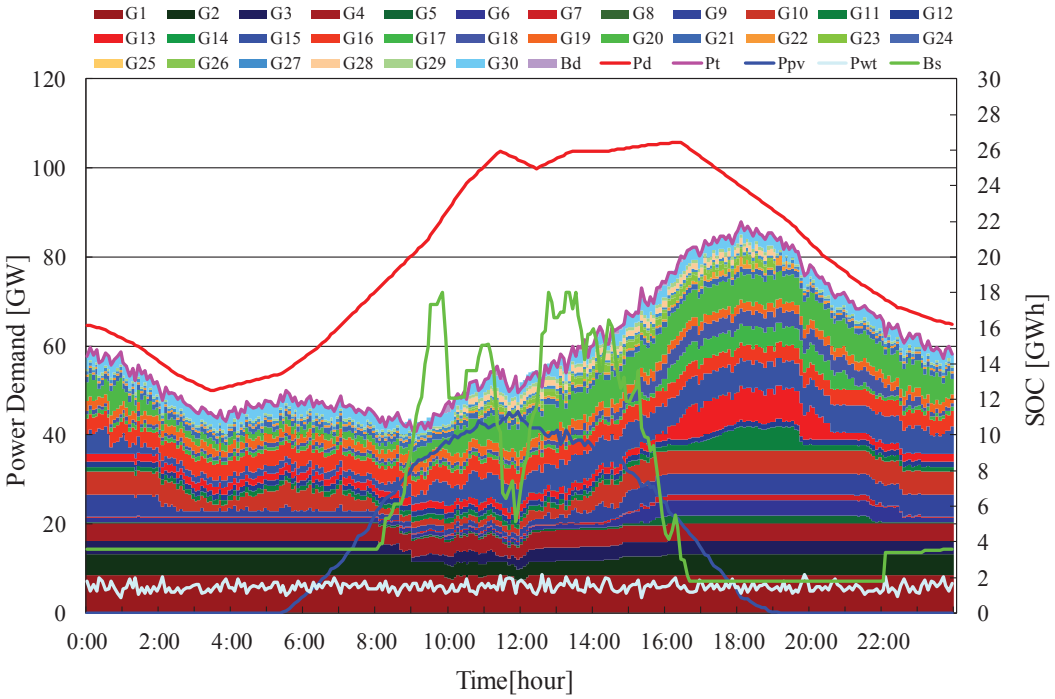

(a) Day-ahead 24-hour GS in Case 3.

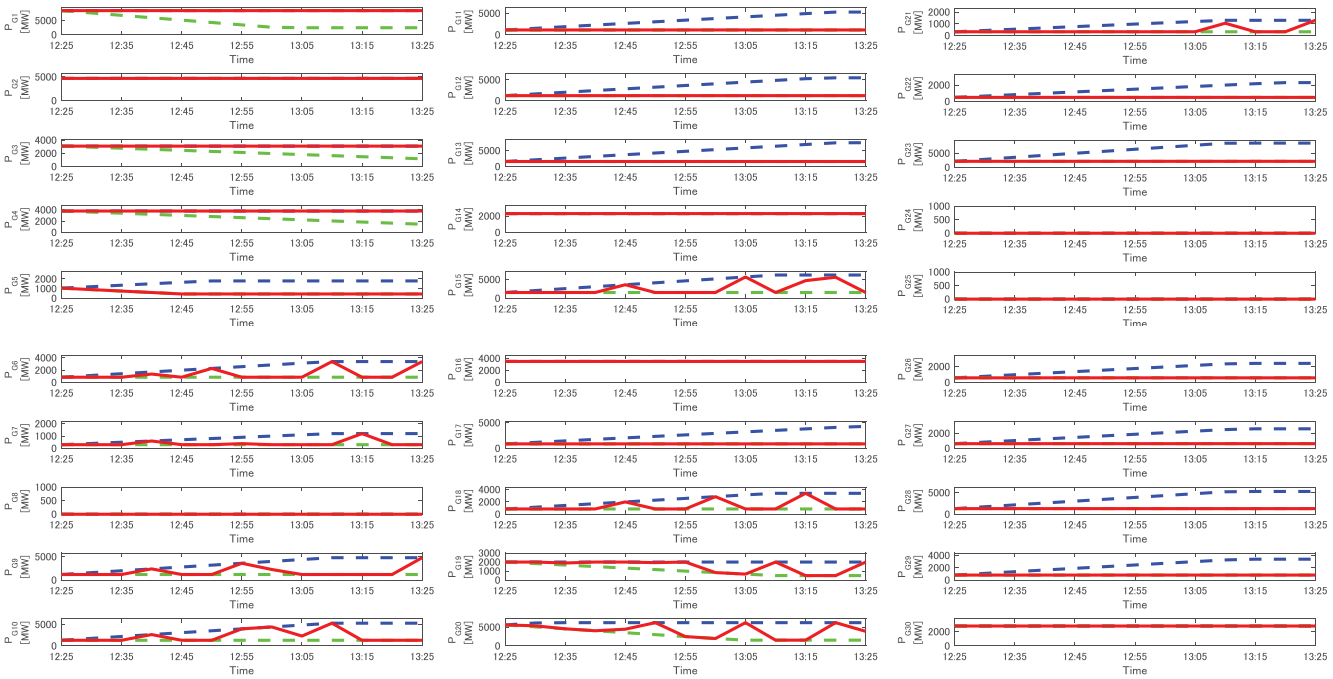

(b) Real-time 1-hour GS with RTDF in Case 3

Day-ahead 24-hour GS and Real-time 1-hour GS with RTDF for West Japan Power System Model in Case 3.

Author Publication

List of Publications

A. Transactions/International Journal Papers

(1) Yutaka Sasaki, Naoto Yorino, **Imam Wahyudi Farid**, Dai Seikoba, Mitsumasa Asada Liying Ma, and Yoshifumi Zoka, "A Simple and Reliable PV Forecasting Method for Local Area Energy Management", IEEJ Trans. on Power and Energy, Vol. 137, No.7, pp.1-8, July 2017.
佐々木豊, 餘利野直人, **Imam Wahyudi Farid**, 清木場大, 朝田光雅, 馬立英, 造賀芳文 "ローカル電力需給制御に適した太陽光発電量の予測手法," 電気学会論文誌 B, Vol. 137, No.7, pp.1-8, 2017.

(2) Yutaka Sasaki, Naoto Yorino, Yoshifumi Zoka, and **Imam Wahyudi Farid** "Robust Stochastic Dynamic Load Dispatch against Uncertainties," *IEEE Trans. on Smart Grid*, Vol. PP, No. 99, pp. 1-8, March 2017.

B. International and domestic Conference Papers Related to This Thesis

(1) Yutaka Sasaki, Naoto Yorino, Yoshifumi Zoka, **Imam Wahyudi Farid,** and Shinya Sekizaki, "Robust Dynamic Load Dispatch under Uncertainties", Proc. of *International Institute of Research and Education in Power System Dynamics Symposium (IREP2017)*, pp.1-13, August 27th– September 1st, 2017, Espinho, Portugal.

(2) Imam Wahyudi Farid, Mitsumasa Asada, Yutaka Sasaki, Naoto Yorino, and Yoshifumi Zoka , "Real-time PV Forecasting Method for Energy Management Operation," Proc. of *International Conference on Electrical Engineering (ICEE2017)*, pp.1-5, July 4th-7th, 2017, Weihai, China.

Robust Stochastic Dynamic Load Dispatch against Uncertainties

Y. Sasaki, *Member, IEEE*, N. Yorino, *Member, IEEE*, Y. Zoka, *Member, IEEE*, F.I. Wahyudi, *Student Member, IEEE*

***Abstract*--At present, electric power systems face difficulties in system operations due to rapid increase in uncontrollable renewable energy sources (RESs), such as photovoltaic power generations (PVs). Reduction of controllable resources also yields concerns about system reliability issues. This paper focuses on a new dynamic load dispatch method for mitigating the irregularity associated with RES. The developed load dispatch method is to schedule the committed generating units outputs so as to meet required irregular load demand estimation which is frequently updated in real-time operation circumstance. A new algorithm is proposed for unit commitment and stochastic dynamic economic load dispatch as an efficient solution for a day-ahead and a real-time generation schedule (GS), respectively, that fully utilizes the limited resources of a power system under uncertainties. Day-ahead and real-time PV forecasts with the co-relations of PV forecasting errors are effectively treated in the proposed method. Special feature of the proposed method different from the existing works lies in a frequent real-time update of GS by using a fast algorithm to maximize robustness against uncertainties.**

***Index Terms*--Uncertainties, Confidence Intervals, PV forecasting, Day-ahead and real-time generation schedule, Stochastic dynamic economic load dispatch.**

I. Introduction

RENEWABLE energy sources (RESs) such as photovoltaic power generations (PVs) and wind-turbine power generations (WTs) are expected to grow substantially in the near future. A reasonable estimation is that 20-30% of the amount of total energy will be delivered through such sources in the upcoming 15 years. PVs are clean and safety energy sources, while they are prone to cause degradation of power quality as well as grid security due to unforeseen weather conditions. Continuous sunlight intermittency, especially during cloudy days, incurs sudden intense changes in their outputs such as unpredictable significant ramp effect. The increasing renewable energy requires additional ramping abilities to maintain the grid stability. Development of sophisticated operation technology is a key subject.

Y. Sasaki is an Assistant professor with Graduate School of Engineering, Hiroshima University, 1-4-1 Kagamiyama, Higashi-Hiroshima, 739-8527 Japan (e-mail: yusasaki@hiroshima-u.ac.jp).

N. Yorino is a Professor with Graduate School of Engineering, Hiroshima University, (e-mail: yorino@hiroshima-u.ac.jp).

Y. Zoka is an Associate professor with Graduate School of Engineering, Hiroshima University (e-mail: zo@hiroshima-u.ac.jp).

F.I. Wahyudi is a Ph.D student with Graduate School of Engineering, Hiroshima University, (e-mail: d140188@hiroshima-u.ac.jp).

Novel methodologies for stochastic dynamic economic load dispatch (SDED) become necessary to guarantee secure operation in real-time scenarios [1]. This particular concern is common to various widely adopted power systems, where smart gird projects make use of all available controls including demand response [2]. In order to fully utilize controllable generators, development of robust and reliable load dispatching method is extremely of importance to effectively treat uncertainties [3] [5].

Various approaches have been proposed so far concerned with SDED problem, classified into two approaches. The first approach repeatedly performs static economic load dispatch (ELD) at each interval by taking into account the ramp rate constraints [6], [7]. The second approach determines generation schedule (GS) by solving a single optimization problem. The approach includes heuristic technique in dynamic programming [8], improved simulated annealing [9], [10], hybrid approach of Hopfield neural network and quadratic programming (QP) [11], variable scaling hybrid differential algorithm [12], re-dispatch algorithms using QP, linear programming (LP) and the Danzig Wolfe's decomposition technique [13], a multi-stage algorithm [14], and the interior point method [15].

However, these conventional approaches cannot fully manage large uncertainty and infeasibility of power system operations. Hafiz et al. [16] and Yorino et al. [17] have proposed time-sequence dynamic feasible region (TDF) approach to fully utilize ramp rate capabilities of controllable generators against uncertainties. The concept of Robust Power System Security [18] has been proposed by Okumoto et al. where safe-side treatment of uncertainty is suggested for important constraints related to system collapse.

In this paper, we propose a new energy management method based on Robust Power System Security. The proposed method is applied to micro energy management system (micro-EMS) controller (Fig. 1), where load and RES predictions are available online. Confidence intervals (CIs) of the RES prediction errors are specified depending on required reliability of system operation against system collapse. The proposed method updates the day-ahead GS a few times a day and provides 1-hour GS every 5 minutes in real-time operation. Contributions of this paper are as follows:

1. CIs and covariance matrix of prediction errors are used respectively in deterministic feasibility detection and probabilistic line flow management. The former realizes effective safe-side reserve management, while

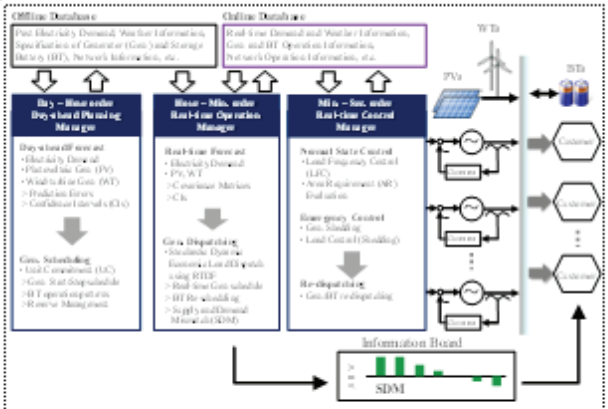

Fig. 1. The proposed micro-EMS controller.

the latter manages soft constraints of line overloading. The approach is new in the treatment of uncertainties.

ii. The paper also proposes new algorithms to realize the proposed uncertainty treatment, which include (1) an improved TDF, Robust TDF (RTDF) that effectively treats CIs, (2) an improved SDED method which combines RTDF, QP and liner stochastic load flow (SLF), and (3) an improved UC algorithm for day ahead 24-hour GS.

Advantage of the proposed method is that the supply and demand balance is kept to the maximum (high feasibility of dispatch) under uncertainties in real time power system operations. In case of a critical situation when the forecasted load cannot match the existing generator's capability, the method will detect the minimum amount of supply and demand mismatch in advance (1-hour before) and handle it reliably for the considered time horizon.

II. Outline Of The Micro-EMS Controller

A. Proposed Approach to Treat Uncertainties

We first carry out PV output forecast and its error analysis. A weather clustering method has been proposed for this purpose in [19]. A covariance matrix of PV output errors is calculated, while CIs of the PV forecast errors are specified depending on required reliability against system collapse.

The covariance matrices will be used in real-time GS in (31) for line flow control, while CIs are used in day-ahead unit commitment (UC) in (15) and real-time RTDF computation in (18) which is further used in real-time SDED in (32) to guarantee the supply and demand balance and reserve management.

B. Outline of the Controller

Our research target is to develop a micro-EMS controller that enforces robustness against uncertainties [19]. Figure 1 shows the configuration of the proposed management system: there are mainly three functions responsible for day-ahead operation planning, minute-order real-time operation, and second-order real-time control. Based on the prediction of RES outputs, the system manages the existing generators, storage battery (BT) and controllable demands in optimal manner.

C. Planning Manager

This manager provides an updated schedule of the output pattern for the limited resources. The output is represented as a 24-hour GS which also comprise the BT operation schedule, where a unit time is 30 minutes. Existing techniques for the UC can be fully utilized in the optimization process. Uncertainties related to the prediction and fluctuation of PV are handled particularly [19].

D. Operation Manager

The proposed method is related mainly to this part. which is the main subject of this paper. The operation manager provides real-time control signal to each generator using most recent real-time PV forecast.

E. Optimization

The optimization is performed in two stages. In stage I optimization, the 24-hour GS, which was planned in the previous day, is refined to determine the start/stop time schedule for generators. A robust GS against prediction error is determined. Stage II optimization utilizes only the start/stop time schedules and the BT operation. The rest of the optimization results of stage I is used only for reference and will be totally updated by stage II optimization, which will be proposed in the next section.

III. Formulation

A. Formulation for Stage I Optimization

The optimization problem is formulated with N_G controllable generators in a time horizon of T intervals ahead from the current moment as follows.

Minimize:

$$C^{OH}(\boldsymbol{P}_G, \boldsymbol{u}) = \sum_{t=1}^{T}\sum_{k=1}^{N_G} u_{kt}\cdot f_{kt} + \sum_{m=1}^{N_T}\sum_{k=1}^{N_G}\left(u_{kT_m} - u_{kT_{m'}}\right)\cdot suc_k \quad (1)$$

$$f_{kt} = a_k P_{Gkt}^2 + b_k P_{Gkt} + c_k \quad (2)$$

suc_k : start-up cost [$] of k-th generator

Subject to:

i. Supply and demand balance constraints.

$$\sum_{k=1}^{N_G} P_{Gkt} + B_{dt} - B_{et} = E[P_{Dt}] - E[P_{pvt}] - E[P_{WTt}] \quad (3)$$

ii. Upper and lower output of generator constraints.

$$P_{Gk}^{\min}\cdot u_{kt} \le P_{Gkt} \le P_{Gk}^{\max}\cdot u_{kt} \quad (4)$$

iii. Ramp-rate constraints.

$$-\delta_k\cdot\Delta t \le P_{Gk(t-1)} - P_{Gkt} \le \delta_k\cdot\Delta t \quad (5)$$

iv. Start/stop variables constraints.

$$0 \le u_{kt} \le 1 \quad (6)$$

v. Minimum continuity down time constraints.

$$if \quad (1-u_{kt})\cdot u_{k(t-1)} = 1$$
$$then \quad \sum_{t}^{t+mdt} (1-u_{kt}) = mdt_k \tag{7}$$

i. Minimum continuity up time constraints.

$$if \quad u_{kt}\cdot(1-u_{k(t-1)}) = 1$$
$$then \quad \sum_{t}^{t+mut} (1-u_{kt}) = mut_k \tag{8}$$

ii. BT charge/discharge output limits constraints.

$$0 \le B_{dt} \le B_d^{\max} \tag{9}$$
$$0 \le B_{ct} \le B_c^{\max} \tag{10}$$

With switching constraint:

$$B_{ct}\cdot B_{dt} = 0 \tag{11}$$

iii. BT upper and lower bounds of the state of charge.

$$B_s^{\min} \le B_{st} \le B_s^{\max} \tag{12}$$

iv. Dynamic transition of BT state of charge.

$$B_{st} = B_{s(t-1)} + \{B_{ct} - B_{dt}/\eta\}\cdot\frac{\Delta t}{60} \tag{13}$$

v. Line flow limits between node i and j.

$$-F_{ij}^{\max} \le F_{ijt} \le F_{ij}^{\max} \tag{14}$$

vi. DC power flow equation (23) in the next section

vii. Operating reserve power constraints.

$$\sum_{k=1}^{N_G} P_{Gk}^{\max}\cdot u_{kt} + B_{dt} - B_{ct} \ge \ddot{P}_{nt} + R_t \tag{15}$$

$$\sum_{k=1}^{N_G} P_{Gk}^{\min}\cdot u_{kt} + B_{dt} - B_{ct} \le \underline{\underline{P}}_{nt} \tag{16}$$

where, $P_{nt} = P_{Dt} - P_{PVt} - P_{WTt}$,

$\ddot{P}_{nt} = P_{Dt} - \underline{\underline{P}}_{PVt} - \underline{\underline{P}}_{WTt}$,

$\underline{\underline{P}}_{nt} = P_{Dt} - \ddot{P}_{PVt} - \ddot{P}_{WTt}$.

Where, C^{DH}: generation cost [$] for day-ahead GS, u_{kt}: start/stop variables of k-th generator at time t, P_{Gkt}: power output [MW] of k-th generator at time t, $\boldsymbol{P_G} \in \mathbb{R}^{N_G\times T}$: vector of P_{Gkt} (k=1,..,N_G, t=1,..,T), $\boldsymbol{u} \in \mathbb{R}^{N_G\times T}$: vector of u_{kt}, a_k, b_k, c_k: quadratic cost coefficients of k-th generator, T_{Pm}: time [min] at local maximum electricity demand (m=1,…,N_P), N_P: number of peak time, T_N: time [min] at minimum electricity demand, B_{ct}, B_{dt}: charge and discharge output power [MW] of BT at time t, respectively, P_{Dt}: electricity demand [MW] at time t, P_{PVt}: PV outputs [MW] at time t, P_{WTt}: WT outputs [MW] at time t, $E[\cdot]$: expected value [MW] at time t, $P_{Gk}^{\max}$, $P_{Gk}^{\min}$: maximum and minimum outputs [MW] of k-th generator, respectively, δ_k: ramp-rate limit [MW/min] of k-th generator, Δt: computational interval [min], mut_k, mdt_k: Minimum operating time [min] and minimum waiting time [min] of k-th generator, respectively, B_c^{max}, B_d^{max}: charge and discharge maximum power [MW] of BT, respectively, B_{st}: state of charge (SOC) [MWh] of BT at time t, B_s^{max}, B_s^{min}: maximum and minimum SOC bounds [MWh] of BT, respectively, η: charge/discharge efficiency of BT, F_{ijt}: line flow [MW] from node i to j governed by DC power flow equation, F_{ij}^{max}: maximum allowable line flow [MW] between node i and j, R_t: operating reserve power [MW] at time t, P_{nt}: net electricity demand at time t, $\ddot{P}_{nt}$, $\underline{\underline{P}}_{nt}$: upper and lower bounds [MW] of P_{nt} including CIs of RES prediction at time t, respectively.

Solution procedure will be given in section III-*E*. After obtaining the solution, we fix the start/stop time schedules and the BT charge/discharge operation, and then perform the next steps as below.

A. RTDF and Supply-Demand Mismatch using CIs

TDF is defined as the region of generator output P_{Gkt} reachable from a specified operating point and satisfying all constraints (3)-(5) with load forecasts $\hat{P}_{Dt}$ for t=1,..,T. TDF evaluation algorithm was proposed in [16] and [17], where the present operating point t=0 is used as a starting point in order to obtain reachable points successively in forward direction to t=T. TDF obtained by this calculation is represented as $TDF(t, \hat{P}_{Dt})$, which implies the region defined by the upper and lower bounds of each generator output at each time t=1…T.

In this paper, Robust TDF (RTDF) is defined taking into account CIs around the latest load predictions $\hat{P}_{Dt}$:

$$RTDF(t, \hat{P}_{Dt}) = \left\{TDF(t, \hat{P}_{Dt} + M_{Ut}) \bigcap TDF(t, \hat{P}_{Dt} - M_{Lt})\right\} \tag{17}$$

Where "$\bigcap$" implies the intersection. M_{Ut} and M_{Lt} are the assumed upper and lower limits of prediction errors, respectively. RTDF is obtained as the upper and lower bounds pair $\bar{\alpha}_{kt}$ and $\underline{\alpha}_{kt}$ (k=1,..,N_G, t=1,..,T) as follows.

$$\underline{\alpha}_{kt} \le P_{Gkt} \le \bar{\alpha}_{kt} \tag{18}$$

Calculation of RTDF is performed in each control cycle before stage II optimization in section III-*D*.

Once the upper and lower limits are obtained, any output values P_{Gkt} inside the limits (18) will be guaranteed as reachable if the latest load forecast errors appear inside CIs, $[\hat{P}_{Dt} - M_{Lt}, \hat{P}_{Dt} + M_{Ut}]$. In this algorithm, when $\bar{\alpha}_{kt} < \underline{\alpha}_{kt}$ is detected, RTDF is nonexistence and the supply-demand mismatch (SDM) is computed by (19).

$$SDM = \begin{cases} \underline{\alpha}_{kt} - \bar{\alpha}_{kt} & (when\ \bar{\alpha}_{kt} < \underline{\alpha}_{kt}) \\ 0 & (when\ \bar{\alpha}_{kt} \ge \underline{\alpha}_{kt}) \end{cases} \tag{19}$$

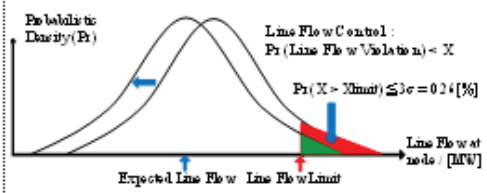

Fig. 2. Stochastic control of line flow.

SDM disappears. Then the optimization process is continued.

C. Stochastic Load Flow [20]-[22]

The prediction errors of loads and RESs result in line flow uncertainty. Line flow constraints are treated in a probabilistic manner as presented in Fig. 2. Assuming the normal distribution for the prediction error characteristic, linear DC power flow calculation method is used to provide the most efficient computation. The SLF method is applied in such a way that the probability of constraint violation is less than a specified value for each line. The stochastic network constraint is represented as in the following form.

$$LBF_l \le F_l = \sum_{i=1}^{N_n} S_{li} P_i \le UBF_l \tag{20}$$

UBF_l and LBF_l are the upper and lower bounds [MW] with respect to the transmission line l, F_l: amount of line flow [MW], N_n: number of nodes, S_{li}: conversion matrix, P_i: injection power [MW] into node i.

The formulation of (20) is given as below. Based on the DC power flow method, the following relationships hold.

$$S_N \theta = P \tag{21}$$

$$F = S_C \theta \tag{22}$$

Where, $\theta \in \mathbf{R}^{N\times 1}$: voltage angle matrices [rad], $P \in \mathbf{R}^{N\times 1}$: real power injection matrices [p.u.], $F \in \mathbf{R}^{N_l\times 1}$: real power line flow [p.u.], $S_N \in \mathbf{R}^{N\times N}$: node susceptance matrices [p.u./rad], $S_C \in \mathbf{R}^{N_l\times N}$: line susceptance matrices. From (21) and (22), we obtain:

$$F = S_C S_N^{-1} P = S \cdot P \tag{23}$$

Node injection P is represented as

$$P = P_G - P_D \tag{24}$$

Where P_D is a probabilistic variable consisting of loads and RES outputs (negative demands), while P_G corresponds to a variable of conventional generator outputs to be determined in the optimization process. Therefore, the expected value $E[P]$ of node injection power P is represented by the following expression:

$$E[P] = P_G - E[P_D] \tag{25}$$

Then, the mean value vector and covariance matrix of line flow are represented as follows:

$$E[F] = S[P_G - E[P_D]] = S \cdot P_G - S \cdot E[P_D] = [\mu_l] \tag{26}$$

$$\begin{aligned} Cov[F] &= E[(F - E[F])(F - E[F])^T] \\ &= S \cdot E[(P - E[P])(P - E[P])^T] \cdot S^T \\ &= S \cdot Cov[P] \cdot S^T = [\sigma_{ij}] \end{aligned} \tag{27}$$

Where, $Cov[P] = \begin{pmatrix} b_{11} & b_{12} & \cdots & b_{1n} \\ b_{21} & b_{22} & \cdots & \vdots \\ \vdots & \vdots & \ddots & b_{(n-1)n} \\ b_{n1} & \cdots & b_{n(n-1)} & b_{nn} \end{pmatrix}$.

The diagonal element b_{nn} is variance of P_{D_i}, the non-diagonal element is the covariance (Cov) of PV generation outputs.

The probability density function for line flow l may be described using the elements from (26) and (27):

$$\xi_{F_l}(F_l) = \frac{1}{\sqrt{2\pi}\sigma_{ll}} \exp\left\{-\frac{1}{2}\frac{(F_l - \mu_l)^2}{\sigma_{ll}^2}\right\} \tag{28}$$

In order to constrain the violation probability to a value less than X, threshold β is defined by the following equations.

$$X \ge 1 - \int_{-\overline{F}_l}^{\overline{F}_l} \xi_{F_l}(x)dx \tag{29}$$

$$\overline{F}_l - \beta \cdot \sigma_{ll} \ge \left|E[F_l]\right| \tag{30}$$

Further substitution of (30) into (28) yields stochastic load flow constraint below, where (31) is identical with (20).

$$-\overline{F}_l + \beta \cdot \sigma_{ll} + D_l \le \sum_{j=1}^{N_n} S_{lj} P_j \le \overline{F}_l - \beta \cdot \sigma_{ll} + D_l \tag{31}$$

where,

$$D_l = \sum_{i=1}^{N_n} S_{li} E[P_D^i].$$

D. Formulation for Stage II Optimization

The optimization problem (Stage II) is formulated with N_G controllable generators in a time horizon of T intervals ahead from the current moment as follows.

Minimize:

$$C^{RT}(P_G, u) = \sum_{i=1}^{T} \sum_{k=1}^{N_G} (a_k P_{Gki}^2 + b_k P_{Gki} + c_k) \tag{32}$$

Subject to:

(3), (5), (18), (31).

Constraints (18) and (31), which are explained in sections III-*B* and *C*, are the novel treatment of uncertainties by the proposed method. That is, the important constraint of the supply and demand balance is treated in deterministic manner by RTDF with CIs to avoid system collapse. On the other hand, soft constraints of line overloading are dealt with by DC probabilistic power flow. Covariance matrix and CIs will be

updated frequently in real-time operation, as is presented in the next section.

A. Computational Procedures

This section describes the computation procedure of the proposed method presented in the previous sections. The following procedures are performed in every control cycle.

< Day-ahead 24-hour GS: Stage I > (A few times a day)

Instead of standard approach using Mixed-Integer Linear Programming (MILP), we have developed a special technique by improving the method in [23] to solve the UC problem by using standard QP software. The effectiveness of the proposed technique has been studied in [24].

The day-ahead GS is obtained by using the following algorithm to determine the generator's output $\boldsymbol{P_G}$, its start/stop variable $\boldsymbol{u}$ and BT charge/discharge operation for 24 hours, where unit time is 30 minutes.

Step I-1 Read day-ahead forecast data for loads and RES.

Step I-2 Set iteration number $d = 0$.

Step I-3 Solve (1) by QP to determine $\boldsymbol{P_G}$ and $\boldsymbol{u}$, treated as continuous variables.

Step I-4 Compute unit fuel cost in (33) using present $\boldsymbol{P_G}$.

$$\mu_{kt}^{d} = a_k P_{Gkt} + b_k + c_k / P_{Gkt} \tag{33}$$

Step I-5 Solve the following problem with penalty function (35) using QP algorithm.

Minimize:

$$g(\boldsymbol{P_G}, \boldsymbol{u}, d, \boldsymbol{\mu}^d) = C^{DH}(\boldsymbol{P_G}, \boldsymbol{u}) + h(d, \boldsymbol{\mu}^d) \tag{34}$$

$$h(d, \boldsymbol{\mu}^d) = \sum_{k=1}^{N_G} \sum_{t=1}^{T} \left\{ 10^{-d+2} (d+2) (\mu_{kt})^d \right\} \tag{35}$$

Subject to: (3)-(16), and (23).

Step I-6 $d = d + 1$.

Step I-7 Repeat Steps I-4 to I-6 until the convergence is obtained.

Step I-8 Determine start/stop variables $\boldsymbol{u}$: if u_{kt}>0.5 (threshold) then set u_{kt}=1 else u_{kt}=0.

Step I-9 By fixing $\boldsymbol{u}$, solve (1) to obtain $\boldsymbol{P_G}$ using QP algorithm.

The obtained start/stop time for generators and BT operation for 24-hour GS will be used in stage II as predetermined schedule. The generator's outputs P_{Gkt} are used as only reference for operators.

< Real-time 1-hour GS: Stage II > (Every 5 minutes)

The real-time GS is carried out to minimize the generator's output and BT charge/discharge operation (if necessary) every 5 minutes.

Step II-1 Read data of day-ahead generator's start/stop variables and BT charge/discharge operations.

Step II-2 Update forecasts (load and RES), covariance matrices, and CIs using most recent data. Perform state estimation to obtain the present operating condition.

Step II-3 Calculate RTDF and Supply-Demand Mismatch (SDM). If SDM is non-zero, arrange relevant reserve by modifying BT operation schedule, or using other resources corresponding to detected value of SDM, and perform RTDF update to confirm zero SDM.

Step II-4 Compute UBF_l and LBF_l.

Step II-5 Solve problem (32) by QP software to obtain GS: P_{Gkt} (k=1,..,N_G, t=5,10,.., 60[min]).

The obtained GS is monitored by system operator, where GS in 5 minutes ahead are sent to the individual generators as real-time control signal.

II. Case Studies

A. Simulation Conditions

The proposed method is demonstrated using an example system in Fig. 3. The generation mix data are from a Japanese smart grid project where the installed PV an WT generation are about 15% of peak load. It is composed of three diesel generators, two load areas with RESs and a BT station. Detail data are given in Tables I. PV prediction data is shown in Fig. 4, which has been given by our forecasting method based on the weather clustering type neural network. Typical load patterns are used in the proposed optimization process.

B. Stage I optimization

Figure 5 shows the result of stage I optimization, describing 24-hours GS for generators (P_{G1}, P_{G2}, P_{G3}), BT operation (P_{BT}=B_d -B_c), electricity demand (P_D), net electricity demand (P_n), PV output (P_{PV}) predictions, WT outputs (P_{WT}), and SOC of BT (B_s). Note that G2 starts up at 11:00 and shuts down at 18:15 shown in Table II, which will be fixed in the stage II optimization.

C. Stage II optimization

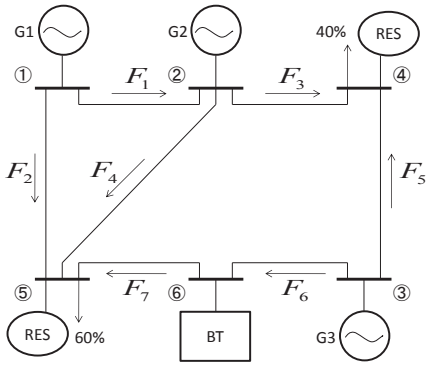

Fig. 3. Test Power System.

TABLE I
Specification of three diesel generators.

k	Output Limit [kW]	Ramp Rate [kW/min]	Start-up Cost (suc_k) [$]	Cost Coefficients[100$]		
				a_k	b_k	c_k
G1	1,000~2,000	66.7	40.00	0.0011	16.416	4,320.00
G2	625~1,250	41.7	25.00	0.0021	17.410	3,667.50
G3	1,125~2,250	75.0	45.00	0.0002	20.178	3,993.70

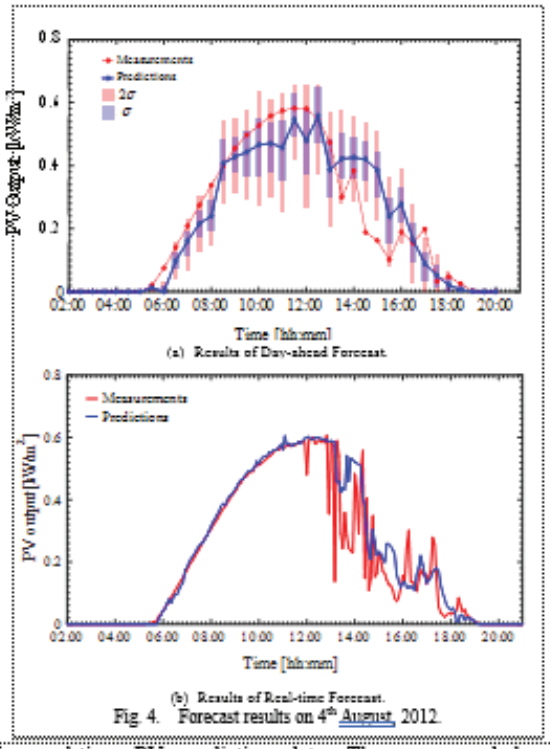

Fig. 4. Forecast results on 4th August, 2012.

on real-time PV prediction data. The upper and lower tolerances of prediction errors in net demands (load – RES) are set as a linear function of time as follows:

$$M_{Dt} = M_{Lt} = \hat{P}_{Dt} \times \frac{t}{T} \times \gamma \quad (36)$$

Where, $\hat{P}_{Dt}$ (t=0,1,…,T) are the most recent forecasted net power demands. T=60 [min], t: prediction time (t=0 for present operating point), γ is a parameter representing 1 hour ahead maximum prediction error, and γ= [0%, 10%, 20%] will be examined. Allowable constraint violation for line flow is set to $X=3\sigma=0.26$[%] in this examination.

Figure 6 shows the result of stage II optimization obtained at 17:30 (weekday, γ=10%). The upper and lower limits of RTDF and 1-hour GS for each generator are provided. The GS at 5 minutes ahead (17:35) is sent to each generating unit as a control signal. RTDF implies reachable area from the operating point at 17:30. The larger RTDF, the larger system capability that copes with uncertainty is expected. RTDF computation also successfully provides SDM 1-hour before the operation, which is given as P_{mis} that appears at 18:25. This advantageous characteristic come from the RTDF computation which identifies the feasible region with high accuracy. Note that the detected SDM is managed by the rescheduling of the BT operation 1-hour before by the proposed method. If BT cannot cope with the situation, we can prepare additional action such as demand response or load shedding at 18:25.

Figure 7 shows the scheduled F_3 line flow, which may vary inside 3σ allowable intervals. The result shows that SLF works successfully to avoid overloads in stage II optimization.

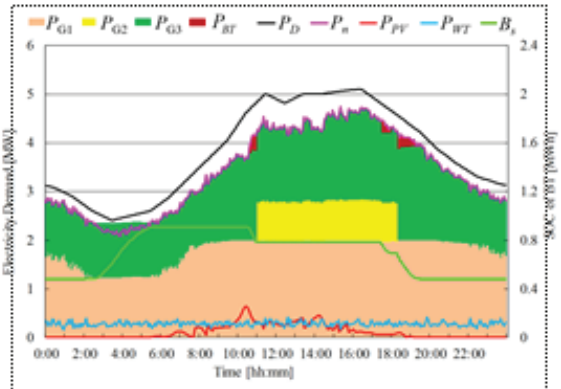

Fig. 5. Day-ahead 24-hour GS.

TABLE II
Start-up and shut-down times data from day-ahead UC.

Demand	Unit k	Start-up time	Shut-down time
Weekday	G1	-	-
	G2	11:00	18:15
	G3	-	-

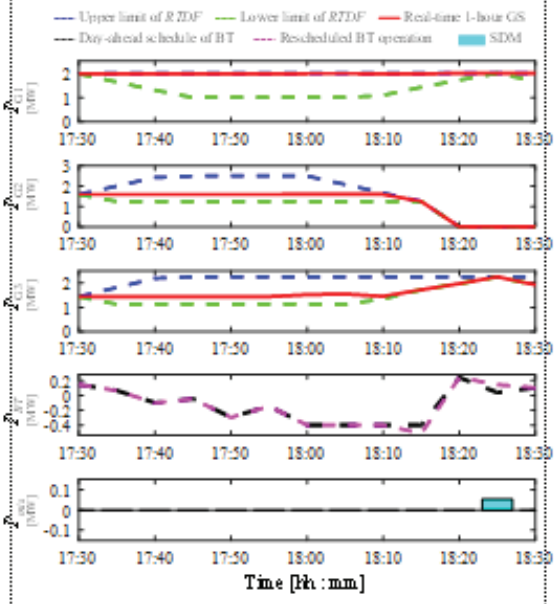

Fig. 6. Real-time 1-hour GS with RTDF and SDM.

Figure 8 describes the simulated results after 24-hour operations by the proposed real-time optimized control method. Descriptions of wave forms are given below the figure caption. We see that the PV prediction 1-hour ahead in the 2nd graph is erroneous. Nevertheless, the proposed method successfully treats the uncertainties to control generators as seen in 4-6th graphs, Rescheduled BT operation in the 7th graph has completely absorbed the SDM detected in Fig. 6. As a result, the frequency deviations are suppressed less than 0.2 Hz as observed in 8th graph. The frequency fluctuation has

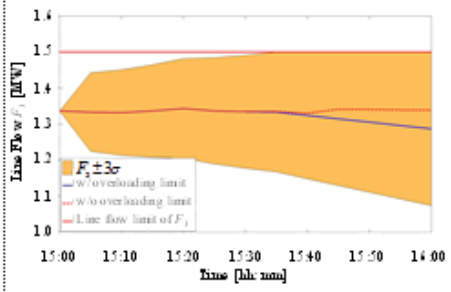

Fig. 7. Line Flow with 3σ allowable intervals at line F_3.

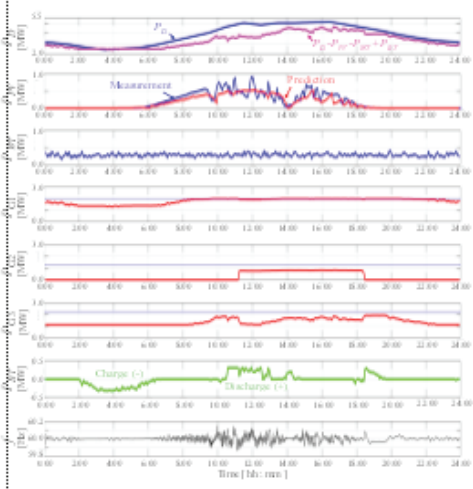

Fig. 8. The results of the 24-hour operations.
(From top: 1: P_D and net demand (=P_D-P_{PV}-P_{WT}+P_{BT}) [2~5.5MW], 2: P_{PV} (prediction 1-hour ahead and measurement) [0~1MW], 3: P_{WT} [0~1MW], 4: P_{G1}, 5: P_{G2}, 6: P_{G3} [0~3MW], 7: P_{BT} [-0.5 ~0.5MW], and 8: f system frequency [59.8~60.2Hz], where [*~**] describes full scale of each graph)

been analyzed by the simulator in the proposed micro-EMS controller in Fig.1. The frequency deviations increase mainly due to PV output fluctuations as well as the prediction errors in the day time. Thus, the proposed method reliably manages the uncertainties in the real-time power system operation.

Table III shows the computational burden (CPU Time), which is evaluated for test power systems with 3, 5, and 10 generators using Intel Core i7, 2.20GHz, 8GB memory.

The CPU time on Stage I implies a total computation time from Steps I-2 to I-9 in Section III-*E* for obtaining a day-ahead 24-hour GS. Stage II computation time is for the calculation of Steps II-3 to II-5 in Section III-*E* for obtaining a real-time 1-hour GS that is to be repeated every 5 minutes. Note that the numbers in the blanket imply the computation time for RTDF and SDM.

TABLE III
CPU Time

Number of Generators	Stage I for day-ahead 24-hour GS [sec]	Stage II for real-time 1-hour GS[sec]
3	3.0	0.37 (0.011)
5	4.4	0.44 (0.012)
10	9.4	1.87 (0.054)

V. Conclusion

Integrating large amounts of intermittent RESs into electric power systems causes various difficulties such as the supply and demand balance and frequency problems. In such situations, treatment of uncertainty by means of limited controllable resources is a critical issue for secure power system operations. Frequent evaluation of generation schedule is effective for minimizing prediction errors in order to establish a reliable operation against sudden changes in RES generations. The paper proposes a new real-time optimization method guaranteeing feasibility of operations. Uncertainties affecting the important constraint of the supply and demand balance are treated in deterministic manner using CIs to avoid system collapse, while those relating to soft constraints of line overloading are dealt with by DC probabilistic power flow.

Although the computation time is a critical issue, the proposed method provides a solution for introducing a large amount of RES into a smart grid operation.

The present version of the proposed method utilizes the DC power calculation method which may degenerate the accuracy when applied to low voltage distribution systems with large values of R/X. The use of extended equations based on a distribution power flow [25], [26] seems an interesting trial in the future.

VI. References

[1] J. Zhu, "Optimization of Power System Operation," Wiley-IEEE Press, Second Edition, Jan. 2015.

[2] A. Ipakchi, and F. Albuyeh, "Grid of the future," *IEEE Power and Energy Magazine*, Vol. 7, No. 2, pp.52-62, Feb. 2009.

[3] N. Yorino, Y. Sasaki, S. Fujita, Y. Zoka, and Y. Okumoto, "Issues for Power System Operation for Future Renewable Energy Penetration: Robust Power System Security," *Electrical Engineering in Japan*, Vol. 182, No. 1, pp. 30-38, Jan. 2013.

[4] [A2 2] N. Yorino, Y. Sasaki, E.P. Hristov, Y. Zoka, and Y. Okumoto, "Dynamic Load Dispatch for Power System Robust Security against Uncertainties," *2013 IREP Symp. Bulk Power System Dynamics and Control - IX Optimization, Security and Control of the Emerging Power Grid*, pp.1-17, Crete, Greece, 25-30 Aug. 2013.

[5] [A2 3] N. Yorino, M. Abdillah, Y. Isoya, Y. Sasaki, and Y. Zoka, "A New Method of Evaluating Robust Power System Security Against Uncertainties," *IEEJ Trans. on Elect. and Electron. Eng.*, Vol.10, No.6, pp. 636-643, Nov. 2015.

[6] D.W. Ross, and S. Kim, "Dynamic Economic Dispatch of Generation," *IEEE Trans. on Power App. and Syst.*, Vol. PAS-99, No. 6, pp.2060-2068, Nov. 1980.

[7] T. Li, and M. Shahidehpour, "Dynamic Ramping in Unit Commitment," *IEEE Trans. on Power Syst.*, Vol. 22, No. 3, pp.1379-1381, Aug. 2007.

[8] W.G. Wood, "Spinning Reserve Constrained Static and Dynamic Economic Dispatch," *IEEE Trans. on Power App. and Syst.*, Vol. PAS-101, No. 2, pp.381-388, Feb. 1982.

[9] D.N. Simopoulos, S.D. Kavatza, and C.D. Vournas, "Unit Commitment by an Enhanced Simulated Annealing Algorithm," *IEEE Trans. on Power Syst.*, Vol. 21, No. 1, pp.68-76, Feb. 2006.

[10] C.L. Chen, "Simulated Annealing-based Optimal Wind-thermal Coordination Scheduling," *IET Gener. Transm. and Distrib.*, Vol. 1, No. 3, pp.447-455, May 2007.
[11] A.Y. Abdelaziz, M.Z. Kamh, S.F. Mekhamer, and M.A.L. Badr, "A Hybrid HNN-QP Approach for Dynamic Economic Dispatch Problem," *Electric Power Systems Research*, Vol. 78, No. 10, pp.1784-1788, Oct. 2008.
[12] J.P. Chiou, "A Variable Scaling Hybrid Differential Evolution for Solving Large-scale Power Dispatch Problem," *IET Gener. Transm. And Distrib.*, Vol. 3, No. 2, pp.154-163, Feb. 2009.
[13] C.E. Somuah, and N. Khunaizi, "Application of Linear Programming Redispatch Technique to Dynamic Generation Allocation," *IEEE Trans. on Power Syst.*, Vol. 5, No. 1, pp.20-26, Feb. 1990.
[14] F.N. Lee, L. Lemonidis, and R.C. Liu, "Price-based Ramp-rate Model for Dynamic Dispatch and Unit Commitment," *IEEE Trans. on Power Syst.*, Vol. 9, No. 3, pp.1233-1242, Aug. 1994.
[15] G. Irisarri, L.M. Kimball, K.A. Clements, A. Bagchi, and P.W. Davis, "Economic Dispatch with Network and Ramping Constrained via Interior Point Methods," *IEEE Trans. on Power Syst.*, Vol. 13, No. 1, pp.236-242, Feb. 1998.
[16] [A2 5] H.M. Hafiz, N. Yorino, Y. Sasaki, and Y. Zoka, "Feasible Operation Region for Dynamic Economic Dispatch and Reserve Monitoring," *European Trans. on Electrical Power*, Vol. 22, No. 7, pp.924-936, Oct. 2012.
[17] [A2 6] N. Yorino, H.M. Hafiz, Y. Sasaki, and Y. Zoka, "High-speed Real-time Dynamic Economic Load Dispatch," *IEEE Trans. on Power Syst.*, Vol. 27, No. 2, pp.621-630, May 2012.
[18] Y. Okumoto, N. Yorino, Y. Zoka, Y. Sasaki, T. Yamanaka, and T. Akiyoshi, "An Application of Robust Power System Security to Power System Operation for High-penetration of PV," *IEEE Innovative Smart Grid Technologies Europe (ISGT Europe 2012)*, pp.1-7, Berlin, Germany, 14-17 Oct. 2012.
[19] Y. Sasaki, D. Saikoba, T. Okihara, K. Kanaya, Y. Zoka, and N. Yorino, "A Robust Supply and Demand Controller against Uncertainties of Renewable Energy Sources," *18th Power Systems Computation Conference (PSCC2014)*, No. ID352, pp.1-6, Wroclaw, Poland, 18-22 Aug. 2014.
[20] B. Borkowsk, "Probabilistic Load Flow," *IEEE Trans. on, Power App and Syst.*, Vol. 93, No. 3, pp.752-759, May 1974.
[21] J.F. Dopazo, O.A. Klitin, and A.M. Sasson, "Stochastic Load Flows," *IEEE Trans. on Power App. and Syst.*, Vol. 94, No. 2, pp.299-309, Mar. 1975.
[22] C.L. Su, "Probabilistic Load-Flow Computation Using Point Estimate Method," *IEEE Trans. on Power Syst.*, Vol. 20, No. 4, pp.1843-1851, Nov. 2005.
[23] T. Sawa and K. Furukawa, "Unit Commitment using Quadratic Programming and Unit Decommitment," *IEEE PES General Meeting 2012*, pp.1-6, San Diego, CA, 22-26 Jul. 2012.
[24] Y. Sasaki, S. Notsunaga, T. Okihara, Y. Zoka, and N. Yorino, "Development of the DS-Manager for Utilizing the Existing Generators," *The International Conference on Electrical Engineering*, No. 272, pp.1-6, Hong Kong, China, 5-9 Jul. 2015.
[25] K. Mahmoud, N. Yorino, and A. Ahmed, "Optimal Distributed Generation Allocation in Distribution Systems for Loss Minimization," *IEEE Trans. on Power Syst.*, Vol. 31, No. 2, pp.960-969, Mar. 2016.
[26] K. Mahmoud, N. Yorino, and A. Ahmed, "Power Loss Minimization in Distribution Systems Using Multiple Distributed Generations," *IEEJ Trans. on Elec. Electron. Eng.*, Vol. 10, No. 5, pp. 521–526, May 2015.

VII. BIOGRAPHIES

Naoto Yorino (M'90) received B.S., M.S. and Ph.D. degrees in Electrical Engineering from Waseda University, Japan, in 1981, 1983, and 1987, respectively. He is a Professor, Vice Dean, Faculty of Engineering, Hiroshima University, Japan. He was with Fuji Electric Co. Ltd., Japan from 1983 to 1984. He was a Visiting Professor at McGill University, Montreal, QC, Canada, from 1991 to 1992, Vice President of PE&S, the IEE of Japan from 2009 to 2011. Dr. Yorino is a member of IEEE, CIGRE, iREP.

Yutaka Sasaki (M'08) received B.S., M.S. and Ph.D degree in Electrical Engineering from Hokkaido University, Japan in 2004, 2006, and 2008, respectively. He is an Assistant Professor at Hiroshima University. He was a Visiting Scholar at Washington State University, Pullman, WA, USA from 2012 to 2013. His research interests include optimal planning and operation of power system including renewable energy resources.

Yoshifumi Zoka (M'99) received B.S. degree in Electrical Engineering, M.S. and Ph.D. degrees in Systems Engineering from Hiroshima University, Japan. He is currently an Associate Professor in Graduate School of Engineering, Hiroshima University. He was a Research Associate at University of Washington, Seattle, WA, USA from 2002 to 2003. His research interest lies in power system planning, stability and control problems.

Farid Imam Wahyudi (S'16) received B.S. degree in Electrical Engineering from Institute Technology of Sepuluh Nopember (ITS), Indonesia in 2012, M.S. degree in 2014. He is currently for pursuing a PhD in the area of PV Forecasting using artificial intelligent at Graduate School of Engineering, Hiroshima University. His research interest lies in power system and application of the artificial intelligent.

電気学会論文誌B（電力・エネルギー部門誌）
IEEJ Transactions on Power and Energy
Vol.137 No.7 pp.●-●●●　DOI: ●●●/ieejpes.●●●●

論　文

ローカル電力需給制御に適した太陽光発電量の予測手法

正　員　佐々木　豊*　上級会員　餘利野　直人*a)　非会員　Farid Imam Wahyudi*
正　員　清木場　大*　学生員　朝田　光雅*　非会員　馬　立英**　上級会員　造賀　芳文*

A Simple and Reliable PV Forecasting Method for Local Area Energy Management

Yutaka Sasaki*, Member, Naoto Yorino*a), Senior Member, Farid Imam Wahyudi*, Non-Member, Dai Seikoba*, Member,
Mitsumasa Asada*, Student Member, Liying Ma**, Non-Member, Yoshifumi Zoka*, Senior Member

(2016年5月9日受付，2017年3月9日再受付)

Various forecasting methods for photovoltaic (PV) generations have been proposed so far. However, the conventional methods cannot be widely used in various situations because they require sophisticated data that cannot easily be obtained. Furthermore, the prediction accuracy of such methods tend to deteriorate especially due to lack of data.

This paper proposes a simple and reliable PV forecasting method for local energy management. The proposed method uses only public weather forecasting data that is easily obtained. The method maintains high accuracy by using the real time correlation data between the target and neighboring areas. Multiple neural networks are effectively used based on a weather clustering technique. It has been confirmed that the proposed method shows the robustness in the prediction accuracy when used for local area PV prediction.

キーワード：不確定性，太陽光発電予測，ローカル電力需給制御
Keywords: Uncertainties, PV Forecasting, Local Energy Management

1. はじめに

環境負荷低減の観点から運用時に化石燃料を消費しない再生可能エネルギー電源（Renewable Energy Source; RES）が注目されている。特に，我が国では太陽光発電（Photovoltaic; PV）の積極的な導入設置が活発に行われている[1]。しかし，PVは，日射量の時間的・空間的変化により出力が不確定になる。そのため，既存の火力発電機やディーゼル発電機等の可制御電源群によって，出力計画と制御を行いながら，電力供給の安定化を図っていく必要がある。一方で，日射量の正確な予測ができれば，既存火力機や水力機，および蓄電池(Battery; BT)を含むエネルギー貯蔵装置の効率的な運用計画が可能となる。さらに，予測誤差やその分布を解析すること安定な需給制御に向けた予備力確保も可能となる。このような背景から，一般に予測手法の開発に加え予測に基づく高度な発電機の需給制御手法が重要視され，著者らも需給制御シミュレータとして図1に示すツール(需給マネージャ)を開発している[2-4]。需給マネージャは，ビル単位の小規模系統から離島系統レベルまでのシステムを対象に，需給計画/運用制御を行うマネージャである。著者らは，小規模系統を対象とした需給マネージャ用の翌日およびリアルタイム予測手法ついて検討おり[5-8]，本論文ではローカルな地域における最小限の気象情報のみを用いた翌日およ

a) Correspondence to: Naoto Yorino. E-mail: yorino@hiroshima-u.ac.jp
* 広島大学大学院工学研究科
〒739-8527　広島県東広島市鏡山1-4-1
Graduate School of Engineering, Hiroshima University.
1-4-1 Kagamiyama, Higashihiroshima, Hiroshima, Japan 739-8527
** Concordia University
7141 Rue Sherbrooke O, Montréal, QC H4B 1R6, Canada

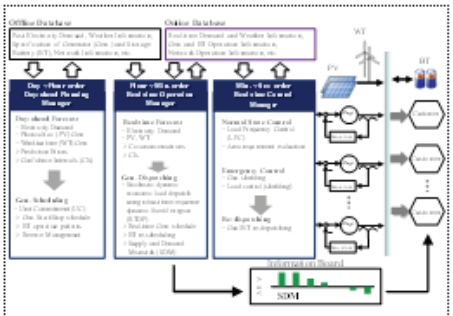

Fig. 1. The proposed supply and demand management controller.

びリアルタイム PV 発電量予測手法について報告する。提案する予測手法では，翌日・リアルタイム予測値とその予測誤差，いわゆる信頼性区間(Confidence Intervals; CIs)を直接的に求め，需給制御にそのまま利用することができる。

PV発電量予測に関する先行事例として，これまでにさまざまな予測手法が提案されている。例えば，地上からの雲画像の観測・解析に基づく手法[9]，気象衛星による雲画像の観測に基づく手法[10]が報告されているが，地上カメラまたは上空衛星から得られる多くの情報を解析しなければならない。一方，容易に入手できる天気予報データを用いた推定式に基づく予測手法[11, 12]が提案されているが，天気予報は簡易的に得られるものの，予測値と信頼区間を直接的に求めることはできていない。また，ディーゼル発電・蓄電池を組み合わせたハイブリッドシステムへのピンポイントPV発電量予測の適用[13]が検討されているが，マイクログリッドなどのローカル需給制御への具体的な適用には至っていない。ローカルな配電システムに適用した事例としては，配電系統に設置される計測機器を用いた相関分析を用いた予測手法[14]が提案されているが，すべての変電所に日射計が備わっていることを前提にしている。従来手法では対象問題毎に，それぞれの問題に対応した，一般には容易に入手できない高度なデータが必要である。また，複数種類のデータを用いることで高精度な予測手法であっても計算負荷が増大する。すなわち，ローカル地域での適用が難しい。

本論文では，ローカル地域の電力需給制御を対象としたより実用的なPV発電量予測手法を提案する。特に，

(1) 一般に容易に入手できるデータだけを用いること
(2) 条件不利地域におけるローカル需給制御を実施可能な精度を有すること

の条件を満足するよう実用的な予測手法を提案する。

このように提案法は，気象に関するデータ取得が困難なローカル地域の電力需給制御における PV 発電量予測手法である。従来法ほどの予測精度は期待できないかもしれないが，小規模系統の需給制御(翌日発電機起動停止計画，リアルタイム発電機運済負荷配分制御)には十分な精度であることを検証済みである[5]。広島大学工学部実験研究棟(広島県東広島市)に設置したPV を対象に検討を実施している。

第 2 章では，提案法を実装する需給マネージャについて論じる。第 3 章では予測学習に用いたニューラルネットワーク(Neural Network; NN)に基づく学習を用いた日射量予測手法を論じる。NN は翌日およびリアルタイム PV 発電量予の両方に用いているが，第 3 章では特に，翌日 PV 発電量予測手法について論ずる。次に，第 4 章ではリアルタイムPV 発電量予測手法について説明する。ここでは時空間的要素を考慮するために「隔たり時間」という考えを提案し，NN 法と組み合わせて予測を行う。

2. 需給マネージャの機能

著者らは，図 1 に示した需給制御シミュレータ(需給マネージャと呼ぶ)を開発している[3,4]。需給マネージャが管理するシステムとしては，ビル単位の小規模系統から離島系統レベルまでのシステムを想定している。小規模系統は，太陽光発電，ディーゼル発電機，蓄電池，負荷需要で構成される。需給マネージャでは数秒から数時間オーダー毎に制御階層を分割し，階層間で必要最低限の情報のやりとりを行うように設計している。また，データ授受の失敗の際にも，各階層が独立して動作できるよう最低限のデータセットを備えている。予測部は，翌日予測部とリアルタイム予測部からなる。主に，前者の予測は，制御可能なディーゼル発電機群の起動停止計画(Unit Commitment; UC)に利用する。後者の情報は，ディーゼル発電機群のダイナミック経済負荷配分(Dynamic Economic Load Dispatch; DELD)に使用する。なお，DELD は UC の起動停止情報を用いるが，独立してリアルタイム需給運用を担当する。さらに，簡易ディーゼル発電機群モデルを準備し，系統の動特性を 4 次のルンゲクッタ法で解くことで周波数変動をシミュレーションしながら負荷周波数制御(Load Frequency Control; LFC)を実施する。

〈2･1〉 翌日需給計画パート　運用対象日の前日に，需要および再生可能エネルギー電源(Renewable Energy Source; RES)発電量を翌日 24 時間分(30 分間隔)予測し，発電機および蓄電池などの既存設備の起動停止計画を策定する。翌日予測部では PV や風力発電(Wind-turbine; WT)をはじめとする RES の翌日発電量や翌日需要を予測する。これらの結果は翌日 UC の策定に反映される。また，翌日 UC が 30 分間隔で行われることを考慮し，翌日の各予測を 30 分間隔で行う。本論文では翌日 PV 発電量予測手法として時間帯や天気別で NN を作成し予測を行う手法について提案する。ある程度大きな予測誤差を含む前日予測データに対応するため，予備力待機計画も併せて需給計画を策定する。

〈2･2〉 リアルタイム需給運用パート　運用対象日の当日に，5 分時間間隔で，1 時間先までの需要および RES 発電量のリアルタイム予測を実施，前日予測に対してさらに予測精度を向上させる。リアルタイム予測部では，当日の 5 分先から 1 時間先までの発電量や需要値をリアルタイムで予測することで，需給制御システムシミュレータにおける当日 UC，発電機の DELD に使用する。本研究では，リアルタイム PV 発電量予測手法として，多地点日射量との相関分析(Correlation Analysis; CA)を用いた発電量予測手法を提案する。日射量の急激な変動が起きるタイミングと大きさを短時間前に予測することで，系統周波数の安定化を実現する。この予測結果に基づいて，5 分毎に 1 時間先まで発電機および蓄電池などの既存設備のリアルタイム運用計画を策定する。また同時に，急激な天候変化や大きな予測外れに対応するため，運転予備力・瞬動予備力待機計画も併せて策定する。

〈2･3〉実時間周波数制御パート　運用対象日の当日に，実時間周波数制御を実施し，シミュレーションによって，周波数変動を評価する。既存ディーゼル発電機と蓄電池によりLFCが実施される。

3. 翌日 PV発電量予測手法

翌日 PV発電量予測手法について，図2の(i)~(vii)に示す順番に従って予測を行う。以降，各項目について説明する。

〈3･1〉入力データに関する前処理　図2(i)について説明する。気象庁 Web サイト[15]で公開されている地域時系列予報より，3時間毎の天気（晴れ，曇り，雨(雪)），気温，風速(4段階)，降水確率の情報を得ることができる。このうち，気温 T 降水の有無 p (1 または 0)は，生データとして利用し，風速は気象庁では，最大風速 v [m/s]について「0~2」，「3~5」，「6~9」，「10以上」の4段階とすでに分けられているので，本論文でもこの分け方に準じて数値化して取り扱う。また，天気予報が更新されない時間帯については，前後のデータを線形補間し，3時間刻みのデータを作成した。

〈3･2〉データの天候分類　次に図2(ii)について説明する。気象庁の天気予報をもとに晴れ，曇り，雨，それぞれに対応する過去日射量データを整理する。それぞれの天候に対応した NN を作成する。すなわち，予測したい時刻の予報が晴れの場合，晴れのデータで作成した NN を使用して予測を行う。なお，天気予報や過去の気象データでは天気データが 3 時間間隔で予報あるいは記録されているため，予報時刻の前後 3 時間は同一天気と考えて天候分類を行う。

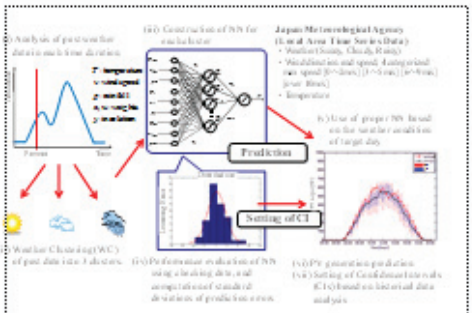

Fig. 2. The proposed scheme of PV forecasting.

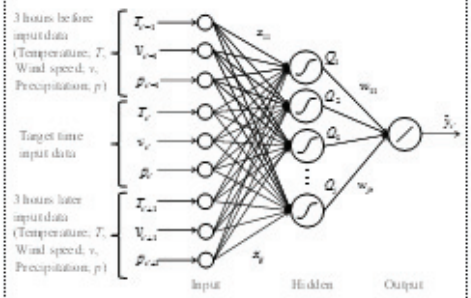

Fig. 3. A three-layer neural network.

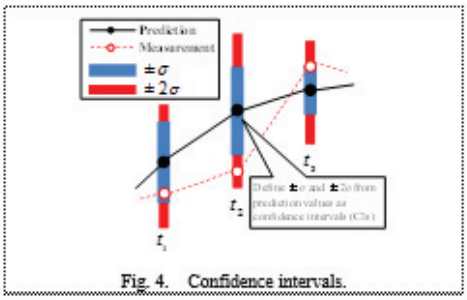

Fig. 4. Confidence intervals.

〈3･3〉NN を用いた日射量予測　<3.2>で分類した天候毎に図3に示す三層 NN を作成し，予測対象日の天気予報から得られたデータを入力して日射量の予測を行う(図2(iii))。ここで，<3.1>の述べたデータ(気温 T，風速 v，降水の有無 p)を学習データとして使用し，教師・評価データには，日射量を使用する。なお，予測対象時間である時刻 t' の日射量を予測するために，時刻 t'-1(t'の3時間前)，t'，t'+1(t'の3時間後)について，気温 T，風速 v，降水の有無 p (0 or 1) を入力している。また，x，w は重み係数，Q は中間(Hidden)層の出力である，本論文では誤差逆伝播法(Backpropagation, BP)を用いて決定する。以上の NN の学習により，翌日対象時間の日射量予測値 $\hat{y}_{t'}$ と学習誤差の分布データ(図2(iv))を得ることができる。

〈3･4〉PV発電量の推定　提案法では，太陽光発電システムの発電電力量推定方法[16]に則り，(2)式によって，<3.3>で得られた予測日射量 $\hat{y}_{t'}$ を予測 PV 発電量 $\hat{P}_{t'}$ に換算する。

$$\hat{P}_{t'} = (K / G_S) \cdot P_{AS} \cdot \hat{y}_{t'} \quad (1)$$

ここで，K は月別総合設計係数，G_S は標準試験条件における日射強度 [kW/m²]，P_{AS} は標準太陽電池アレイ出力[kW]である。なお，月別総合設計係数 K は(2)式から計算できる。

$$K = K_{HD} \cdot K_{PD} \cdot K_{PA} \cdot K_{PM} \cdot \eta_{INO} \cdot K_{PT} \quad (2)$$

ここで，K_{HD}: 日射量変動補正係数，K_{PD}: 経時変化補正係数，K_{PA}: アレイ回路補正係数，K_{PM}: アレイ負荷整合補正係数，η_{INO}: パワーコンディショナ実行効率，K_{PT}: 温度補正係数である。各係数等は広島大学工学部実験研究棟に設置したPVシステムのデータを使用する。

以上より，図2(v)(vi)の PV 発電量を推定できる。

〈3･5〉信頼性区間の設定　天候の急激な変化による日射量の変化幅について，曇り日などの天気が不明瞭な日には大幅な予測誤差が生じる可能性がある。本論文では天気予報データを用いているため，天気予報が外れてしまった場合や天気予報が行われていない時間帯について大幅な予測外れが懸念される。また，PV発電量予測の大幅な誤差は系統運用にも大きく影響を与えてしまう可能性がある。事前に予測の信頼性を把握することができれば，柔軟な系統

運用が可能となる。そこで，本論文では，予測結果の上下にある程度の誤差を許容する幅(信頼性区間，CIs)を設けることで予測結果の信頼性を視覚的に把握できるようにしている(図 2(vii))。予測の際に作成をした NN を過去の気象データを用いてテストすることで，予測誤差の算出を行う。NN の学習から得られた予測誤差の標準偏差 σ を求め，翌日 PV 発電量予測値を平均値としてそこから $\pm\sigma$，$\pm 2\sigma$ の範囲を信頼性区間と定義した(図 4)。

4. リアルタイム PV 発電量予測手法

〈4･1〉リアルタイム予測の考え方　本論文では，他地点の日射量を考慮した地点間の距離に基づく相関性を考慮した相関分析(Correlation Analysis; CA)手法を提案し，リアルタイム PV 発電量予測に実装する。図 5 に概念図を示す。ここでは，2 地点(A, B)を想定する。各地点の PV 発電量予測には，第 3 章で述べた翌日 PV 発電量予測手法のニューラルネットワークを適用する。なお，リアルタイム予測で与えるデータなどの条件については第 5 章のシミュレーションによる検証で説明する。図 5 のローカルな 2 地点間の雲の移動の時間的な遅れを利用してリアルタイム予測を行うものである。雲の流れにおける上流地点の日射変動パターンは下流地点に遅れ時間を伴って現れると仮定する。CA 手法によって 2 地点の相関を分析し，相関の高い上流地点の日射量を下流地点の日射量予測に適用する。

〈4･2〉CA 手法による日射量予測　地点日射量の相関分析によって地点間の日射変動の類似性を考慮して日射変動が現れる隔たり時間を導く。また，その値から予測に使用する地点を選別する。(3)式より，予測対象地点 k と他地点 l の日射量の相関係数 r_{kl} を 5 分おきに算出する。まず，地点 k の日射量過去データをある一定期間抽出し，地点 l では，地点 k で抽出した期間より τ 分前の日射量過去データを同じ時間窓で一定期間抽出する。

$$r_{kl}=\frac{\sum_t\left(y_k(t)-\bar{y}_k\right)\left(y_l(t-\tau)-\bar{y}_l\right)}{\sqrt{\sum_t\left(y_k(t)-\bar{y}_k\right)^2}\sqrt{\sum_t\left(y_l(t-\tau)-\bar{y}_l\right)^2}} \quad (3)$$

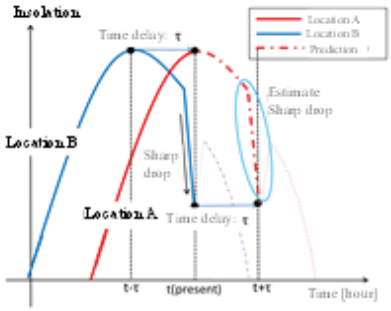

Fig. 5. The proposed method for real-time forecasting.

ここで，t：時刻[min]，τ：隔たり時間[min]，y_l：他地点日射量[kW/m²]，y_k：予測対象地点日射量[kW/m²]，$\bar{y}$：y の期間内平均[kW/m²]である。

次に，(3)式の隔たり時間 τ を刻み幅 5 分で変更し相関係数を求める。最も相関の高い隔たり時間 τ_{max} を選定し，τ_{max} 分前の地点 l の日射量を地点 k の日射量予測に使用する。

〈4･3〉多地点による日射量予測　安定した予測精度を得るため，多地点との相関分析をリアルタイムで行い，5 分毎に予測に使用する地点の選別を行う。比較的高い相関を持つ上位数地点を選別する。その後，上流地点にデータの重みを乗じる。最終的に地点毎の予測結果を統合して予測対象地点の日射量を推定する。具体的な手法として，〈4･2〉の相関分析を複数の地点に対して行う。各地点の相関係数 r_{kl} を重みとし，予測日射量の加重平均値を(4)式により計算する。

$$\hat{Y}_k(t)=\frac{\sum_l\left(r_{kl}\cdot\hat{y}_{kl}(t)\right)}{\sum_l r_{kl}} \quad (4)$$

ここで，$\hat{y}_{kl}$：地点 l による k 地点での日射量予測値[kW/m²]，$\hat{Y}_k$：全地点による地点 k の日射量予測値[kW/m²]。

5. シミュレーションによる検証

〈5･1〉シミュレーション条件　これまでに経済産業省補助事業の「分散型新エネルギー大量導入促進系統安定対策事業」による中国地方の日射量データや，気象庁が提供している過去の気象データを使用して提案法の検討を行ってきた。そこで，比較的良好な予測性能が得られることを確認した[6]。例えば，提案法の翌日発電量予測誤差を比較すると，文献[11]の予測誤差 MAE = 100～120 [Wh/(m²･h)]に対して，提案法は，MAE = 70～110 [Wh/(m²･h)]で比較的良好な結果が得られている。また，文献[12]の手法を用いた予測誤差率 24.5[%]に対して，提案法は 24.8[%]とこちらも比較的良好な結果といえる。以上を踏まえて，本論文では予測対象地点を広島大学工学部実験研究棟に設置した PV パネル(10[kW] × 4[台]，傾斜角 30[°]，パワーコンディショナ 10[kW] × 4[台])とし，気象庁で公開されているデータのみを用いて翌日 PV 発電量予測およびリアルタイム PV 発電量予測を行う。予測結果の精度検証を行うために，比較的よく用いられている自己回帰(Autoregressive; AR)手法を従来法とした。

まず，翌日 PV 発電量予測について，<3.2>の天候分類を行った場合と行わない場合との予測誤差の違い，信頼性区間の有効性を検証する。2012 年の 1 年間について予測を行った。NN は図 3 を使用し，学習には予測対象月前後 3 か月間のデータを過去 4 年分(2009～2012 年)使用している。例えば，8 月の予測を行う場合は 2009～2011 年における 7，8，9 月のデータと 2012 年における 7 月のデータを使用する。また，入力データに許容数以下のデータ欠損が生じた場合には線形補間を行い，許容数以上ならばその日のデータを

使用しない。天気データの存在しない時間帯は存在する時間帯の前後 3 時間を同一天気として扱っている。例えば，12 時が晴れの場合，10 時 31 分から 13 時 30 分までを晴れとして扱う。リアルタイム PV 発電量予測では予測対象地点の他，中国地域の代表 10 地点の過去日射量データを使用し，相関の高い上位 4 地点を選択して予測に適用する。AR モデルとの比較を行い CA モデルの有効性を検証する。

(5･2) 翌日 PV 発電量予測結果

（1）予測結果　図 6，7 に比較的発電量の変化が激しい日の PV 発電量の予測結果を示す。縦軸は PV 発電量の 30 分間積算値である。また，予測値から上下に伸びている青色の線が予測値から±σ の範囲，赤色の線が±2σ の範囲である。図の下部に記している天気は，左から 3，6，9，12，15，18，21 時における天気(晴，曇，雨のいずれか)である。天候が緩やかに変化している場合，どちらの結果も比較的精度よく予測が出来ていることが確認できる。信頼性区間について見てみると，基本的に実測値が区間内に収まっている。朝方や夕方の発電出力量が小さいときには区間幅が小さくなっており，変動が顕著となる日中は幅が大きい。天候分類を行った場合と行わなかった場合を比べると区間幅が狭くなっていることが確認できる。

（2）予測誤差　図 8 に各月における平均予測誤差，最大予測誤差の推移を示す。予測誤差の算出には(5)式で表される 2 乗平均平方根誤差(Root Mean Square Error; RMSE)を使用している。ここで，N がデータ数，y が実測値，$\hat{y}$ が予測値である。

$$RMSE = \sqrt{\frac{1}{N}\sum_{t=1}^{N}\left(y(t)-\hat{y}(t)\right)^2} \qquad (5)$$

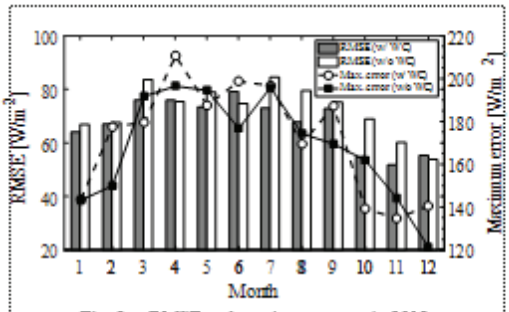

Fig. 8. RMSE and maximum errors in 2012.

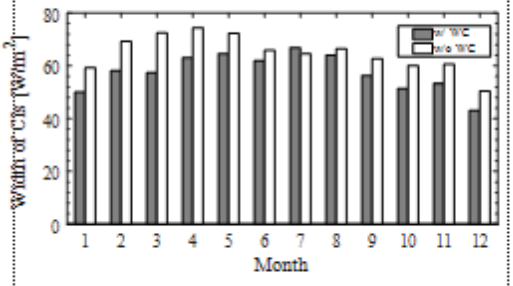

Fig. 9. Width of confidence intervals (CIs) in 2012.

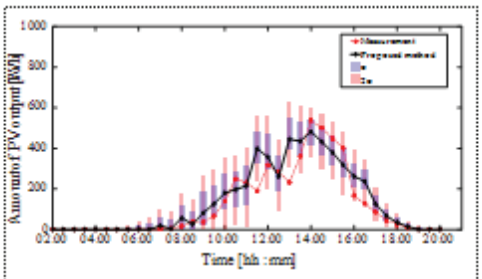

Fig. 6. PV forecasting with weather clustering.

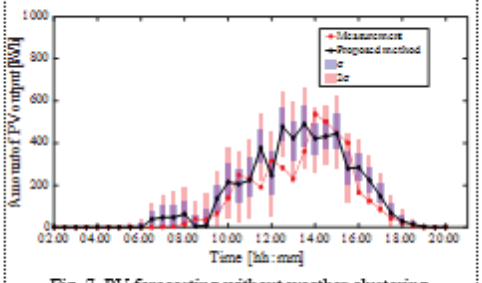

Fig. 7. PV forecasting without weather clustering.

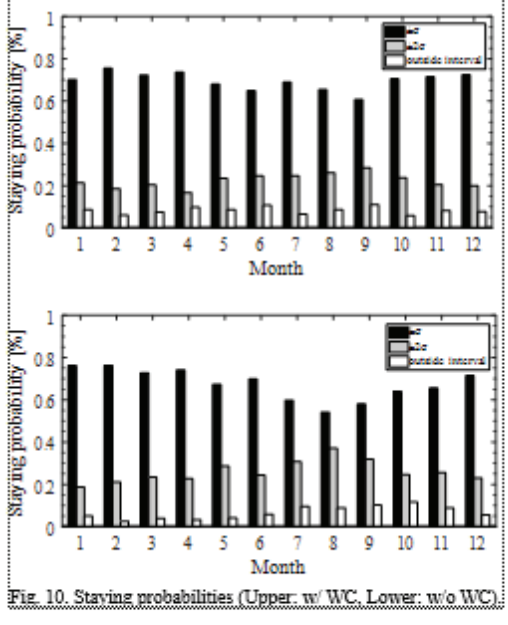

Fig. 10. Staying probabilities (Upper: w/ WC, Lower: w/o WC).

Table1. Prediction Errors [%]

	5min ahead	10min ahead	20min ahead	40min ahead	60min ahead
ε (AR) [%]	16.09	19.00	20.75	23.76	25.07
ε (CA) [%]	16.50	18.47	19.84	21.20	22.26
η (AR) [%]	32.87	36.74	36.56	39.10	40.65
η (CA) [%]	31.43	32.48	33.91	34.89	35.12

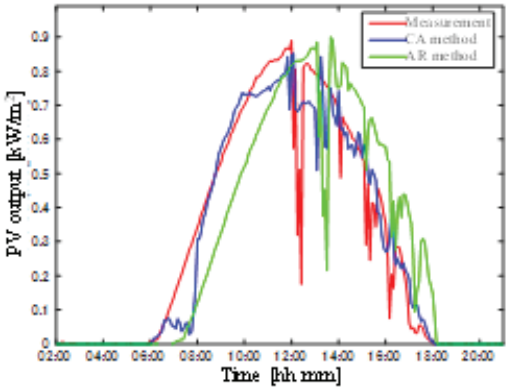

Fig.11. 60-min ahead predictions.

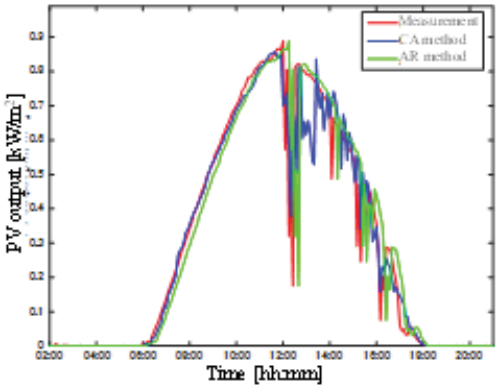

Fig.12. 10-min ahead predictions.

天候分類を行った場合，ほとんどの月で平均誤差が低減されていることが分かる。しかし，最大誤差に関してみると，天候分類をした場合に誤差が増えている月が多く見られた。天候分類を行う場合，3時間は同一天気として扱うため，3時間内に急激に天候の変動があった場合にうまく予測が行えなかったためと考えられる。

（3）信頼性区間　次に，信頼性区間の有効性について検証を行う。図9には各月における信頼性区間の大きさ，図10には信頼性区間内にPV実測値が入った割合である滞在確率を示している。図9を見ると天候分類を行った場合，1年間を通して区間幅が小さくなっていることが分かる。滞在確率について見てみると，シミュレーションを行った期間については，80%以上の確率で区間内に収まることが確認

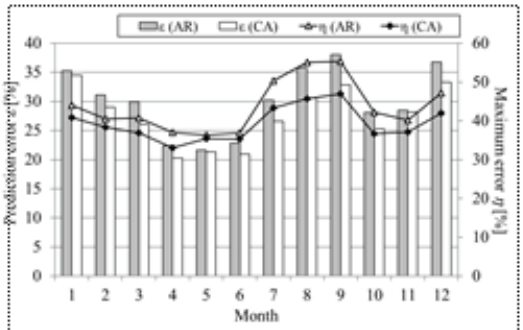

Fig.13. Prediction errors [%]

できる。図10の2つのグラフを比較すると信頼性区間$\pm\sigma$あるいは$\pm 2\sigma$の中に納まっている割合が向上している。これらのことから，信頼性区間の信頼性が天候分類によって向上したことが確認できた。

〈5･3〉リアルタイムPV発電量予測結果

予測精度を比較するための指標として，以下の(6)，(7)式で表される予測誤差率ε，最大予測誤差率ηを用いる。大気外日射量とは，その日の理想的な最大日射量を表す理論値である。2012年6月の予測対象時間毎の予測誤差率の平均値と最大予測誤差率の平均値を表1に示す。図11，図12に日射量の60分先，10分先の予測値と実績値を示す。ARモデルにおける最大予測誤差率ηは，5分から10分にかけて大きく増大している。結果として，ARモデルと同等程度の予測精度が得られた。

$$\varepsilon = \frac{\sqrt{\frac{1}{m}\sum_{i=1}^{m}\left(\hat{Y}_i - Y_i\right)^2}}{\frac{1}{m}\sum_{i=1}^{m} I_i} \times 100\,[\%] \qquad (6)$$

$$\eta = 100 \times \left| Y_{max} - \hat{Y}_{max} \right| / I_{max}\ [\%] \qquad (7)$$

ただし，$\hat{Y}$: 日射量予測値[kW/m²]，$\hat{Y}_{max}$: 最大予測誤差を与える日射量予測値[kW/m²]，Y: 日射量実績値[kW/m²]，Y_{max}: 最大予測誤差を与える日射量実績値[kW/m²]，I: 大気外日射量[kW/m²]，I_{max}: 大気外日射量最大値である。

さらに，気象条件の異なるすべての季節において予測精度の検証を行う。使用データの関係上，10～12月は2011年度，1～9月は2012年度のデータを使用している。図13に30分先予測の月別予測誤差率を示している。本手法では日射変動をある程度事前に予測することが可能となり，ARモデルと比較して，季節ごとの日射量予測誤差率，最大誤差率を抑えられていることが確認できた。

6. おわりに

本論文では，需給マネージャのための翌日・リアルタイムPV発電量予測手法を提案し，その有効性の検証を行った。また，多地点に分布する日射量計から得られる日射量データをリアルタイムで収集し，各地点の予測を行うシステム

を想定して，CAモデルによるPV発電量の予測を行った。

今後，翌日PV発電量予測については予測精度の向上や提案したPV発電量予測手法をシミュレータに実装し，予測誤差や設定した信頼性区間が系統へ与える影響度について検証を行うという課題がある。リアルタイム予測については日射量以外の気象条件についても他地点との関係性を考慮する必要がある。また，予測外れを考慮した信頼区間の設定や現在のモデルを利用した短時間先のランプ変動を検知するシステムの構築などが課題である。以上より，予測精度向上による，需給マネージャのさらなるパフォーマンス向上が見込まれる。

文　　献

（1） NEDO：「太陽光発電ロードマップ（PV2030+）概要版」，2030年に向けた太陽光発電ロードマップに関する見直し検討委員会報告書 (2009.6)

（2） Y. Sasaki, D. Seikoba, J. Okihara, K. Kanaya, Y. Zoka, and N. Yorino, "A Robust Supply and Demand Controller Against Uncertainties of Renewable Energy Sources," *18th Power Systems Computation Conference*, No. ID352 (2014)

（3） Y. Sasaki, N. Yorino, and Y. Zoka, "Probabilistic Economic Load Dispatch Applied to a micro-EMS Controller," *19th Power Systems Computation Conference*, No. ID574 (2016)

（4） Y. Sasaki, K. Kanaya, D. Seikoba, J. Okihara, Y. Zoka, and N. Yorino," Probabilistic Constrained Dynamic Economic Load Dispatch for Renewable Energy Sources," Grand Renewable Energy 2014 International Conference and Exhibition (2014)

（5） 津木場大，金谷浩平，沖原 潤，清鳥翔太，佐々木豊，造賀芳文，餘利野直人，「需給制御マネージャにおけるPV発電量予測の影響評価」，平成26年電気学会電力・エネルギー部門大会，P21，pp.41-42 (2014)

（6） 朝田光雅，津木場大，佐々木豊，造賀芳文，餘利野直人，「需給制御マネージャにおける翌日・短時間先PV発電量予測の検討」，P22，pp.43-44 (2015)

（7） L. Ma and K. Khorasani, "Constructive Feedforward Neural Networks using Hermite Polynomial Activation Functions," *IEEE Trans. on Neural Networks*, Vol. 16, No. 4, pp.821-833 (2005)

（8） L. Ma, N. Yorino, and K. Khorasani, "Solar Radiation (Insolation) Forecasting Using Constructive Neural Networks," *Proc. of IEEE World Congress on Computational Intelligence (WCCI)*, No.16433, 24-29 July (2016)

（9） 山本茂広，片木 猛，朴 在健，「風の履歴解析による太陽光発電の出力変動予測」，電学論B，Vol.119，No.8/9，pp.909-915 (1999)

(10) 下瀬健一，大竹秀明，Joao Gari da Silva Fonseca Junior，高島 工，大関 崇，山田芳則，「気象庁メソモデルの日射量予測誤差要因の解析」，電学論B，Vol.134，No.6，pp.518-526 (2014)

(11) 細東一郎，村田浩之，東山 伸，滝川浩史，「全国各地の日日射量誤差予測のための気候区代表モデル法」，電学論B，Vol.128，No.1，pp.151-156 (2008)

(12) 嶋田健彦，黒川浩助，「天気予報と天気変化パターンを用いた日射予測」，電学論B，Vol.127，No.11，pp.1219-1225 (2007)

(13) 山本茂広，橋本 岳，橋本 武，「太陽光発電のための日射量積算値の予測に関する基礎的研究」，電学論B，Vol.121，No.12，pp.1708-1715 (2001)

(14) 松田勝弘，有松健司，山根憲一郎，渡辺雅浩，山崎 潤，村越 潤，「空間的相関分析に基づく配電運用管理向け短期太陽光発電量予測手法」，電学論B，Vol.134，No.9，pp.759-766 (2014)

(15) 気象庁Webサイト，「地域時系列予報」，URL：http://www.jma.go.jp/jma/kishou/know/kurashi/jikeiretsu.html (2016.10.14確認済)

(16) 日本工業規格協会，「太陽光発電システムの発電電力量推定方法」，日本工業規格 JIS-8907 (2005)

佐々木豊　（正員）2008年3月北海道大学大学院情報科学研究科博士課程後期修了。同年4月広島大学大学院工学研究科助教，現在に至る。博士（情報科学）。2012年Washington State University客員研究員。主として，電力システムの計画・運用および制御に関する研究に従事。IEEE，IET，電気設備学会，エネルギー・資源学会会員。

餘利野直人　（上級会員）1983年早稲田大学大学院修士課程修了。富士電機製造（株）入社。1984年同博士課程進学。1985年早稲田大学助手。1987年同博士課程修了。広島大学助手，1990年同助教授，2005年同教授。1991年MacGill大学客員研究員。工学博士。2005年中国電気保安協会理事。1985年George Montefiore受賞。IEEE，CIGRE，電気設備学会会員。

Farid Imam Wahyudi　（非会員）　2014年スラバヤ工科大学電気工学専攻修了。2015年4月広島大学大学院工学研究科博士課程後期課程（システムサイバネティクス専攻）入学，現在に至る。主として，ニューラルネットワークを用いた太陽光発電量予測に関する研究に従事。

津木場大　（正員）2013年4月広島大学大学院工学研究科博士課程前期課程（システムサイバネティクス専攻）入学，2015年3月同専攻修了。在学中，主として翌日太陽光発電量予測に関する研究に従事。

朝田光雅　（学生員）2015年4月広島大学大学院工学研究科博士課程前期課程（システムサイバネティクス専攻）入学，現在に至る。主として，主として，リアルタイム太陽光発電量予測に関する研究に従事。

馬立英　（非会員）2015年4月広島大学大学院工学研究科博士課程前期課程（システムサイバネティクス専攻）外国人客員研究員，2016年4月，Concordia University教授，現在に至る。主として，ニューラルネットワークを用いた各種予測アルゴリズムに関する研究に従事。

Robust Dynamic Load Dispatch under Uncertainties

Yutaka Sasaki, Naoto Yorino, Yoshifumi Zoka, Imam Wahyudi Farid, Shinya Sekizaki
Graduate School of Engineering
Hiroshima University
Higashi-Hiroshima, Japan
yusasaki@hiroshima-u.ac.jp

***Abstract*—At present, electric power systems face difficulties in system operations due to rapid increase in uncontrollable renewable energy sources (RESs), such as photovoltaic power generations (PVs). Reduction of controllable resources also yields concerns about system reliability issues. This paper focuses on a new dynamic load dispatch method for mitigating the irregularity associated with RES. The developed load dispatch method is to schedule the committed generating units outputs so as to meet required irregular load demand estimation which is frequently updated in real-time operation circumstance. A new algorithm is proposed for unit commitment and stochastic dynamic economic load dispatch as an efficient solution for a day-ahead and a real-time generation schedule (GS), respectively, that fully utilizes the limited resources of a power system under uncertainties. Day-ahead and real-time PV forecasts with the co-relations of PV forecasting errors are effectively treated in the proposed method. Special feature of the proposed method different from the existing works lies in a frequent real-time update of GS by using a fast algorithm to maximize robustness against uncertainties.**

Keywords—Uncertainties, Confidence Intervals, PV forecasting, Day-ahead and real-time generation schedule, Stochastic dynamic economic load dispatch.

I. INTRODUCTION

Renewable energy sources (RESs) such as photovoltaic power generations (PVs) and wind-turbine power generations (WTs) are expected to grow substantially in the near future. A reasonable estimation is that 20-30% of the amount of total energy will be delivered through such sources in the upcoming 15 years. PVs are clean and safety energy sources, while they are prone to cause degradation of power quality as well as grid security due to unforeseen weather conditions. Continuous sunlight intermittency, especially during cloudy days, incurs sudden intense changes in their outputs such as unpredictable significant ramp effect. The increasing renewable energy requires additional ramping abilities to maintain the grid stability. Development of sophisticated operation technology is a key subject.

Novel methodologies for stochastic dynamic economic load dispatch (SDED) become necessary to guarantee secure operation in real-time scenarios [1]. This particular concern is common to various widely adopted power systems, where smart gird projects make use of all available controls including demand response [2]. In order to fully utilize controllable generators, development of robust and reliable load dispatching method is extremely of importance to effectively treat uncertainties [3]–[5].

Various approaches have been proposed so far concerned with SDED problem, classified into two approaches. The first approach repeatedly performs static economic load dispatch (ELD) at each interval by taking into account the ramp rate constraints [6], [7]. The second approach determines generation schedule (GS) by solving a single optimization problem. The approach includes heuristic technique in dynamic programming [8], improved simulated annealing [9], [10], hybrid approach of Hopfield neural network and quadratic programming (QP) [11], variable scaling hybrid differential algorithm [12], re-dispatch algorithms using QP, linear programming (LP) and the Danzig Wolfe's decomposition technique [13], a multi-stage algorithm [14], and the interior point method [15].

However, these conventional approaches cannot fully manage large uncertainty and infeasibility of power system operations. Hafiz et al. [16] and Yorino et al. [17] have proposed time-sequence dynamic feasible region (TDF) approach to fully utilize ramp rate capabilities of controllable generators against uncertainties. The concept of Robust Power System Security [18] has been proposed by Okumoto et al. where safe-side treatment of uncertainty is suggested for important constraints related to system collapse.

In this paper, we propose a new energy management method based on Robust Power System Security. The proposed method is applied to micro energy management system (micro-EMS) controller (Fig. 1), where load and RES predictions are available online. Confidence intervals (CIs) of the RES

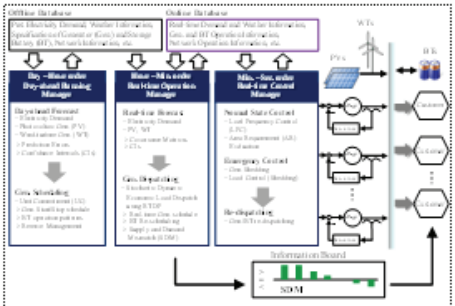

Fig. 1. The proposed micro-EMS controller.

prediction errors are specified depending on required reliability of system operation against system collapse. The proposed method updates the day-ahead GS a few times a day and provides 1-hour GS every 5 minutes in real-time operation. Contributions of this paper are as follows:

In this paper, we propose a new energy management method based on Robust Power System Security. The proposed method is applied to micro energy management system (micro-EMS) controller (Fig. 1), where load and RES predictions are available online. Confidence intervals (CIs) of the RES prediction errors are specified depending on required reliability of system operation against system collapse. The proposed method updates the day-ahead GS a few times a day and provides 1-hour GS every 5 minutes in real-time operation. Contributions of this paper are as follows:

i. CIs and covariance matrix of prediction errors are used respectively in deterministic feasibility detection and probabilistic line flow management. The former realizes effective safe-side reserve management, while the latter manages soft constraints of line overloading. The approach is new in the treatment of uncertainties.

ii. The paper also proposes new algorithms to realize the proposed uncertainty treatment, which include (1) an improved TDF, Robust TDF (RTDF) that effectively treats CIs, (2) an improved SDED method which combines RTDF, QP and liner stochastic load flow (SLF), and (3) an improved UC algorithm for day ahead 24-hour GS.

Advantage of the proposed method is that the supply and demand balance is kept to the maximum (high feasibility of dispatch) under uncertainties in real time power system operations. In case of a critical situation when the forecasted load cannot match the existing generator's capability, the method will detect the minimum amount of supply and demand mismatch in advance (1-hour before) and handle it reliably for the considered time horizon.

II. Outline Of The Micro-EMS Controller

A. Proposed Approach to Treat Uncertainties

We first carry out PV output forecast and its error analysis. A weather clustering method has been proposed for this purpose in [19]. A covariance matrix of PV output errors is calculated, while CIs of the PV forecast errors are specified depending on required reliability against system collapse.

The covariance matrices will be used in real-time GS in (31) for line flow control, while CIs are used in day-ahead unit commitment (UC) in (15) and real-time RTDF computation in (18) which is further used in real-time SDED in (32) to guarantee the supply and demand balance and reserve management.

B. Outline of the Controller

Our research target is to develop a micro-EMS controller that enforces robustness against uncertainties [19]. Figure 1 shows the configuration of the proposed management system: there are mainly three functions responsible for day-ahead operation planning, minute-order real-time operation, and second-order real-time control. Based on the prediction of RES outputs, the system manages the existing generators, storage battery (BT) and controllable demands in optimal manner.

C. Planning Manager

This manager provides an updated schedule of the output pattern for the limited resources. The output is represented as a 24-hour GS which also comprise the BT operation schedule, where a unit time is 30 minutes. Existing techniques for the UC can be fully utilized in the optimization process. Uncertainties related to the prediction and fluctuation of PV are handled particularly [19].

D. Operation Manager

The proposed method is related mainly to this part. which is the main subject of this paper. The operation manager provides real-time control signal to each generator using most recent real-time PV forecast.

E. Optimization

The optimization is performed in two stages. In stage I optimization, the 24-hour GS, which was planned in the previous day, is refined to determine the start/stop time schedule for generators. A robust GS against prediction error is determined. Stage II optimization utilizes only the start/stop time schedules and the BT operation. The rest of the optimization results of stage I is used only for reference and will be totally updated by stage II optimization, which will be proposed in the next section.

III. Formulation

A. Formulation for Stage I Optimization

The optimization problem is formulated with N_G controllable generators in a time horizon of T intervals ahead from the current moment as follows.

Minimize:

$$C^{DH}(\boldsymbol{P_G}, \boldsymbol{u}) = \sum_{t=1}^{T}\sum_{k=1}^{N_G} u_{kt} \cdot f_{kt} + \sum_{t=1}^{N_T}\sum_{k=1}^{N_G}\left(u_{kT_{1n}} - u_{kT_{1f}}\right) \cdot suc_k \quad (1)$$

$$f_{kt} = a_k P_{Gkt}^2 + b_k P_{Gkt} + c_k \quad (2)$$

suc_k : Start-up cost [$] of k-th generator

Subject to:

i. Supply and demand balance constraints.

$$\sum_{k=1}^{N_G} P_{Gkt} + B_{at} - B_{et} = E[P_{Dt}] - E[P_{PVt}] - E[P_{WTt}] \quad (3)$$

ii. Upper and lower output of generator constraints.

$$P_{Gk}^{min} \cdot u_{kt} \le P_{Gkt} \le P_{Gk}^{max} \cdot u_{kt} \quad (4)$$

iii. Ramp-rate constraints.

$$-\delta_k \cdot \Delta t \le P_{Gk(t-1)} - P_{Gkt} \le \delta_k \cdot \Delta t \quad (5)$$

iv. Start/stop variables constraints.

$$0 \le u_{kt} \le 1 \quad (6)$$

v. Minimum continuity down time constraints.

$$if \quad (1-u_{kt}) \cdot u_{k(t-1)} = 1$$
$$then \quad \sum_{t}^{t+mdt} (1-u_{kt}) = mdt_k \quad (7)$$

vi. Minimum continuity up time constraints.

$$if \quad u_{kt} \cdot (1-u_{k(t-1)}) = 1$$
$$then \quad \sum_{t}^{t+mut} (1-u_{kt}) = mut_k \quad (8)$$

vii. BT charge/discharge output limits constraints.

$$0 \le B_{dt} \le B_d^{max} \quad (9)$$

$$0 \le B_{ct} \le B_c^{max} \quad (10)$$

With switching constraint:

$$B_{ct} \cdot B_{dt} = 0 \quad (11)$$

viii. BT upper and lower bounds of the state of charge.

$$B_s^{min} \le B_{st} \le B_s^{max} \quad (12)$$

ix. Dynamic transition of BT state of charge.

$$B_{st} = B_{s(t-1)} + \{B_{ct} - B_{dt} / \eta\} \cdot \frac{\Delta t}{60} \quad (13)$$

x. Line flow limits between node i and j.

$$-F_{ij}^{max} \le F_{ijt} \le F_{ij}^{max} \quad (14)$$

xi. DC power flow equation (23) in the next section

xii. Operating reserve power constraints.

$$\sum_{k=1}^{N_G} P_{Gk}^{max} \cdot u_{kt} + B_{dt} - B_{ct} \ge \bar{P}_{nt} + R_t \quad (15)$$

$$\sum_{k=1}^{N_G} P_{Gk}^{min} \cdot u_{kt} + B_{dt} - B_{ct} \le \underline{P}_{nt} \quad (16)$$

where, $\bar{P}_{nt} = P_{Dt} - \underline{P}_{pvt} - \underline{P}_{wtt}$,

$\underline{P}_{nt} = P_{Dt} - \bar{P}_{pvt} - \bar{P}_{wtt}$,

$\underline{P}_{nt} = P_{Dt} - \underline{P}_{pvt} - \underline{P}_{wtt}$.

Where, C^{DA}: generation cost [$] for day-ahead GS, u_{kt}: start/stop variables of k-th generator at time t, P_{Gkt}: power output [MW] of k-th generator at time t, $P_G \in \mathbf{R}^{N_G \times T}$: vector of P_{Gkt} (k=1,..,N_G, t=1,..,T), $u \in \mathbf{R}^{N_G \times T}$: vector of u_{kt}, a_k, b_k, c_k: quadratic cost coefficients of k-th generator, T_{Dm}: time [min] at local maximum electricity demand (m=1,…,N_P), N_P: number of peak time, T_N: time [min] at minimum electricity demand, B_{ct}, B_{dt}: charge and discharge output power [MW] of BT at time t, respectively, P_{Dt}: electricity demand [MW] at time t, P_{pvt}: PV outputs [MW] at time t, P_{wtt}: WT outputs [MW] at time t, $E[\cdot]$: expected value [MW] at time t, P_{Gk}^{max}, P_{Gk}^{min}: maximum and minimum outputs [MW] of k-th generator, respectively, δ_k: ramp-rate limit [MW/min] of k-th generator, Δt: computational interval [min], mut_k, mdt_k: Minimum operating time [min] and minimum waiting time [min] of k-th generator, respectively, B_c^{max}, B_d^{max}: charge and discharge maximum power [MW] of BT, respectively, B_{st}: state of charge (SOC) [MWh] of BT at time t, B_s^{max}, B_s^{min}: maximum and minimum SOC bounds [MWh] of BT, respectively, η: charge/discharge efficiency of BT, F_{ijt}: line flow [MW] from node i to j governed by DC power flow equation, F_{ij}^{max}: maximum allowable line flow [MW] between node i and j, R_t: operating reserve power [MW] at time t, P_{nt}: net electricity demand at time t, $\bar{P}_{nt}$, $\underline{P}_{nt}$: upper and lower bounds [MW] of P_{nt} including CIs of RES prediction at time t, respectively.

Solution procedure will be given in section III-*E*. After obtaining the solution, we fix the start/stop time schedules and the BT charge/discharge operation, and then perform the next steps as below.

B. RTDF and Supply-Demand Mismatch using CIs

TDF is defined as the region of generator output P_{Gt} reachable from a specified operating point and satisfying all constraints (3)-(5) with load forecasts $\hat{P}_{Dt}$ for t=1,..,T. TDF evaluation algorithm was proposed in [16] and [17], where the present operating point t=0 is used as a starting point in order to obtain reachable points successively in forward direction to t=T. TDF obtained by this calculation is represented as $TDF(t, \hat{P}_{Dt})$, which implies the region defined by the upper and lower bounds of each generator output at each time t=1…T.

In this paper, Robust TDF (RTDF) is defined taking into account CIs around the latest load predictions $\hat{P}_{Dt}$:

$$RTDF(t, \hat{P}_{Dt}) = \left\{ TDF(t, \hat{P}_{Dt} + M_{Ut}) \bigcap TDF(t, \hat{P}_{Dt} - M_{Lt}) \right\} \quad (17)$$

Where "$\bigcap$" implies the intersection. M_{Ut} and M_{Lt} are the assumed upper and lower limits of prediction errors, respectively. RTDF is obtained as the upper and lower bounds pair $\bar{\alpha}_{kt}$ and $\underline{\alpha}_{kt}$ (k=1,…,N_G, t=1,..,T) as follows.

$$\underline{\alpha}_{kt} \le P_{Gkt} \le \bar{\alpha}_{kt} \quad (18)$$

Calculation of RTDF is performed in each control cycle before stage II optimization in section III-*D*.

Once the upper and lower limits are obtained, any output values P_{Gkt} inside the limits (18) will be guaranteed as reachable if the latest load forecast errors appear inside CIs $[\hat{P}_{Dt} - M_{Lt}, \hat{P}_{Dt} + M_{Ut}]$. In this algorithm, when $\bar{\alpha}_{kt} < \underline{\alpha}_{kt}$ is detected, RTDF is nonexistence and the supply-demand mismatch (SDM) is computed by (19).

$$SDM = \begin{cases} \underline{\alpha}_{tc} - \overline{\alpha}_{tc} & (when\ \overline{\alpha}_{tc} < \underline{\alpha}_{tc}) \\ 0 & (when\ \overline{\alpha}_{tc} \geq \underline{\alpha}_{tc}) \end{cases} \quad (19)$$

When SDM is detected, it must be compensated by additional power provision or load reduction. After the management of SDM, we recalculate RTDF to confirm that SDM disappears. Then the optimization process is continued.

C. Stochastic Load Flow [20]-[22]

The prediction errors of loads and RESs result in line flow uncertainty. Line flow constraints are treated in a probabilistic manner as presented in Fig. 2. Assuming the normal distribution for the prediction error characteristic, linear DC power flow calculation method is used to provide the most efficient computation. The SLF method is applied in such a way that the probability of constraint violation is less than a specified value for each line. The stochastic network constraint is represented as in the following form.

$$LBF_l \leq F_l = \sum_{j=1}^{N_n} S_{lj} P_j \leq UBF_l \quad (20)$$

UBF_l and LBF_l are the upper and lower bounds [MW] with respect to the transmission line l, F_l: amount of line flow [MW], N_n: number of nodes, S_{lj}: conversion matrix, P_j: injection power [MW] into node j.

The formulation of (20) is given as below. Based on the DC power flow method, the following relationships hold.

$$\boldsymbol{S}_N \boldsymbol{\theta} = \boldsymbol{P} \quad (21)$$

$$\boldsymbol{F} = \boldsymbol{S}_C \boldsymbol{\theta} \quad (22)$$

Where, $\boldsymbol{\theta} \in \mathbf{R}^{N \times 1}$: voltage angle matrices [rad], $\boldsymbol{P} \in \mathbf{R}^{N \times 1}$: real power injection matrices [p.u.], $\boldsymbol{F} \in \mathbf{R}^{M \times 1}$: real power line flow [p.u.], $\boldsymbol{S}_N \in \mathbf{R}^{N \times N}$: node susceptance matrices [p.u./rad], $\boldsymbol{S}_C \in \mathbf{R}^{M \times N}$: line susceptance matrices. From (21) and (22), we obtain:

$$\boldsymbol{F} = \boldsymbol{S}_C \boldsymbol{S}_N^{-1} \boldsymbol{P} = \boldsymbol{S} \cdot \boldsymbol{P} \quad (23)$$

Node injection $\boldsymbol{P}$ is represented as

$$\boldsymbol{P} = \boldsymbol{P}_G - \boldsymbol{P}_D \quad (24)$$

Where P_D is a probabilistic variable consisting of loads and RES outputs (negative demands), while P_G corresponds to a

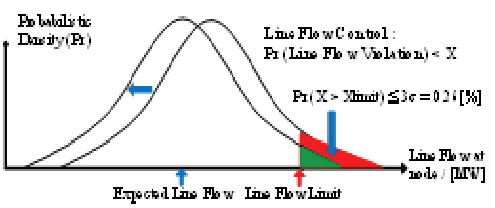

Fig. 2. Stochastic control of line flow.

variable of conventional generator outputs to be determined in the optimization process. Therefore, the expected value $E[\boldsymbol{P}]$ of node injection power $\boldsymbol{P}$ is represented by the following expression:

$$E[\boldsymbol{P}] = \boldsymbol{P}_G - E[\boldsymbol{P}_D] \quad (25)$$

Then, the mean value vector and covariance matrix of line flow are represented as follows:

$$E[\boldsymbol{F}] = \boldsymbol{S}[\boldsymbol{P}_G - E[\boldsymbol{P}_D]] = \boldsymbol{S} \cdot \boldsymbol{P}_G - \boldsymbol{S} \cdot E[\boldsymbol{P}_D] = [\mu_l] \quad (26)$$

$$\begin{aligned} Cov[\boldsymbol{F}] &= E[(\boldsymbol{F} - E[\boldsymbol{F}])(\boldsymbol{F} - E[\boldsymbol{F}])^T] \\ &= \boldsymbol{S} \cdot E[(\boldsymbol{P} - E[\boldsymbol{P}])(\boldsymbol{P} - E[\boldsymbol{P}])^T] \cdot \boldsymbol{S}^T \\ &= \boldsymbol{S} \cdot Cov[\boldsymbol{P}] \cdot \boldsymbol{S}^T = [\sigma_{ij}] \end{aligned} \quad (27)$$

Where, $Cov[P] = \begin{pmatrix} b_{11} & b_{12} & \cdots & b_{1n} \\ b_{21} & b_{22} & \cdots & \vdots \\ \vdots & \vdots & \ddots & b_{(n-1)n} \\ b_{n1} & \cdots & b_{n(n-1)} & b_{nn} \end{pmatrix}$.

The diagonal element b_{nn} is variance of $\boldsymbol{P}_D$, the non-diagonal element is the covariance (Cov) of PV generation outputs.

The probability density function for line flow l may be described using the elements from (26) and (27):

$$\xi_{F_l}(F_l) = \frac{1}{\sqrt{2\pi}\sigma_{ll}} \exp\left\{-\frac{1}{2}\frac{(F_l - \mu_l)^2}{\sigma_{ll}^2}\right\} \quad (28)$$

In order to constrain the violation probability to a value less than X, threshold β is defined by the following equations.

$$X \geq 1 - \int_{-\overline{F}_l}^{\overline{F}_l} \xi_{F_l}(x)dx \quad (29)$$

$$\overline{F}_l - \beta \cdot \sigma_{ll} \geq |E[F_l]| \quad (30)$$

Further substitution of (30) into (28) yields stochastic load flow constraint below, where (31) is identical with (20).

$$-\overline{F}_l + \beta \cdot \sigma_{ll} + D_l \leq \sum_{j=1}^{N_n} S_{lj} P_j \leq \overline{F}_l - \beta \cdot \sigma_{ll} + D_l \quad (31)$$

Where ,

$$D_l = \sum_{j=1}^{N_n} S_{lj} E[P_D^j].$$

D. Formulation for Stage II Optimization

The optimization problem (Stage II) is formulated with N_G controllable generators in a time horizon of T intervals ahead from the current moment as follows.

Minimize:

$$C^{RT}(P_G, u) = \sum_{t=1}^{T} \sum_{k=1}^{N_G} (a_k P_{Gkt}^2 + b_k P_{Gkt} + c_k) \quad (32)$$

Subject to:

(3), (5), (18), (31).

Constraints (18) and (31), which are explained in sections III-*B* and *C*, are the novel treatment of uncertainties by the proposed method. That is, the important constraint of the supply and demand balance is treated in deterministic manner by RTDF with CIs to avoid system collapse. On the other hand, soft constraints of line overloading are dealt with by DC probabilistic power flow. Covariance matrix and CIs will be updated frequently in real-time operation, as is presented in the next section.

E. Computational Procedures

This section describes the computation procedure of the proposed method presented in the previous sections. The following procedures are performed in every control cycle.

< Day-ahead 24-hour GS: Stage I > (A few times a day)

Instead of standard approach using Mixed-Integer Linear Programming (MILP), we have developed a special technique by improving the method in [23] to solve the UC problem by using standard QP software. The effectiveness of the proposed technique has been studied in [24].

The day-ahead GS is obtained by using the following algorithm to determine the generator's output $\boldsymbol{P_G}$, its start/stop variable $\boldsymbol{u}$ and BT charge/discharge operation for 24 hours, where unit time is 30 minutes.

Step I-1 Read day-ahead forecast data for loads and RES.

Step I-2 Set iteration number $d = 0$.

Step I-3 Solve (1) by QP to determine $\boldsymbol{P_G}$ and $\boldsymbol{u}$, treated as continuous variables.

Step I-4 Compute unit fuel cost in (33) using present $\boldsymbol{P_G}$.

$$\mu_{Gt}^{d} = a_t P_{Gt} + b_t + c_t / P_{Gt} \qquad (33)$$

Step I-5 Solve the following problem with penalty function (35) using QP algorithm.

Minimize:

$$g(\boldsymbol{P_G}, \boldsymbol{u}, d, \boldsymbol{\mu^d}) = C^{\overline{GR}}(\boldsymbol{P_G}, \boldsymbol{u}) + h(d, \boldsymbol{\mu^d}) \qquad (34)$$

$$h(d, \boldsymbol{\mu^d}) = \sum_{k=1}^{N_G} \sum_{t=1}^{T} \left\{ 10^{-d+2} (d+2)(\mu_{Gt})^d \right\} \qquad (35)$$

Subject to: (3)-(16), and (23).

Step I-6 $d = d + 1$.

Step I-7 Repeat Steps I-4 to I-6 until the convergence is obtained.

Step I-8 Determine start/stop variables $\boldsymbol{u}$: if $u_{kt} > 0.5$ (threshold) then set $u_{kt}=1$ else $u_{kt}=0$.

Step I-9 By fixing $\boldsymbol{u}$, solve (1) to obtain $\boldsymbol{P_G}$ using QP algorithm.

The obtained start/stop time for generators and BT operation for 24-hour GS will be used in stage II as predetermined schedule. The generator's outputs P_{Gkt} are used as only reference for operators.

< Real-time 1-hour GS: Stage II > (Every 5 minutes)

The real-time GS is carried out to minimize the generator's output and BT charge/discharge operation (if necessary) every 5 minutes.

Step II-1 Read data of day-ahead generator's start/stop variables and BT charge/discharge operations.

Step II-2 Update forecasts (load and RES), covariance matrices, and CIs using most recent data. Perform state estimation to obtain the present operating condition.

Step II-3 Calculate RTDF and Supply-Demand Mismatch (SDM). If SDM is non-zero, arrange relevant reserve by modifying BT operation schedule, or using other resources corresponding to detected value of SDM, and perform RTDF update to confirm zero SDM.

Step II-4 Compute UBF_k and LBF_k.

Step II-5 Solve problem (32) by QP software to obtain GS P_{Gkt} (k=1,..,N_G, t=5,10,.., 60[min]).

The obtained GS is monitored by system operator, where GS in 5 minutes ahead are sent to the individual generators as real-time control signal.

IV. Case Studies

A. Simulation Conditions

The proposed method is demonstrated using an example system in Fig. 3. The generation mix data are from a Japanese smart grid project where the installed PV an WT generation are about 15% of peak load. It is composed of three diesel generators, two load areas with RESs and a BT station. Detail data are given in Tables I. PV prediction data is shown in Fig. 4, which has been given by our forecasting method based on the weather clustering type neural network. Typical load patterns are used in the proposed optimization process.

B. Stage I optimization

Figure 5 shows the result of stage I optimization, describing 24-hours GS for generators (P_{G1}, P_{G2}, P_{G3}), BT operation ($P_{BT}=B_{t-1}-B_t$), electricity demand (P_D), net electricity demand (P_{net}), PV output (P_{PV}) predictions, WT outputs (P_{WT}), and SOC of BT (B_t). Note that G2 starts up at 11:00 and shuts down at 18:15 shown in Table II, which will be fixed in the stage II optimization.

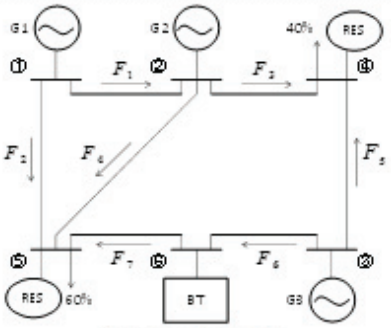

Fig. 3. Test Power System.

TABLE I
Specification of three diesel generators.

k	Output Limit [kW]	Ramp Rate [kW/min]	Start-up Cost (suc$_k$) [$]	Cost Coefficients[100$]		
				a_k	b_k	c_k
G1	1,000~2,000	66.7	40.00	0.0011	16.416	4,320.00
G2	625~1,250	41.7	25.00	0.0021	17.410	3,667.50
G3	1,125~2,250	75.0	45.00	0.0002	20.178	3,993.70

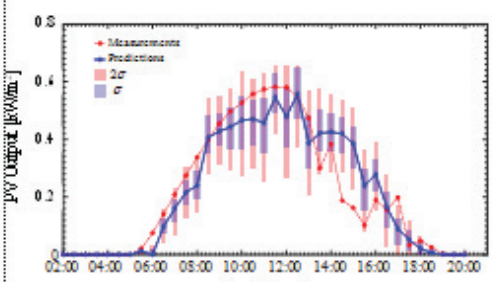

(a) Results of Day-ahead Forecast.

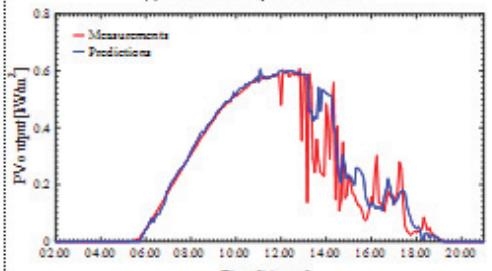

(b) Results of Real-time Forecast.

Fig. 4. Forecast results on 4th August, 2012.

C. Stage II optimization

1-hour GS is computed and updated every 5 minutes based on real-time PV prediction data. The upper and lower tolerances of prediction errors in net demands (load – RES) are set as a linear function of time as follows:

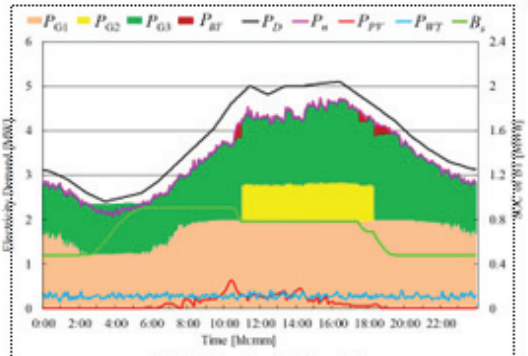

Fig. 5. Day-ahead 24-hour GS.

TABLE II
Start-up and shut-down times data from day-ahead UC.

Demand	Unit k	Start-up time	Shut-down time
Weekday	G1	-	-
	G2	11:00	18:15
	G3	-	-

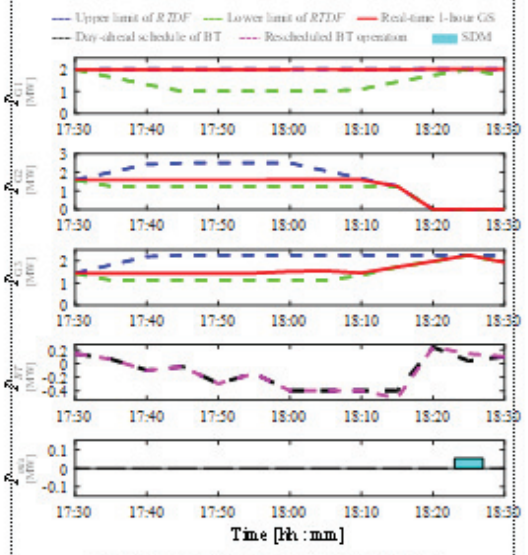

Fig. 6. Real-time 1-hour GS with RTDF and SDM.

$$M_{Lt} = M_{L1} = \hat{P}_{Dt} \times \frac{t}{T} \times \gamma \quad (36)$$

Where, $\hat{P}_{Dt}$ (t=0,1,…,T) are the most recent forecasted net power demands. T=60 [min], t: prediction time (t=0 for present operating point), γ is a parameter representing 1 hour ahead maximum prediction error, and γ= [0%, 10%, 20%] will be examined. Allowable constraint violation for line flow is set to X=3σ=0.26[%] in this examination.

Figure 6 shows the result of stage II optimization obtained at 17:30 (weekday, γ=10%). The upper and lower limits of RTDF and 1-hour GS for each generator are provided. The GS at 5 minutes ahead (17:35) is sent to each generating unit as a control signal. RTDF implies reachable area from the operating point at 17:30. The larger RTDF, the larger system capability that copes with uncertainty is expected. RTDF computation also successfully provides SDM 1-hour before the operation, which is given as P_{cmd} that appears at 18:25. This advantageous characteristic come from the RTDF computation which identifies the feasible region with high accuracy. Note that the detected SDM is managed by the rescheduling of the BT operation 1-hour before by the proposed method. If BT cannot cope with the situation, we can prepare additional action such as demand response or load shedding at 18:25.

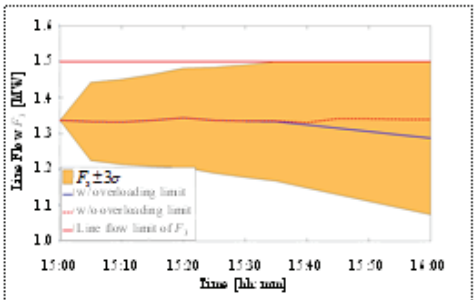

Fig. 7. Line Flow with 3σ allowable intervals at line F_3.

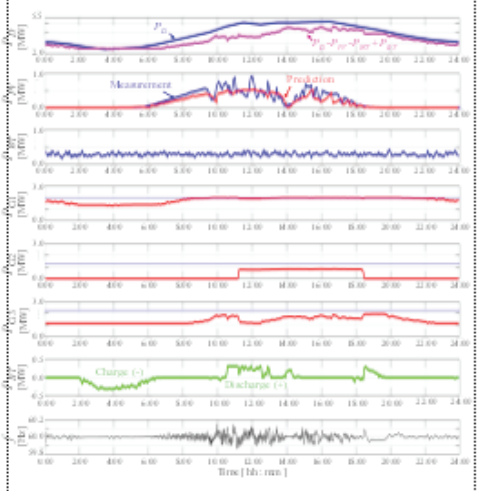

Fig. 8. The results of the 24-hour operations.
(From top: 1: P_{Σ} and net demand (=P_{Σ}-P_{rv}-P_{wt}+P_{batt}) [2~5.5MW], 2: P_{rv} (prediction 1-hour ahead and measurement) [0~1MW], 3: P_{wt} [0~1MW], 4: P_{G1}, 5: P_{G2}, 6: P_{G3} [0~3MW], 7: P_{BT} [-0.5 ~0.5MW], and 8: f system frequency [59.8~60.2Hz], where [*~**] describes full scale of each graph)

Figure 7 shows the scheduled F_3 line flow, which may vary inside 3σ allowable intervals. The result shows that SLF works successfully to avoid overloads in stage II optimization.

Figure 8 describes the simulated results after 24-hour operations by the proposed real-time optimized control method. Descriptions of wave forms are given below the figure caption. We see that the PV prediction 1-hour ahead in the 2nd graph is erroneous. Nevertheless, the proposed method successfully treats the uncertainties to control generators as seen in 4-6th graphs, Rescheduled BT operation in the 7th graph has completely absorbed the SDM detected in Fig. 6. As a result, the frequency deviations are suppressed less than 0.2 Hz as observed in 8th graph. The frequency fluctuation has been analyzed by the simulator in the proposed micro-EMS controller in Fig.1. The frequency deviations increase mainly due to PV output fluctuations as well as the prediction errors in the day time. Thus, the proposed method reliably manages the uncertainties in the real-time power system operation.

D. Application to West Japan Power System

The proposed controller is applied to West Japan power system, which consists of six regions (Kyushu, Chugoku, Shikoku, Kansai, Hokuriku, and Chubu) shown in Fig. 9. We

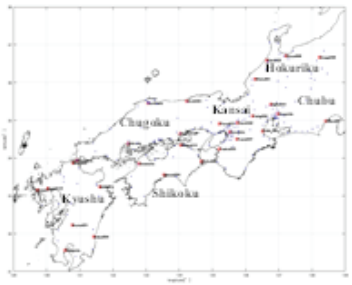

Fig. 9. West Japan area consists of six regions.

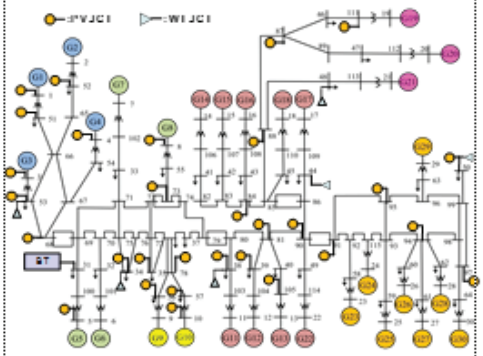

Fig. 10. West Japan 30-Gen. system model with RES, BT.

use the power system model [27] depicted in Fig.10, where the total generation capacity is 100.2 [GW]. The system consists of 30-generators, 31-load areas with RESs and a BT station. Taking into account the scenarios of PV generation of Japan [28], we set three cases:

Case 1: 19 GW of PV installation (All Japan is 32GW)

Case 2: 38 GW (64 GW)

Case 3: 67 GW (112 GW)

Here, we demonstrate (1) PV forecasts, (2) Stage I: day-ahead 24-hour GS, and (3) Stage II: real-time 1-hour GS in the following sections.

1) Day-ahead and real-time PV forecasts

Figure 11 shows the results of PV output forecast using the weather data on 3rd Aug. 2012 (sunny/cloudy day with relatively high PV generation outputs) in Case 1. The blue line indicates the prediction by the proposed method, the blue bars around the prediction line shows the confidence interval (CI) of the prediction where the errors are less than the standard deviation $\pm\sigma$, and the red bars, $\pm 2\sigma$. We see that the predictions for different areas have different CIs depending on learning data of the areas. This implies that reliability of the predictions is different from area to area even though the same prediction method is used. These predictions with CIs will be used in the computations of Stages I and II in order to obtain reliable GS.

2) StageI: Day-ahead 24-hour GS

Figures 12-14 (a) show the results of stage I optimization for cases 1-3, respectively. The Figures describe 24-hours GS, which include the schedules of the followings:

Generators (P_{G1}, P_{G2}, ..., P_{G10}), BT operation ($P_{BT}=B_d-B_d$),

Electricity demand (P_D), Predicted net demand (P_n),

PV output (P_{PV}) predictions, WT outputs (P_{WT}),

SOC of BT (B_d).

3) StageII: Real-time 1-hour GS

We have carried out real-time power system operations for 24 hours by the proposed real-time optimized control method. Figures 12-14 (b) show one hour GS at 12:25 for cases 1-3, respectively. We can observe that reliable schedule for each device is obtained inside its feasible region, RTDF.

E. Computational Burden

Table III shows the computational burden (CPU Time), which is evaluated for the test power systems with 3, 5, 10 and 30 generators using Intel Core i7, 2.20GHz, 8GB memory.

The CPU time on Stage I implies a total computation time from Steps I-2 to I-9 in Section III-*E* for obtaining a day-ahead 24-hour GS. Stage II computation time is for the calculation of Steps II-3 to II-5 in Section III-*E* for obtaining a real-time 1-hour GS that is to be repeated every 5 minutes. Note that the numbers in the blanket imply the computation time for RTDF and SDM.

TABLE III
CPU Time

Number of Generators	Stage I for day-ahead 24-hour GS [sec]	Stage II for real-time 1-hour GS[sec]
3	3.0	0.37 (0.011)
5	4.4	0.44 (0.012)
10	9.4	1.87 (0.054)
30	20.0	3.86 (0.109)

V. Conclusion

Integrating large amounts of intermittent RESs into electric power systems causes various difficulties such as the supply and demand balance and frequency problems. In such situations, treatment of uncertainty by means of limited controllable resources is a critical issue for secure power system operations. Frequent evaluation of generation schedule is effective for minimizing prediction errors in order to establish a reliable operation against sudden changes in RES generations. The paper proposes a new real-time optimization method guaranteeing feasibility of operations. Uncertainties affecting the important constraint of the supply and demand balance are treated in deterministic manner using CIs to avoid system collapse, while those relating to soft constraints of line overloading are dealt with by DC probabilistic power flow.

Although the computation time is a critical issue, the proposed method provides a solution for introducing a large amount of RES into a smart grid operation.

The present version of the proposed method utilizes the DC power calculation method which may degenerate the accuracy when applied to low voltage distribution systems with large values of R/X. The use of extended equations based on a distribution power flow [25], [26] seems an interesting trial in the future.

VI. References

[1] [AT 1] J. Zhu, "Optimization of Power System Operation," Wiley-IEEE Press, Second Edition, Jan. 2015.

[2] [AT 2] A. Ipakchi, and F. Albuyeh, "Grid of the future," *IEEE Power and Energy Magazine*, Vol. 7, No. 2, pp.52-62, Feb. 2009.

[3] [AT 3] N. Yorino, Y. Sasaki, S. Fujita, Y. Zoka, and Y. Okumoto, "Issues for Power System Operation for Future Renewable Energy Penetration: Robust Power System Security," *Electrical Engineering in Japan*, Vol. 182, No. 1, pp. 30-38, Jan. 2013.

[4] [AT 4] N. Yorino, Y. Sasaki, E.P. Hristov, Y. Zoka, and Y. Okumoto, "Dynamic Load Dispatch for Power System Robust Security against Uncertainties," *2013 IREP Symp. Bulk Power System Dynamics and Control - IX Optimization, Security and Control of the Emerging Power Grid*, pp.1-17, Crete, Greece, 25-30 Aug. 2013.

[5] [AT5] N. Yorino, M. Abdillah, Y. Isoya, Y. Sasaki, and Y. Zoka, "A New Method of Evaluating Robust Power System Security Against Uncertainties," *IEEJ Trans. on Elect. and Electron. Eng.*, Vol.10, No.6, pp. 636-643, Nov. 2015.

[6] [AT 6] D.W. Ross, and S. Kim, "Dynamic Economic Dispatch of Generation," *IEEE Trans. on Power App. and Syst.*, Vol. PAS-99, No. 6, pp.2060-2068, Nov. 1980.

[7] [AT 7] T. Li, and M. Shahidehpour, "Dynamic Ramping in Unit Commitment," *IEEE Trans. on Power Syst.*, Vol. 22, No. 3, pp.1379-1381, Aug. 2007.

[8] [AT 8] W.G. Wood, "Spinning Reserve Constrained Static and Dynamic Economic Dispatch," *IEEE Trans. on Power App. and Syst.*, Vol. PAS-101, No. 2, pp.381-388, Feb. 1982.

[9] [AI 9] D.N. Simopoulos, S.D. Kavatza, and C.D. Vournas, "Unit Commitment by an Enhanced Simulated Annealing Algorithm," *IEEE Trans. on Power Syst.*, Vol. 21, No. 1, pp.68-76, Feb. 2006.

[10] [AI 10] C.L. Chen, "Simulated Annealing-based Optimal Wind-thermal Coordination Scheduling," *IET Gener. Transm. and Distrib.*, Vol. 1, No. 3, pp.447-455, May 2007.

[11] [AI 11] A.Y. Abdelaziz, M.Z. Kamh, S.F. Mekhamer, and M.A.L. Badr, "A Hybrid HNN-QP Approach for Dynamic Economic Dispatch Problem," *Electric Power Systems Research*, Vol. 78, No. 10, pp.1784-1788, Oct. 2008.

[12] [AI 12] J.P. Chiou, "A Variable Scaling Hybrid Differential Evolution for Solving Large-scale Power Dispatch Problem," *IET Gener. Transm. And Distrib.*, Vol. 3, No. 2, pp.154-163, Feb. 2009.

[13] [AI 13] C.E. Soumah, and N. Khaouam, "Application of Linear Programming Redispatch Technique to Dynamic Generation Allocation," *IEEE Trans. on Power Syst.*, Vol. 5, No. 1, pp.20-26, Feb. 1990.

[14] [AI 14] F.N. Lee, L. Lemonidis, and K.C. Liu, "Price-based Ramp-rate Model for Dynamic Dispatch and Unit Commitment," *IEEE Trans. on Power Syst.*, Vol. 9, No. 3, pp.1233-1242, Aug. 1994.

[15] [AI 15] G. Irisarri, L.M. Kimball, K.A. Clements, A. Bagchi, and P.W. Davis, "Economic Dispatch with Network and Ramping Constrained via Interior Point Methods," *IEEE Trans. on Power Syst.*, Vol. 13, No. 1, pp.236-242, Feb. 1998.

[16] [AI 16] H.M. Hafiz, N. Yorino, Y. Sasaki, and Y. Zoka, "Feasible Operation Region for Dynamic Economic Dispatch and Reserve Monitoring," *European Trans. on Electrical Power*, Vol. 22, No. 7, pp.924-936, Oct. 2012.

[17] [AI 17] N. Yorino, H.M. Hafiz, Y. Sasaki, and Y. Zoka, "High-speed Real-time Dynamic Economic Load Dispatch," *IEEE Trans. on Power Syst.*, Vol. 27, No. 2, pp.621-630, May 2012.

[18] [AI 18] Y. Okumoto, N. Yorino, Y. Zoka, Y. Sasaki, T. Yamanaka, and T. Akiyoshi, "An Application of Robust Power System Security to Power System Operation for High-penetration of PV," *IEEE Innovative Smart Grid Technologies Europe (ISGT Europe 2012)*, pp.1-7, Berlin, Germany, 14-17 Oct. 2012.

[19] [AI 19] Y. Sasaki, D. Seikoba, J. Ushiara, K. Kamiya, Y. Zoka, and N. Yorino, "A Robust Supply and Demand Controller against Uncertainties of Renewable Energy Sources," *18th Power Systems Computation Conference (PSCC2014)*, No. ID352, pp.1-6, Wroclaw, Poland, 18-22 Aug. 2014.

[20] [AI 20] B. Borkowsk, "Probabilistic Load Flow," *IEEE Trans. on Power App. and Syst.*, Vol. 93, No. 3, pp.752-759, May 1974.

[21] [AI 21] J.F. Dopazo, O.A. Klitin, and A.M. Sasson, "Stochastic Load Flows," *IEEE Trans. on Power App. and Syst.*, Vol. 94, No. 2, pp.299-309, Mar. 1975.

[22] [AI 22] C.L. Su, "Probabilistic Load-Flow Computation Using Point Estimate Method," *IEEE Trans. on Power Syst.*, Vol. 20, No. 4, pp.1843-1851, Nov. 2005.

[23] [AI 23] T. Sawa, and K. Furukawa, "Unit Commitment using Quadratic Programming and Unit Decommitment," *IEEE PES General Meeting 2012*, pp.1-6, San Diego, CA, 22-26 Jul. 2012.

[24] [AI 24] Y. Sasaki, S. Nobunaga, J. Ushiara, Y. Zoka, and N. Yorino, "Development of the DS-Manager for Utilizing the Existing Generators," *The International Conference on Electrical Engineering*, No. 272, pp.1-6, Hong Kong, China, 5-9 Jul. 2015.

[25] [AI 25] K. Mahmoud, N. Yorino, and A. Ahmed, "Optimal Distributed Generation Allocation in Distribution Systems for Loss Minimization," *IEEE Trans. on Power Syst.*, Vol. 31, No. 2, pp.960-969, Mar. 2016.

[26] [AI 26] K. Mahmoud, N. Yorino, and A. Ahmed, "Power Loss Minimization in Distribution Systems Using Multiple Distributed Generations," *IEEJ Trans. on Elec. Electron. Eng.*, Vol. 10, No. 5, pp.521–526, May 2015.

[27] Japanese Power System Models, IEEJ West 30-machine System Models," http://www.iee.jp/pes/?page_id=507.

[28] IEA, "Energy Polices of IEA Countries: Japan 2016 Review," URL: https://www.iea.org/publications/

Real-time PV Forecasting Method for Energy Management Operation

IMAM WAHYUDI FARID, MITSUMASA ASADA,
YUTAKA SASAKI, NAOTO YORINO, YOSHIFUMI ZOKA

Graduate School of Engineering, Hiroshima University

Abstract:

Renewable energy sources (RESs) have been attracted great attention to reduce environmental impact. In particular, the installation of photovoltaic power generations (PVs) are strongly promoted in Japan. However, the PV output is uncertain due to spatially different and time-varying solar radiation. Therefore, controllable generators are necessary to achieve stable power supply based on well-suited generation planning, operation, and control. Various forecasting methods for output of PVs have been proposed. The conventional methods cannot be widely used in various situations because they require sophisticated data that cannot easily be obtained. Furthermore, the prediction accuracy of such methods tend to deteriorate especially due to lack of data.

In this paper, we focused on the real-time PV forecast for energy management operation. We use the public historical insolation and weather (temperature, wind speed, and precipitation) data that can be easily obtained from the meteorological agency website of Japan. We propose the novel method using these data to predict the real-time PV output. By considering the correlation between the target and the neighboring areas, a 5-minute ahead high-accurate prediction for energy management operation can be achieved. By using the correlation coefficients between several areas, we can analysis and compare the autoregressive (AR), proposed solar radiation correlation analysis (SRCA), and using extreme learning machine (ELM).

On the target day, this part performs the real-time prediction of load demand and RES outputs for up to 1 hour in advance with 5-minute intervals, and improves the accuracy comparing to the day-ahead prediction. These processes are executed every 5 minutes and the results are used in the UC on the day and the real-time economic load dispatch (ELD) of the generators.

In this study, as a remarkable point, a SRCA technique is proposed and applied to the real-time prediction, in which the correlations of solar radiation are evaluated between multiple locations and used to estimate timing and magnitude of rapid changes of solar radiation in advance. Based on this prediction, a real-time operational plan of the existing equipment, such as generators and storage batteries for up to 1 hour ahead in every 5 minutes. In order to cope with rapid weather changes and unavoidable prediction errors, a stand-by planning of operating and spinning reserve should be made at the same time.

Keywords:

Uncertainties, Real-time PV forecast, Energy Management Operation

1. Introduction

The Japanese government has recently put great deal of attention on the renewable energy sources (RESs). The operation of RESs are planned to be integrated with the existing electric power system. However, PV power output is inherently uncertain due to different locations, time-varying seasonal and daily solar radiation intensity.

Previous works are reported that various methods can be used to predict the PV output from publicly available weather data. However, the methods in obtaining and processing the raw data prior to the forecasting tend to be complicated, on top of that the forecasting methods also tend to be sophisticated [1-4]. Others one reported using other methods to forecast PV output power. Numerical weather prediction [5,8], sky imagery [6,9], and neural network [7,10] have been used by several reserch.

Here we utilize simple data and reliable method that can be applied to the energy management operation, we can achieve an applicable research result. We use the public historical insolation and weather (temperature, wind speed, and precipitation) data. The data can be easily obtained from the meteorological agency website of Japan.

Since PV output forecast become important in energy management planning, a reliable method particularly 1 until 5 minutes forecast is substantial for real-time PV output forecasting. Recently, real-time PV output forecast is required a sophisticated data process [11-13]. Neural network (NN) as the one of common modeling forecast method is commonly used by researchers to model and forecast the PV output. However, NN process need more computation time for modeling and forecasting. This part is one of the laxity in NN method [14]. In real-time PV forecast, computation time is one of the important thing to yield the results. Real-time PV forecast is presented for up to 1 hour in advance with 5-minutes intervals. This forecast requires a fast calculation and high accurate prediction to be applied on a real-time operation and planning of generators or batteries.

In this paper, we present two groups of real-time forecasting. First is neighboring area real-time forecast and second is pin point real-time forecast. For pin point real-time forecast, we use extreme learning machine (ELM) using simple weather data. ELM provide a fast computation time for modeling and forecasting PV output. ELM facilitate a faster computation time for modeling than general neural networks [15]. By using this advantage, ELM is used for real-time forecasting in this research. More detail of ELM explanation is described in section 2.

This paper also provides SRCA method to calculate the insolation ahead value. SRCA is selected for real-time PV output forecasting. This method is considering the correlation of two or more neighboring areas. The correlation of several areas calculation is presented in section 3. Correlation factor is considered as PV output calculation. AR is selected to analysis and compare the real-time PV output forecast.

We also present an energy management system that represents an existing power system management. Real-time forecast result is applied on real-time economic load dispatch (ELD) of generators. The advantages of real-time ELD is to keep the power system secure and robust. Reference [21] mention that the real-time PV forecast output is needed by the operator of generator dispatch. This clearly mentioned that real-time PV forecast is become a very important due to the application. High accurate of real-time PV output forecast is very important and needed.

The rest of paper is organized as follows. Section 2 we describe the theory ELM and solar radiation correlation analysis (SRCA). Section 3 shows data sources and the forecast methodology. Section 4 presents the experimental result and comparison. Finally, in section 5 the experimental conclusion and future step are shown.

2. PV Forecasting using ELM and SRCA

In this paper, the authors focus on real-time forecasting of PV. The real- time PV forecasting is provide a PV output forecast at less than 10 minutes intervals using ELM and SRCA. In general, real-time PV output forecast is required high accuracy and high speed forecasting process to operate a target system.

2.1 ELM

Reference [15] mentioned a new training algorithm for machine learning. This algorithm does not spend much time to train the network. This method also does not need iterative process to reach the minimum error. Empirical calculation proof that ELM can process generalization better and faster than neural network [16]. The fundamental thing about ELM is start from single hidden layer feed forward network. The scheme of single layer neural network is shown in figure 1.

The forecasting process is conducted in 7 step as shown in the figure.

1. Set the input and output data, labeled as $\boldsymbol{X}$, $\boldsymbol{Y}$, respectively.
2. Set the number of nodes in the hidden layer. This step is labeled as $\boldsymbol{L}$.
3. Set the activation function for the nodes in hidden layer. The label for this process is $g(.)$.
4. Set the weight input and bias input randomly. The input weight can be mention as $\boldsymbol{W}$ and the bias input as $\boldsymbol{b}$.
5. Calculate the hidden layer and group it as one matrix. This step generally mention as $\boldsymbol{M}$. In this step, we also obtain the result of activation function calculation.

$$\boldsymbol{M} = \boldsymbol{X} \cdot \boldsymbol{W} \tag{1}$$

6. Calculate and analyze the output weight of single layer neural network. This step is labeled as β.

$$g(\boldsymbol{M}) \cdot \beta = \boldsymbol{Y} \tag{2}$$

$$\beta = \boldsymbol{H}^{+} \cdot \boldsymbol{Y} \tag{3}$$

In step 6, β is directly connect with $\boldsymbol{Y}$. ELM proposed a solution for this linear problem. To obtained the value of β, ELM use Moore-Penrose generalized inverse. In this case β is the calculation result of $g(\boldsymbol{M})$.

$\boldsymbol{H}^{+}$ is the Moore-Penrose generalized inverse of $\boldsymbol{H}$ [17]. The calculation of $\boldsymbol{H}^{+}$ is mentioned in (4).

$$\boldsymbol{H}^{+} = (\boldsymbol{H}^{T}\boldsymbol{H})^{-1}\boldsymbol{H}^{T} \tag{4}$$

In this part, the β value must be calculated correctly to obtain a small error between forecast result and data output ($\boldsymbol{Y}$).

7. Calculate the error between forecast result and data output. Forecast result is labeled as ($\hat{\boldsymbol{Y}}$). To calculate the ELM error, we use RMSE formulation.

$$RMSE = \sqrt{\sum_{i=1}^{N} \frac{\left(\hat{Y}_i - Y_i\right)^2}{N}} \tag{5}$$

Where, i: first value of forecast result and data output. Data is valued as N.

Finally, ELM provide a faster learning speed than general neural network algorithm. For the

implementation of ELM is simpler based on the matrix Moore-Penrose generalized inverse.

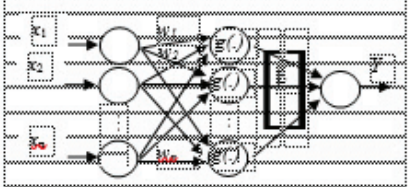

Fig. 1. ELM Architecture.

Where, x_i: input data, i=1…n, w_{ij}: weight between input and middle layer, i=1…n.

2.2 SRCA

In this section, we explain about SRCA method. We use SRCA as real-time forecast in 5 minutes interval. Fundamentally, SRCA is consider the gap correlation between several areas. The amount of insolation is calculated between two or more neighboring areas. We derive solar radiation correlation coefficient, mentioned as (r_{ij}), of the prediction target point i and other point j every 5 mins. Then we extract solar radiation amount past data in a certain period of point i. Then we extract solar radiation amount past data in the same time window period of point j, τ minutes before point i period. Here.

$$r_{ij} = \frac{\sum_t \left(x_i(t)-\bar{x}_i\right)\left(x_j(t-\tau)-\bar{x}_j\right)}{\sqrt{\sum_t \left(x_i(t)-\bar{x}_i\right)^2}\sqrt{\sum_t \left(x_j(t-\tau)-\bar{x}_j\right)}} \quad (6)$$

t: time (min), τ : time interval (min), x_0 : other point's solar radiation amount (kW/m^2), x_i predicted point's solar radiation amount (kW/m^2), $\bar{x}$: x period average (kW/m^2). Next, we change the gap time τ by 5 mins. and look for the correlation coefficient. Select the gap time τ_{max} with highest correlation, use the τ_{max} before solar radiation amount of point j to point i solar radiation prediction.

In order to obtain prediction in high accuracy, we performed real time of correlation analysis with multiple spots, choosing the points used in every 5 minutes prediction. We selected areas which have high correlation, and by setting each correlation coefficient as main object, integrated the prediction result of each spot. As a specific method, correlation analysis is performed towards multiple spots. Every area's correlation coefficient r_{ij} is emphasized, then we calculate weighted average value of the solar radiation prediction as shown in formula (7). Here.

$$\hat{Y}_i(t) = \frac{\sum_j \left(r_{ij} \cdot \hat{y}_{ij}(t)\right)}{\sum_j r_{ij}} \quad (7)$$

where $\hat{y}_{ij}(t)$ denotes the predicted solar radiation value at location i by using location j at time t [kW/m^2], and $\hat{Y}_i(t)$ denotes the predicted solar radiation value at location i by all screened locations at time t [kW/m^2].

Fig. 2 shows the prediction concept in real-time. Conventional authors have considered the prediction method [18-20]. As a simple real-time prediction method, we propose AR (autoregressive) model according to the least squares method of the predicted area's past data. This is a useful technique to avoid excessive error and can ensure accuracy to certain level. Although it enables high accuracy prediction for the latest time, error tends to increase as the predicted time elapses.

Furthermore, due to delay fluctuation of solar radiation actual value characteristics, we may obtain stable prediction accuracy of all times, however if the solar radiation suddenly changed, there must be high prediction error occurred to some extent. To solve these problems, we applied real-time PV output prediction method according to SRCA model that's been considered in other region's solar radiation amount. Solar radiation amount varies on cloud movement. Solar radiation fluctuation pattern, which is the upstream point of cloud flow, is assumed to appear in the downstream point with a delay time. We analyze 2 points according to correlation analysis, applying solar radiation with high correlation upstream to downstream solar radiation prediction.

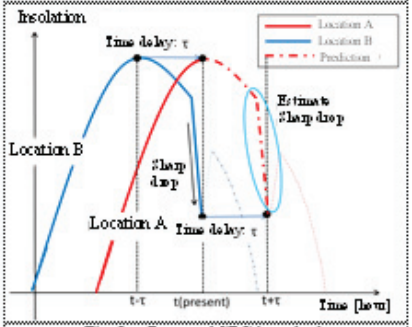

Fig. 2. Proposed SRCA method.

3. Data sources and Methodology

The data set used for two step of ELM calculation. The first step is dataset used for

training phase and the second step is dataset used for testing phase. The dataset is amount of insolation, humidity and temperature value. As detailed described as 10 days data on early of January 2009 will be used as training phase. For the testing phase, we also used 10 days data on early January 2009. Whole data set has 8641samples with 10 second interval. We used the past weather data offered by Japan Meteorological Agency (JMA) to conduct study on proposed method, and it is confirmed as highly performed prediction. The areas that have been prediction target in this paper were installed as PV by Hiroshima University. Using only the data published by Japan Meteorological Agency, we performed the real-time prediction of PV output. For the number of nodes in the hidden layer of ELM, we set it with 50 nodes at the first training. We also compare the different nodes value to knowing the error value and obtain the most effective number of nodes. Table 1 shows the training and testing error with several number of nodes. For the prediction target spot of SRCA method, we use past insolation data of 10 representative areas in Chugoku region. Then, we select the top 4 spot with high level of correlation, and apply forecast. We compare to AR model and verify SRCA model's effectiveness.

4. Case Study

ELM is applied as a regression analysis which can allow to obtain the PV output forecast. Real-time PV forecast with 10 second intervals is presented in this section. Table 1 shows that the increasing number of hidden nodes can affect CPU time.

Table 1. Comparison of Forecast Error and CPU Time between ELM and NN in 2 input data.

No. of Hidden Nodes	Forecast Error (ELM)	Forecast Error (NN)	CPU Time [s] (ELM)	CPU Time [s] (NN)
50	1.22	11.1	0.22	5.35
100	0.46	10.6	0.29	5.48
150	0.18	10.4	0.42	5.43
200	0.23	10.9	0.52	5.80

Figure 2 shows the ELM result with two available meteorological data.

Table 2. Comparison of Forecast Error and CPU Time between ELM and NN in 3 input data.

No. of Hidden Nodes	Forecast Error (ELM)	Forecast Error (NN)	CPU Time [s] (ELM)	CPU Time [s] (NN)
50	2.00	12.4	0.16	4.17
100	1.50	10.7	0.26	4.23
150	3.76	10.9	0.43	4.31
200	1.79	14.0	0.63	5.18

Table 2 indicates that the forecast accuracy is strongly influenced by the meteorological data. It is proof that the meteorological data type has a strong correlation with amount of insolation. SRCA result is shown in figure 4.

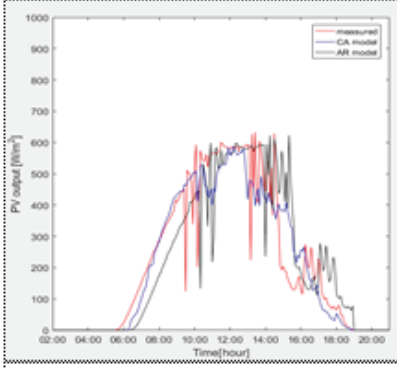

Fig. 3. Comparison of SRCA and AR.

As an indicator for comparing the prediction accuracy, we use the prediction error ratio ε, maximum prediction error ratio η, as shown in formula (8) and (9) below.

$$\varepsilon = \frac{100\times\sqrt{\frac{1}{m}\sum_{i=1}^{m}\left(\hat{X}_i - X_i\right)^2}}{\frac{1}{m}\sum_{i=1}^{m} Q} \ [\%] \qquad (8)$$

$$\eta = 100\times\left|X_{\max} - \hat{X}_{\max}\right| / Q_{\max} \ [\%] \qquad (9)$$

Out atmosphere solar radiation is theoretical value representing ideal maximum solar radiation of the day. Table 1 shows the average value of maximum prediction error ratio and average value of prediction error ratio of every prediction targeted time period in June 2012. Fig. 11 and 12 shows measured value and 10 mins. or 60 mins. away prediction value of solar radiation amount. The maximum prediction error η which occurs in model AR increased sharply over 5 to 10 mins. As the result, we managed to obtain the equivalent degree of prediction accuracy. The responsiveness towards ramp change is also improving.

Table 3. Prediction Errors [%]

	5min ahead	10min ahead	20min ahead	40min ahead	60min ahead
ε (AR)[%]	16.09	19.00	20.75	23.76	25.07
ε(CA)[%]	16.50	18.47	19.84	21.20	22.26
η(AR)[%]	32.87	36.74	36.56	39.10	40.65
η(CA)[%]	31.43	32.48	33.91	34.89	35.12

5. Conclusion

In this paper, we proposed real-time PV output forecast using SRCA and ELM. The interval time is set to 10 seconds. By using ELM proof that computational time can be decreased than conventional method such as neural network. Based on the ELM result, also mentioned the effect of meteorological data. The forecast researcher should choose data that have a strong correlation with the mount of insolation. As described above, according to forecast accuracy improvement, further performance of development of energy management is expected.

References

[1] R. K. Swartman, "Correlation of Solar Radiation with Common Parameters in Toronto, Canada," *Solar Energy*, Vol. 13, No. 3, pp. 345-347 (1971).

[2] R. K. Swartman, "Solar Radiation Estimates from Common Parameters," *Solar Energy*, Vol. 11, No.3-4, pp.170-172 (1967).

[3] D. Yang, Z. Dong, T. Reindl, P. Jirutitijaroen, and W. M. Walsh, "Solar Irradiance Forecasting Using Spatio-temporal Empirical Kriging and Vector Autoregressive Models With Parameter Shrinkage," *Solar Energy*, Vol. 103, pp.550-562, (2014).

[4] G. Notton, C. Paoli, S. Vasileva, M. L. Nivet, J. L. Canaletti, and C. Cristofari, "Estimation of Hourly Global Solar Irradiation on Tilted Planes From Horizontal One Using Artificial Neural Networks," *Energy*, Vol. 39, No.1, pp.166-179 (2012).

[5] R. Perez, E. Lorenz, S. Pelland, M. Beauharnois, G. V. knowe, K. H. Jr., D. Heinemann, J. Remund, S. C. Muller, and W. Traunmuller, "Comparison of Numerical Weather Prediction Solar Irradiance Forecasts in the US, Canada and Europe," *Solar Energy*, Vol. 94, pp.305-326 (2013).

[6] R. Perez, P. Ineichen, K. Moore, M. Kmiecik, C. Chain, R. George, and F. Vignola, "A New Operational Model For Satellite-derived Irradiances: Description and Validation," *Solar Energy*, Vol. 73, No. 5, pp.307-317 (2002).

[7] C. Cornaro, "Solar radiation forecast using neural networks for the prediction of grid Connected pv plants energy production (dsp project)," *Proc. on WIRE: Weather Intelligence for Renewable Energies*, 22 October 2014.

[8] [A2 25] E. Lorenze, et. all, "Irradiance Forecasting for the Power Prediction of Grid-Connected Photovoltaic Systems," *IEEE Journal of Selected Topics in Applied Earth Observations and Remote Sensing*, Vol. 2, No.1, pp. 2-10 (2009).

[9] M. S. Ghonima, et all, "A method for cloud detection and opacity classification based on ground based sky imagery," *Atmospheric Measurement Techniques*, Vol. 5, No. 11, pp. 2881-2892 (2012).

[10] G. Capizzi, C. Napoli, and F. Bonanno, "Innovative Second-Generation Wavelets Construction With Recurrent Neural Networks for Solar Radiation Forecasting," *IEEE Trans. on Neural Networks and Learning Systems*, Vol. 23, No.11, pp.1805-1815 (2012).

[11] W. F. Holmgren, A. Lorenzo, M. Leuthold, C. K. K. A. D. Cronin, and E. A. Betterton, "An Operational, Real-Time Forecasting System for 250 MW of PV Power Using NWP, Satellite, and DG Production data," *Photovoltaic Specialist Conference (PVSC)*, No. 14683377, 8-13 June 2014.

[12] A.T. Lorenzo, et.al, "Short-Term PV Power Forecasts Based on a Real-Time Irradiance Monitoring Network," *Photovoltaic Specialist Conference (PVSC)*, No. 14683253, 8-13 June 2014.

[13] N. Haghdadi, J. Dennis, A. Bruce, I. MacGill, "Real-time Generation Mapping of distributed PV for Network Planning and Operations," *Proc. on Power and Energy Engineering Conference (APPEEC)*, 2015.

[14] M. Benghanem, A. Mellit, S.N. Alamri, "ANN-based modelling and estimation of daily global solar radiation data: A case study. Science Direct," *Energy Conversion and Management*, Vol.50, No.7, pp.1644-1655 (2009).

[15] G.Huang, Q. Zhu, C.K. Siew, "Extreme Learning Machine: A New Learning Scheme of Feedforward Neural Networks," *Proc. on International Joint Conference on Neural Networks (IJCNN2004)*, 25-29 July 2004.

[16] G.B. Huang, Q.Y. Zhu, and C.K. Siew, "Extreme learning machine: Theory and applications," *Neurocomputing*, Vol. 70, pp.489-501 (2006).

[17] Serre, D. Matrices, "Theory and Application," Springer, New York(2002).

[18] Y. Sasaki, K. Kanaya, D. Seikoba, J. Okihara, Y. Zoka, and N. Yorino," Probabilistic Constrained Dynamic Economic Load Dispatch for Renewable Energy Sources," *Grand Renewable Energy 2014 International Conference and Exhibition (2014)*.

[19] [A2 19] L. Ma, N. Yorino, and K. Khorasani, "Solar Radiation (Insolation) Forecasting Using Constructive Neural Networks," *IEEE World Congress on Computational Intelligence (WCCI)*, No.16433, 24-29 July (2016).

[20] L. Ma and K. Khorasani, "Constructive feedforward neural networks using Hermite polynomial activation functions," *IEEE Trans. on Neural Networks*, Vol. 16, No. 4, pp.821-833 (2005).

[21] [A2 7] Y. Sasaki, N. Yorino, Y. Zoka, F.I. Wahyudi, "Robust Stochastic Dynamic Load Dispatch against Uncertainties," *IEEE Trans. on Smart Grid*, Vol. PP, No. 99, pp.1-1 (2017) to be appeared.